Helsinki Institute of Physics Internal Report Series

HIP-2006-1

Reconstruction of B Hadron Decays at DELPHI

Laura Salmi

Helsinki Institute of Physics
P.O. BOX 64, FI-00014 University of Helsinki, Finland

Dissertation for the degree of Doctor of Science in Technology to be presented with due permission of the Department of Engineering Physics and Mathematics, Helsinki University of Technology, for public examination and debate in Auditorium F1 at Helsinki University of Technology (Espoo, Finland) on the 24th of March, 2006, at 12 o'clock noon.

Helsinki 2006

ISBN 952-10-1697-3 (printed)
ISBN 952-10-1698-1 (PDF)
ISSN 1455-0563

Helsinki 2006
Yliopistopaino

Abstract

This thesis describes three analyses related to heavy quarks.

The analysis with the largest impact is the extraction of parameters of heavy quark decays using the lepton energy spectrum and the hadronic mass spectrum in semileptonic B decays. The extraction of the parameters allows to test the framework used to theoretically describe the decay of heavy mesons, and more accurate knowledge of the parameter values results in greater accuracy in the determination of the element $|V_{cb}|$ of the Cabibbo-Kobayashi-Maskawa (CKM) quark mixing matrix. The determination described in this thesis is important, since it is so far the only one where the full lepton energy spectrum has been used. The other determinations are based on using only a part of the spectrum. The first extraction of the parameters in the kinetic mass scheme was based on the statistical moments of the lepton energy spectrum and hadronic mass spectrum measured using the data collected at DELPHI.

In the second analysis, the angular distribution of fragmentation particles in $Z \to b\bar{b}$ and $Z \to c\bar{c}$ events was studied using the DELPHI data. The analysis gave the first direct experimental evidence of the dead cone effect, or the depletion of fragmentation particles at small emission angles, predicted by perturbative quantum chromodynamics.

The third analysis is a simulation study of top quark pair production at a possible future e^+e^- linear collider with a 3 TeV center-of-mass energy. The study allowed to estimate the accuracies with which the cross-section and forward-backward asymmetry could be measured.

Acknowledgements

This thesis is based on research work carried out during the years 2000-2005 as a member of the Helsinki Institute of Physics (HIP) group in the DELPHI collaboration. Most of the work was done at CERN, while some of the publications and this thesis were finalised at HIP in Helsinki.

The help and support of a large number of people has been essential for my research work for this thesis. I wish to thank Professor Risto Orava for the opportunity to work in his group at CERN. Professor Martti M. Salomaa was always able to fit me into his busy schedule for discussions concerning my studies, and Professor Rainer Salomaa has had an important role as my thesis supervisor.

I am grateful to Marco Battaglia for supervising my work, especially during the first years of my activity at CERN. Collaboration with Marta Calvi, Patrick Roudeau and Arantza Oyanguren on the DELPHI moment analysis was a pleasure.

My colleagues from HIP both at CERN and in Helsinki have provided me with an interesting and inspiring working athmosphere. Especially I would like to thank Kenneth Österberg for his thorough reading of this thesis starting from the earliest drafts and for the many valuable comments and suggestions.

My work has been supported financially by the GRASPANP graduate school program and by the following foundations: Magnus Ehrnroothin säätiö, Naisten Tiedesäätiö, Waldemar von Frenckellin säätiö and Yrjö, Ville ja Kalle Väisälän säätiö.

I want to thank my friends at CERN, Helsinki and elsewhere for keeping me in touch with the world outside of physics research and for the many experiences we have shared.

Most of all I thank my parents Satu and Mikko and my brother Sampo for their love and support, and for the pride and enthusiasm they are showing now that I am about to reach an important milestone in my career.

Contents

List of Publications

I J. Abdallah *et al.* with L. Salmi (The DELPHI collaboration), Determination of heavy quark non-perturbative parameters from spectral moments in semileptonic B decays, European Physical Journal **C45** (2006) 35-59

II M. Battaglia *et al.* with L. Salmi, Heavy Quark Parameters and V_{cb} from Spectral Moments in Semileptonic B Decays, Physics Letters **B556** (2003) 41-49

III L. Salmi on behalf of the DELPHI collaboration, OPE parameter determinations from semileptonic B decays at DELPHI, Nuclear Physics B (Proceedings Supplement) **142** (2005) 167-172

IV M. Battaglia, M. Calvi, L. Salmi, A study of the Lepton Spectrum Moments in $B \to X_c \ell \bar{\nu}$ Decays with the DELPHI Detector at LEP, DELPHI 2002-071 CONF 605, Contributed paper to International Conference on High Energy Physics 2002, Amsterdam

V L. Salmi on behalf of the DELPHI collaboration, Recent b physics results from DELPHI, Nuclear Physics B (Proceedings Supplement) **133** (2004) 133-136

VI M. Battaglia, R. Orava and L. Salmi, A study of depletion of fragmentation particles at small angles in b-jets with the DELPHI detector at LEP, DELPHI 2004-037 CONF 712, Contributed paper to International Conference on High Energy Physics 2004, Beijing

VII L. Salmi, $t\bar{t}$ Cross-section and forward-backward asymmetry at CLIC, in *Proceedings of International Workshop on Linear e^+e^- Colliders, Jeju, Korea*, edited by J. S. Kang and S. K. Oh, pp. 310-314, Korean Physical Society (2003)

Publication I: Determination of heavy quark non-perturbative parameters from spectral moments in semileptonic B decays

J. Abdallah *et al.* with L. Salmi (the DELPHI collaboration)

European Physical Journal C45 (2006) 35-59

Non-perturbative parameters used in the theoretical description of the decay of heavy mesons can be extracted from the spectra of the lepton energy and the hadronic mass in semileptonic B decays. The publication describes the measurements of the statistical moments of these two spectra using the DELPHI data. The extraction of the parameter values leads to a more accurate determination of the Cabibbo-Kobayashi-Maskawa (CKM) quark mixing matrix element $|V_{cb}|$.

The author of this thesis was responsible for the reconstruction of the lepton energy spectrum, including the reduction of background in the sample. She also participated in the extraction of the parameters and in the writing of the publication.

Publication II: Heavy Quark Parameters and V_{cb} from Spectral Moments in Semileptonic B Decays

M. Battaglia *et al.* with L. Salmi

Physics Letters B556 (2003) 41-49

The publication contains the first extraction of the heavy quark parameters in the kinetic mass scheme using experimental measurements of statistical moments of the lepton energy spectrum and the hadron mass spectrum. Today, most of the experimental measurements are interpreted using the kinetic mass scheme.

In addition to providing the measurement of the lepton energy spectrum, the author of this thesis participated in the development of the fitting algorithms used to extract the parameters.

Publication III: OPE parameter determinations from semileptonic B decays at DELPHI

L. Salmi on behalf of the DELPHI collaboration

Nuclear Physics B (Proceedings Supplement) 142 (2005) 167-172

The DELPHI measurement of the statistical moments of the lepton energy spectrum and the hadronic mass spectrum along with the extraction of heavy quark parameters is described in this conference contribution.

The author of this thesis was responsible for the lepton spectrum measurement and has written the publication.

Publication IV: A study of the Lepton Spectrum Moments in $B \to X_c \ell \bar{\nu}$ Decays with the DELPHI Detector at LEP

M. Battaglia, M. Calvi, L. Salmi

DELPHI-2002-071 CONF 605 (ICHEP '02)

This conference contribution describes the approach adapted by DELPHI for measuring the lepton energy spectrum and extracting the heavy quark parameters from the moments of the lepton energy spectrum and the hadronic mass spectrum. It is one of the first reports of the measurement of the moments of the lepton energy spectrum and the results have been also used by authors outside the DELPHI collaboration.

The author was responsible for the reconstruction of the B hadron decay and the reduction of background. She also participated in the writing of the article.

Publication V: Recent b physics results from DELPHI

L. Salmi on behalf of the DELPHI collaboration

Nuclear Physics B (Proceedings Supplement) 133 (2004) 133-136

This publication summarises the results of several analysis carried out by the DELPHI collaboration related to B hadrons: the measurement of the branching fraction to B_u^+ mesons, measurement of the b quark fragmentation function, the study of the production of orbitally excited B meson states, the determination of CKM matrix element $|V_{cb}|$ using exclusive $B \to D^* \ell \nu$ decays, the extraction of the heavy quark parameters from semileptonic B decays, the determination of Δm_d from $B_d^0 - \overline{B}_d^0$ oscillations and the search for $B_s^0 - \overline{B}_s^0$ oscillations.

The author of this thesis has written the publication and carried out, with four colleagues, the analysis that extracted the heavy quark parameters from semileptonic B decays.

Publication VI: A study of depletion of fragmentation particles at small angles in b-jets with the DELPHI detector at LEP

M. Battaglia, R. Orava and L. Salmi

DELPHI 2004-037 CONF 712 (ICHEP'04)

Perturbative QCD predicts that the radiation of soft gluons off an energetic heavy quark is suppressed at small emission angles (the dead cone effect). This leads to a depletion of fragmentation particles at small angles with respect to the direction of the heavy hadron in heavy quark jets. The paper describes an experimental study of the phenomenon performed using the DELPHI data. The angular distributions of fragmentation particles in c and b jets were compared, which provided the first experimental evidence of the dead cone effect.

The author of this thesis has performed the analysis and written the paper.

Publication VII: $t\bar{t}$ Cross-section and forward-backward asymmetry at CLIC

L. Salmi

Proceedings of International Workshop on Linear e^+e^- Colliders, Jeju, Korea, edited by J. S. Kang and S. K. Oh, Korean Physical Society (2003)

The publication describes the studies performed to estimate the accuracy with which the production cross-section and the forward-backward asymmetry of $t\bar{t}$ pairs could be measured at a linear collider with 3 TeV center-of-mass energy. The results have also been included in the report of the CLIC Physics Working Group, "Physics at the CLIC multi-TeV linear collider", CERN report CERN-2004-005

The author of this thesis has performed the analysis and written the article.

Chapter 1

Introduction

The physics of heavy quarks, the charm (c), bottom (b) and top (t) quarks, is currently one of the key areas of interest in high energy physics. At the moment, the heaviest quarks, the top quarks, are only produced at the TEVATRON facility in FERMILAB, USA, but in a few years they will also be studied at LHC at CERN. The bottom quarks are the main topic of study at the B factories BABAR at SLAC, USA and BELLE at KEK in Japan. The physics of the charm quarks and hadrons, although studied since 1973, is experiencing a new revival due to the start of a new experiment, CLEO-C, at Cornell, USA. In addition, an important amount of b and c decays were collected in the 1990s by the four LEP experiments at CERN, known as ALEPH, DELPHI, L3 and OPAL. The LEP data provide a complementary environment from the B factories for B physics studies, and many pioneering measurements have been performed based on the LEP data.

The main interest in heavy quark physics is measuring the parameters of the quark mixing matrix, the so-called Cabibbo-Kobayashi-Maskawa (CKM) matrix. The matrix is a powerful test of the Standard Model in the flavour sector, and huge effort is put into measuring the elements at an accuracy of a few percent. Reaching such an accuracy demands improvement both on the experimental and theoretical sides. The advances in heavy quark physics since 1990 have been tremendous. Experimentalists have benefited from the introduction of high resolution silicon vertex detectors that allow precise decay reconstruction. The B factories that started operation in 1999 have already collected and analysed over 150 million B decays each, with more to come.

The Heavy Quark Expansion (HQE) approach uses the quark mass as an expansion parameter. Important progress has been made by experimentally measuring the values of parameters needed to theoretically describe the decays of B hadrons. This reduces the theoretical uncertainty related to the extraction

of certain CKM matrix elements. The consistency of several measurements in different environments supports the theoretical description and assumptions therein. Of specific importance in the extraction of the parameters are the quark masses m_b and m_c, both of which are fundamental parameters of the Standard Model, and are highly correlated with the CKM matrix elements.

Voloshin [1] first suggested that the mass difference, $m_b - m_c$, could be extracted by measuring the first moments of the lepton energy spectrum. The proposal has been since expanded by a variety of authors to include the use of the moments of hadronic mass spectrum and photon energy in $B \to X_s\gamma$ decays in order to extract also other parameters of the expansion.

Publications I, II, III, and IV describe the progress of the DELPHI measurement of the lepton energy and hadronic mass moments and the extraction of the heavy quark parameters and $|V_{cb}|$. Publication IV describes the first results of the lepton energy spectrum measurement. It also contains the first extraction of the parameters by DELPHI. At the time, only other collaboration to have results on the lepton energy spectrum was CLEO. These preliminary results were then used in publication II, where the parameters were extracted using the kinetic mass scheme. This was the first time the kinetic mass scheme was used to interpret the moments in terms of the heavy quark parameters. Today, most collaborations interpret their results using the kinetic mass scheme. The results of publication IV were also used by other authors [2] in their extraction of heavy quark parameters in several mass schemes. Publication III describes the measurement in its nearly final form, and the final results, together with a description of the details of the measurement, are given in publication I.

Publication V summarises several CKM matrix related analyses performed by the DELPHI collaboration, including the determination of the heavy quark parameters using moments of the lepton energy spectrum and hadronic mass spectrum.

In addition to the CKM mixing matrix studies, the physics of heavy quarks is also a good testing ground for Quantum Chromo Dynamics. In the theoretical calculation, the large quark mass gives a natural cut-off scale, keeping the relevant phenomena away from the domain of strong coupling.

Publication VI describes the study of the angular distribution of fragmentation particles in b, c and light quark jets at DELPHI. The observed distributions are compared with the perturbative QCD prediction of the depletion of particles at small angles in heavy quark jets, known as the dead cone effect. This measurement provides the first direct experimental evidence of the effect.

The next generation of colliders after the hadron colliders TEVATRON and LHC will be linear colliders. At CERN, a concept for a 3 TeV linear collider, CLIC, has

been developed. Precision measurements of top quark pair production cross-section and forward-backward asymmetry will allow probing for new physics beyond the center-of-mass energy of the collider. Performance studies carried out at the early stage of the collider design help fully exploit the potential of the collider and to build optimal detectors.

Publication VII describes a simulation study of reconstruction of top quark decays at the CLIC collider in order to estimate the accuracy with which the top production cross-section and the forward-backward asymmetry could be measured, taking into account the expected main backgrounds.

The publications presented in this thesis represent three rather different topics: an extraction of parameters of the electroweak theory, a study of a phenomenon predicted by perturbative QCD, and a study of the possibility of observing physics beyond the Standard Model. In practise, the analyses themselves contain several common features. Most important are the two steps common to all of them: the reconstruction of the decay of the heavy quark and the selection of signal events. These two steps are crucial to the success of the analysis and for each of the analyses, a dedicated algorithm was developed. For practical reasons, they are described very concisely in the publications. Therefore, the decay reconstruction and the signal selection are discussed in detail in this thesis. For other details of the analyses, the reader is referred to the respective publications.

This thesis is organised as follows.

The first chapters give the background of the analyses, starting with an introduction to the Standard Model of particle physics, with emphasis on the CKM matrix and QCD (Chapter 2). It is followed by a description of the LEP accelerator and the DELPHI experiment (Chapter 3). Then, the evolution of $Z \to b\bar{b}$ events at LEP (Chapter 4) is described and models of B meson decays (Chapter 5) are discussed, including the Heavy Quark Expansion and its parameters. This is followed by a description of the top quark production at CLIC (Chapter 6) together with motivation for the cross-section and asymmetry measurements.

Then the methods developed for the decay reconstruction and the background reduction are described in Chapters 7 and 8, respectively.

The comparison of the results with those from other collaborations and the conclusions are given in Chapter 9. A brief summary is in Chapter 10.

Chapter 2

The Standard Model

The Standard Model is a quantum field theory that contains all the known fundamental particles and three of the four known interactions. It consists of the Glashow-Weinberg-Salam model of electromagnetic and weak interactions and of the Quantum Chromo Dynamics (QCD), which describes the strong interactions. Only gravity is not included in the Standard Model.

In this chapter, a brief introduction to the particles and interactions of the Standard Model is given, followed by a more detailed discussion on the quark mixing matrix and QCD. Comprehensive reviews of the Standard Model can be found in particle physics textbooks, such as [3].

2.1 Particles and interactions

There are two kinds of fundamental particles, quarks and leptons. They come in three families, each consisting of two quarks and two leptons. All stable matter is made of particles from the first family, the up and down quarks and the electrons. The other two families are copies of the first family, except that the particles are more massive and unstable. The quarks and leptons, with their charges and masses, are shown in Table 2.1.

The quarks come in three different colours. The strong force binds the quarks into colour-neutral hadrons, and no free quarks have been experimentally observed.

The interactions are mediated by gauge bosons. The electromagnetic interaction between charged particles is mediated by massless and neutral photons, γ. The weak interaction is carried by neutral Z^0 bosons with a mass $m_Z \approx 91.2$ GeV/c^2, and charged W^+ and W^- bosons, with a mass $m_W \approx$

Table 2.1: The fundamental fermions, their electric charges and masses as evaluated in Ref. [4]. The quark masses are given in the $\overline{\text{MS}}$ scheme, except for the t quark mass, for which the pole mass is given.

quark	charge (e)	mass (MeV/c^2)	lepton	charge (e)	mass (MeV/c^2)
up (u)	2/3	1.5 to 4	electron (e)	-1	0.511
down (d)	-1/3	4 to 8	e neutrino (ν_e)	0	$< 3 \cdot 10^{-6}$
charm (c)	2/3	1150 to 1350	muon (μ)	-1	106
strange (s)	-1/3	80 to 130	μ neutrino (ν_μ)	0	< 0.19
top (t)	2/3	172700 ± 2900	tau (τ)	-1	1777
bottom (b)	-1/3	4100 to 4400	τ neutrino (ν_τ)	0	< 18.2

80.4 GeV/c^2. The gluons that carry the strong force between quarks are massless, but carry a colour-anticolour charge. Due to this, also gluons interact strongly (self-interaction). The Higgs boson that would generate the masses of the weak gauge bosons is yet to be discovered.

The Standard Model has been remarkably successful and its predictions have been proved correct with remarkable precision. For example, electroweak observables were used to estimate the top quark mass m_t before the top quark was found. A determination by the DELPHI Collaboration in 1994 suggested $m_t = 157^{+36+19}_{-48-20}$ GeV/c^2 [5], consistent with the current average of direct measurements, $m_t = 172.7 \pm 2.9$ GeV/c^2 [6]. Current determination of the top quark mass through electroweak observables results in a top quark mass of $m_t = 178.1^{+10.4}_{-8.3}$ GeV/c^2 [4]. Today, using the top quark mass, the most probable range for the mass of the Higgs boson can be inferred.

The Standard Model contains 18 free parameters. They are

- the six quark masses and the three charged lepton masses,
- the two electroweak coupling constants g and g' and the strong coupling constant α_s,
- the three mixing angles and one complex phase in the quark flavour mixing matrix and
- the vacuum expectation value of the Higgs field and the Higgs boson mass (or the Higgs field self-coupling).

In the Standard Model the neutrinos are assumed to be massless. In the recent years observations of neutrino flavour change have provided compelling evidence that their mass is in fact non-zero. This increases the number of free parameters by seven: the three neutrino masses, and the three mixing angles and one complex phase of the lepton flavour mixing matrix.

2.2 The CKM matrix

The quark mass eigenstates are not eigenstates of the weak interaction. The weak eigenstates d', s', b' are connected to the mass eigenstates d, s, b via transformation matrix V^{CKM},

$$\begin{pmatrix} d' \\ s' \\ b' \end{pmatrix} = V^{\mathrm{CKM}} \begin{pmatrix} d \\ s \\ b \end{pmatrix} = \begin{pmatrix} V_{ud} & V_{us} & V_{ub} \\ V_{cd} & V_{cs} & V_{cb} \\ V_{td} & V_{ts} & V_{tb} \end{pmatrix} \begin{pmatrix} d \\ s \\ b \end{pmatrix}. \tag{2.1}$$

The matrix is known as the CKM matrix, after Cabibbo [7], Kobayashi and Maskawa [8]. The matrix contains three mixing angles, θ_{12}, θ_{13} and θ_{23}, and one complex phase δ_{13}. Because of the mixing angles, interactions between the quark families are possible, and the complex phase is responsible for all processes that violate combined charge conjugation and parity conservation (CP-violation) in the flavour sector.

$$V^{\mathrm{CKM}} = \begin{pmatrix} c_{12}c_{13} & s_{12}c_{13} & s_{13}e^{-i\delta_{13}} \\ -s_{12}c_{23} - c_{12}s_{23}s_{13}e^{i\delta_{13}} & c_{12}c_{23} - s_{12}s_{23}s_{13}e^{i\delta_{13}} & s_{23}c_{13} \\ s_{12}s_{23} - c_{12}s_{23}s_{13}e^{i\delta_{13}} & -c_{12}s_{23} - s_{12}c_{23}s_{13}e^{i\delta_{13}} & c_{23}c_{13} \end{pmatrix}, \tag{2.2}$$

where the shorthand notations $s_{ij} = \sin\theta_{ij}$ and $c_{ij} = \cos\theta_{ij}$ have been used. The widely used Wolfenstein parametrisation, valid to order λ^6, brings out the hierarchical structure of the matrix,

$$V^{\mathrm{CKM}} \approx \begin{pmatrix} 1 - \frac{1}{2}\lambda^2 & \lambda & A\lambda^3(\rho - i\eta + \frac{1}{2}\eta\lambda^2) \\ -\lambda & 1 - \frac{1}{2}\lambda^2 - i\eta A^2\lambda^4 & A\lambda^2(1 + i\eta\lambda^2) \\ A\lambda^3(1 - \rho - i\eta) & -A\lambda^2 & 1 \end{pmatrix}, \tag{2.3}$$

where $\lambda = \sin\theta_C = 0.2235 \pm 0.0033$ [4] is the so-called Cabibbo angle. The parameter $A \approx 0.82$ with an accuracy of about 5%, while ρ and the phase η are less well known. From Eq. (2.3) one can see that all diagonal elements are close to unity, while the off-diagonal elements are much smaller. The current

measured absolute values of the elements are, at a 90% confidence level, [4]

$$|V^{\rm CKM}| = \begin{pmatrix} 0.9739 \text{ to } 0.9751 & 0.221 \text{ to } 0.227 & 0.0029 \text{ to } 0.0045 \\ 0.221 \text{ to } 0.227 & 0.9730 \text{ to } 0.9744 & 0.039 \text{ to } 0.044 \\ 0.0048 \text{ to } 0.014 & 0.037 \text{ to } 0.43 & 0.9990 \text{ to } 0.9992 \end{pmatrix}, \quad (2.4)$$

where unitarity has been applied as a constraint.

The matrix has to be unitary, if weak interactions are described by a single SU(2) gauge theory, as in the Standard Model. The unitarity implies that

$$\sum_{l=1}^{3} (V_{il})^* V_{lj} = \delta_{ij}. \quad (2.5)$$

The cases $i \neq j$ can be expressed as triangles in the complex plane. The six triangles have very different shapes, but they all have the same area [9], which reflects the fact that there is a single irreducible complex phase for the three families. The most interesting of these triangles is known as the unitarity triangle (Figure 2.1), obtained from the third row and the third column. The sides of the triangle are of the same order of magnitude, which makes it especially sensitive to physics beyond the Standard Model. New physics would result in different measurements giving inconsistent values for the location of the apex of the triangle.

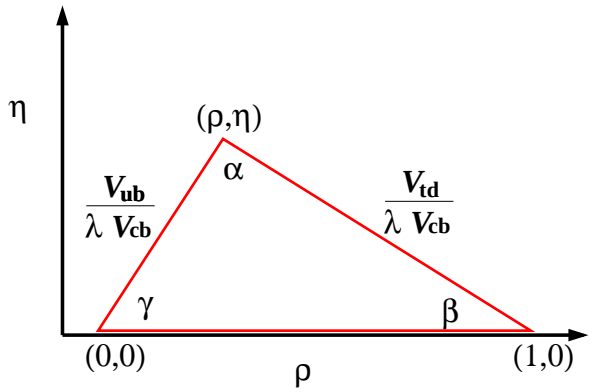

Figure 2.1: The unitarity triangle.

The triangle is scaled such that its base extends from $(0, 0)$ to $(1, 0)$ and its apex is at (ρ, η). The other two sides are proportional to $|V_{ub}|/|V_{cb}|$ and $|V_{td}|/|V_{cb}|$. The three angles are known as α, β and γ, or ϕ_1, ϕ_2 and ϕ_3.

The CKM matrix and the unitarity triangle are over-constrained. The sides of the triangles can be inferred from measurements of rates that are insensitive

to CP-violation. The angles are related to each other and they all depend on the phase δ_{13}.

Current knowledge on the location of the apex of the triangle is based on several very different measurements: V_{cb}, V_{ub}, ϵ from kaon decays, and $B^0 - \bar{B}^0$ oscillation for both B^0_d and B^0_s. The angles are measured directly using exclusive decay modes. The angle β is obtained, for example, from decays $B^0 \to J/\psi K_S$, the angle α using decays $B^0 \to \pi^+\pi^-$, $\pi^\pm\rho^\mp$, $\rho^+\rho^-$ and the angle γ from $B^+ \to \bar{D}^0 K^+$ and $B^+ \to D^0 K^+$. The measurements of α and γ require reconstruction and identification of rare B decays that are dominated by several orders of magnitude larger backgrounds.

Two complementary methods are used to measure V_{cb}. The inclusive method is based on the measurement of the semileptonic decay width of the b [10–18], which is related to V_{cb} through

$$\Gamma_{\rm sl} = \frac{G_F^2 m_b^5}{192\pi^3}|V_{cb}|^2\left\{z_0\left(1-\frac{\mu_\pi^2-\mu_G^2}{2m_b^2}\right)-2\left(1-\frac{m_c^2}{m_b^2}\right)^4\frac{\mu_G^2}{m_b^2}-\frac{2\alpha_S}{3\pi}z_0^{(1)}+\dots\right\}, \quad (2.6)$$

where G_F is the Fermi constant, m_b (m_c) is the mass of the b (c) quark, z_0 and $z_0^{(1)}$ are known parton phase space factors that depend on m_c^2/m_b^2, and μ_G^2 and μ_π^2 are Operator Product Expansion (OPE) parameters (for definition, see Chapter 5). An accurate determination of V_{cb} requires knowledge of the values of m_b, m_c, and OPE parameters μ_π, μ_G, and also ρ_D and ρ_{LS} that appear in the higher order terms (see Chapter 5). Alternatively, V_{cb} can be determined by using the exclusive reconstruction of $B \to D^*\ell\nu$ decays [19–24]. In this exclusive method the dominating uncertainty comes from the extrapolation of the form factor to zero recoil.

In a similar manner to the inclusive measurement of V_{cb}, the element V_{ub} can be obtained from inclusive measurement of $B \to X_u\ell\nu$ decays. The measurement is complicated by the dominating $B \to X_c\ell\nu$ decays that easily contaminate the sample. This can be overcome by either using only events where the lepton energy exceeds the largest kinematically allowed lepton energy in b decays to charm [25, 26], in which case the result depends on the modelling of the rate below the endpoint, or by detailed control over the background, as in [27–29].

The $B^0 - \bar{B}^0$ oscillation frequencies are related to the CKM elements via the mass difference between the eigenstates

$$\Delta m_{B_{d,s}} = \frac{G_F^2}{6\pi^2}\eta_B m_{B_{d,s}} m_W^2 S_0(x_t) f^2_{B_{d,s}} \mathrm{B}_{B_{d,s}} |V_{td,ts}V_{tb}^*|^2, \quad (2.7)$$

where η_B is a QCD parameter, $m_{B_{d,s}}$ is the mass of $B^0_{s,d}$, m_W is the W mass, $f_{B_{d,s}}$ is the $B_{s,d}$ decay constant, and $\mathrm{B}_{B_{d,s}}$ is the so called bag parameter of

the $B_{d,s}\bar{B}_{d,s}$ system. S_0 are the Inami-Lim functions [30] that depend on the squared mass ratio of the top (m_t) and charm (m_c) quark to W boson, $x_{t,c} = m_{t,c}^2/m_W^2$[1]. In the ratio

$$\frac{\Delta m_{B_s}}{\Delta m_{B_d}} = \frac{m_{B_s}}{m_{B_d}} \xi^2 \frac{|V_{ts}V_{tb}^*|^2}{|V_{td}V_{tb}^*|^2} \tag{2.8}$$

some uncertainties common to both measurements cancel each other out. The remaining constants are collected into the term ξ^2. While Δm_{B_d} has been measured [31–37], for the time being there exist only limits on Δm_{B_s} [38–42].

The parameters of the unitarity triangle can also be accessed in K decays. Mixing-induced CP violation in the $K^0\bar{K}^0$ system can be expressed by the parameter

$$\epsilon_K = \frac{\mathcal{A}(K_L \to (\pi\pi)_{I=0})}{\mathcal{A}(K_S \to (\pi\pi)_{I=0})}, \tag{2.9}$$

which is related to the unitarity triangle via [43]

$$|\epsilon_K| = CB_K\bar{\eta}|V_{cb}|^2\lambda^2\{[\eta_1 S_0(x_c) - \eta_3 S_0(x_c, x_t)] - |V_{cb}|^2(1-\bar{\rho})\eta_2 S_0(x_t)\}, \tag{2.10}$$

where shorthand notations $\bar{\rho} = \rho(1 - \lambda^2/2)$ and $\bar{\eta} = \eta(1 - \lambda^2/2)$ have been used. C is a constant and B_K denotes the bag factor of the $K^0\bar{K}^0$ system. η_1, η_2 and η_3 are QCD parameters.

The angle β (ϕ_1) can be measured by studying the asymmetry of time-dependent rates for B^0 and $\overline{B}^0$ decays to a common CP eigenstate f_{CP},

$$A(t) = \frac{\Gamma(\overline{B}^0(t) \to f_{\mathrm{CP}}) - \Gamma(B^0(t) \to f_{\mathrm{CP}})}{\Gamma(\overline{B}^0(t) \to f_{\mathrm{CP}}) + \Gamma(B^0(t) \to f_{\mathrm{CP}})} = -\eta_f \sin 2\beta \sin \Delta m_{B_d} t, \tag{2.11}$$

where η_f is the CP eigenvalue of f_{CP}. The following final states f_{CP} are usually studied: $J/\psi K_L^0$, $\psi(2S)K_S^0$, $\chi_{c1}K_S^0$, $\eta_c K_S^0$ and $J/\psi K_S^0$ [44, 45].

The angle α (ϕ_2) can be extracted from $B^0 \to \pi\pi$, $B^0 \to \rho\rho$ or $B^0 \to \pi\rho$. The theoretical uncertainty in the extraction using $B^0 \to \rho^+\rho^-$ is relatively small, which is why it allows the most accurate determination of the angle. The asymmetry of decay rates R

$$A = \frac{R(\Delta t) - \overline{R}(\Delta t)}{R(\Delta t) + \overline{R}(\Delta t)} = S \sin \Delta m_{B_d} \Delta t - C \cos \Delta m_{B_d} \Delta t \tag{2.12}$$

contains parameters S and C that depend on the angle α. The $B^0 \to \rho^+\rho^-$ decays are rare and the asymmetry analysis is not very straightforward; therefore the accuracy of some of the recent measurements is remarkable [46, 47]. Determinations of the angle α using the other decays also exist.

[1] $S_0(x_t) = \frac{4x_t - 11x_t^2 + x_t^3}{4(1-x_t)^2}$, $S_0(x_c) = x_c$, $S_o(x_c, x_t) = x_c\big(\ln\frac{x_t}{x_c} - \frac{3x_t}{4(1-x_t)} - \frac{3x_t^2 \ln x_t}{4(1-x_t)^2}\big)$

The angle γ (ϕ_3) is considered to be the most difficult to measure, due to the smallness of the interference terms that provide the sensitivity to γ combined with experimental challenges.

2.3 Quantum Chromo Dynamics

QCD is the theory describing the strong force that binds the quarks and gluons into hadrons, such as the proton. The gauge bosons of QCD are the gluons. Both quarks and gluons carry colour quantum numbers. Since the gluons are coloured, they interact strongly with each other, which makes the behaviour of the strong force radically different from the other three fundamental forces of nature. The quarks are always bound into colour-neutral objects, hadrons, made either of three quarks, or of a quark and an anti-quark.

In high energy reactions, the quark and gluon constituents of hadrons act as quasi-free particles, partons. Such reactions can therefore be factorised into two parts, the process-independent structure functions that describe the distribution of partons in the hadron, and process-dependent cross-sections calculated as a perturbative expansion in terms of the strong coupling constant α_S.

Interesting descriptions of the developement of QCD are presented in Refs. [48] and [49].

The QCD Lagrangian for n quarks with masses m_i and four-component Dirac spinors q_i is

$$\mathcal{L}_{\mathrm{QCD}} = -\frac{1}{4}F^A_{\mu\nu}F^{\mu\nu}_A + \sum_i^n \bar{q}^a_i(i\not{D} - m_i)_{ab}q^b_i - \frac{1}{2\lambda}(\partial^\mu A^A_\mu)^2, \tag{2.13}$$

where A^A_μ are coloured vector fields and $F^A_{\mu\nu}$ is the non-Abelian field-strength tensor,

$$F^A_{\mu\nu} = \partial_\mu A^A_\nu - \partial_\nu A^A_\mu - 2\sqrt{\alpha_S\pi}f^{ABC}A^B_\mu A^C_\nu \tag{2.14}$$

and

$$\not{D} = \gamma^\mu(D_\mu)_{ab} = \gamma^\mu(\delta_{ab}\partial_\mu + 2i\sqrt{\alpha_S\pi}\sum_A \frac{\lambda^A_{a,b}}{2}A^A_\mu). \tag{2.15}$$

f^{ABC} are the structure constants and λ the generators of the SU(3) algebra.

The Lagrangian contains seven parameters: the six quark masses and the strong coupling constant α_S. The third term in Eq. (2.14) will lead to the gluon self-interactions through three and four-point vertices.

Two important features of QCD, asymptotic freedom and confinement, are explained by the anti-screening by the gluons. A red quark, for example, is surrounded by polarised vacuum oriented such that the anti-red colour charge is closest to the quark, just like an electric charge is surrounded by electrically polarised vacuum. In contrast to the case of the electric charge, the quark can emit gluons, which change the colour charge of the quark. After the emission of a red-anti-green gluon, for example, the colour of the quark is green.

The quark is therefore surrounded by a cloud of emitted gluons. When the colour charge of the quark is measured with a long distance (or low-energy) probe, the full charge is measured. With a short-distance, high-energy probe, a smaller colour charge is observed. Therefore, at high energies, the coupling α_S is small, and perturbative calculations are well-behaved, leading to asymptotic freedom. At low energies α_S is close to unity, and perturbative treatment is no longer justified. The coupling constant α_S is said to run, and the expression for the running can be obtained by renormalisation, giving [50, 51], to first order,

$$\alpha_S(Q^2) = \frac{\alpha_S(\mu^2)}{1 + \frac{\alpha_S(\mu^2)}{12\pi}(33 - 2N_f)\log(Q^2/\mu^2)}, \tag{2.16}$$

where μ is the renormalisation scale and Q the scale where the value of α_S is needed.

Similarly, the colour cloud restricts the measurement of the quark mass. While the mass of a lepton can be unambiguously defined, the same cannot be done with quarks. The colour cloud leads to a running (i.e. scale-dependent) quark masses. Again, renormalisation can be used to find an expression for the quark masses, at leading order

$$m(\mu^2) = M[\alpha_S(\mu^2)]^{\frac{1}{\pi\beta_0}}, \tag{2.17}$$

where M is a constant independent of the renormalisation method, and

$$\beta_0 = \frac{11C_A - 4T_R N_f}{12\pi} = \frac{33 - 2N_f}{12\pi}, \tag{2.18}$$

where N_f is the number of flavours with masses below the scale μ, and $C_A = 3$ and $T_R = 1/2$. According to Eq. (2.18), the quarks appear to be lighter when they are probed at scales larger than their mass.

Chapter 3

LEP and DELPHI

The Large Electron Positron collider (LEP) was a circular accelerator with a 27 km circumference that collided electrons and positrons. It was situated near the border of France and Switzerland, in the vicinity of Geneva, and was operated by the European Organization for Nuclear Research, CERN. The electrons and positrons had equal but opposite momenta, and the collisions took place at zero angle. During the first phase of LEP operation, from the start-up in 1989 until 1995, the center-of-mass energy of the collisions was chosen to be close to the Z boson mass 91.2 GeV. The second phase, known as LEP2, saw the energy increase up to 209 GeV. First the energy was increased above the W boson pair production threshold of 161 GeV in order to study the properties of the W boson. Further energy increases were motivated by the search for new particles, such as the Higgs boson and possible supersymmetric particles. Despite pushing the collider to its limits and beyond, no new particles were found. In 2000 the accelerator was shut down and dismantling was started to prepare for the next large accelerator at CERN, LHC.

The electron and positron beams were made to collide at four interaction points around the accelerator. Each of these collision points was surrounded by a massive general-purpose experiment, known as DELPHI, ALEPH, L3 and OPAL.

The data used in the analyses described in this thesis was collected by the DELPHI experiment, mainly in 1994 and 1995. The data consist of approximately two million Z^0 boson decays. Data from 1992 and 1993 is used only to obtain large enough sample of c quark jets in the dead cone analysis. The data from these two years include about 1.5 million Z^0 events.

The DELPHI detector (Figure 3.1) consisted of several layers nearly covering the full solid angle. It was made of a cylindrical barrel-part and two end-caps. In

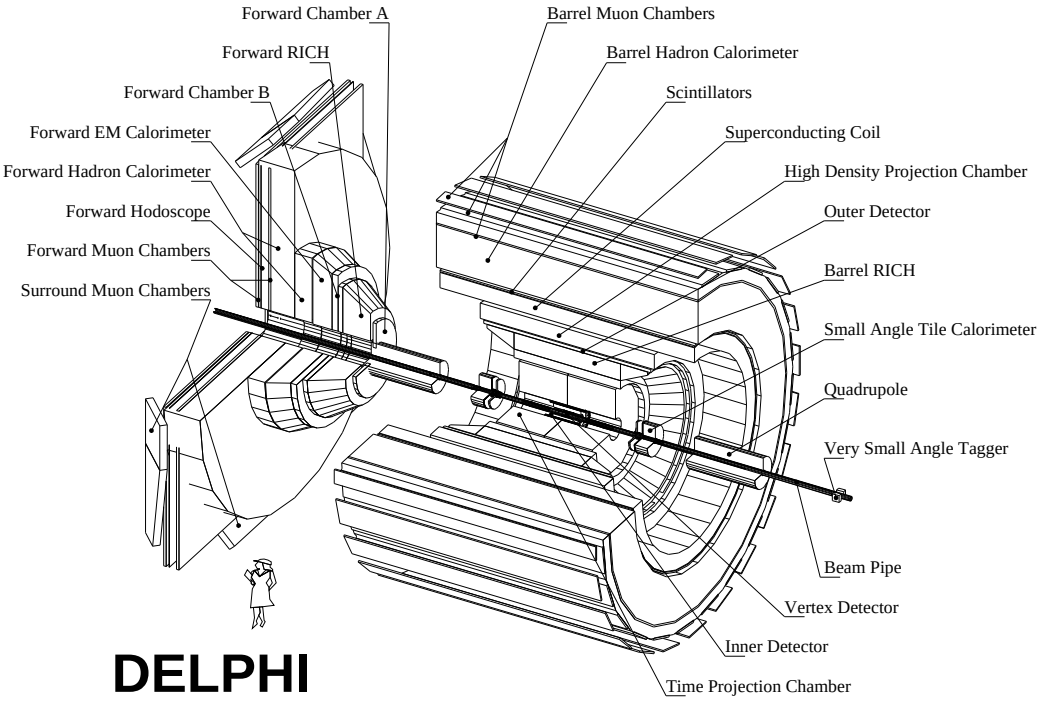

Figure 3.1: Schematic layout of the DELPHI detector.

the barrel part, the innermost detectors, the Vertex Detector (VD), the Inner Detector (ID), the Time Projection Chamber (TPC) and the Outer Detector (OD) were mainly used for the reconstruction of the particle trajectories. The Ring Imaging Cherenkov detector (RICH) was used for hadron identification and the High Density Projection Chamber (HPC) for electron and photon identification as well as for energy measurement. Both tracking and particle identification were aided by the 1.2 T magnetic field provided by the superconducting solenoid magnet. Outside the magnet were the Hadron Calorimeter (HCAL) and the Muon Chambers (MUC). The structure was similar in the end-caps. The coordinate system of DELPHI was chosen such that the z axis was along the electron direction, the x axis pointed towards the centre of LEP and the y axis upwards. The azimuthal angle, ϕ, and the radial coordinate, R, were defined in the $x-y$ plane, and the polar angle, θ, in $R-z$ plane.

The detector and its performance are described in detail elsewhere [52, 53]. Only the aspects most crucial to the analyses described in this thesis, the

Vertex Detector and lepton identification, will be discussed here.

VD is essential for the reconstruction of the decay vertices of heavy particles, such as the B and D mesons, that fly in average a few millimetres before decaying. A detector with a high spatial resolution, placed as close to the interaction point as possible enables the extrapolation of the particle trajectories back to the region close to the interaction point. This allows the determination as to whether a particle originated from the interaction point or from a secondary decay point displaced from the interaction point.

VD underwent several upgrades during the operation of LEP. The first version in 1990 had only two layers, then in 1991 another layer was added closest to the interaction point when the beam pipe radius was reduced. In 1994, the innermost and outermost layers were equipped with double-sided detectors to allow a measurement in both the $R\phi$ and Rz planes. The VD configuration in 1994 and 1995 is illustrated in Figure 3.2. In 1996, the length of VD was extended to increase the coverage in the forward direction. The addition of the double-sided layers improved the performance of the detector significantly, and explains the different quality of the data taken in 1994 and 1995 compared to 1992 and 1993.

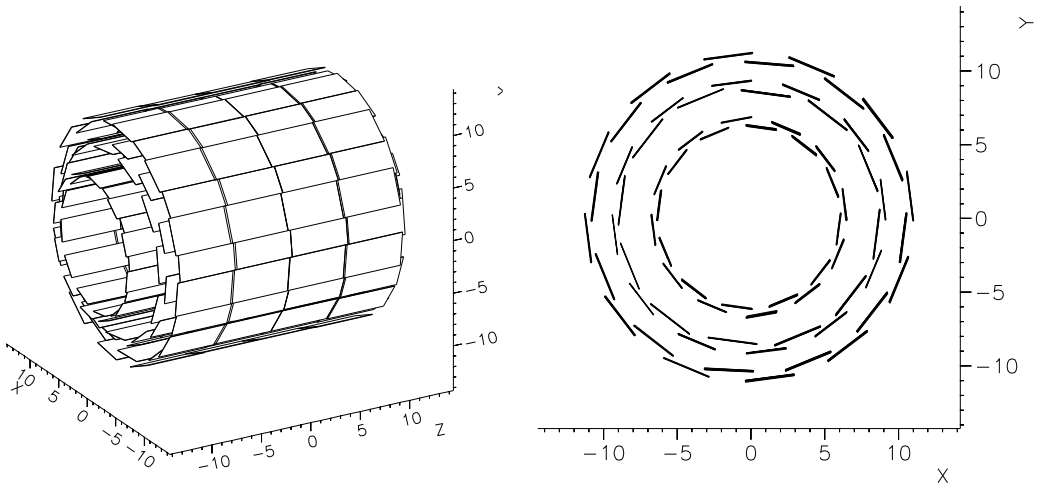

Figure 3.2: The layout of the DELPHI Vertex Detector in 1994-1995, viewed from the side (left) and from the beam direction (right), from [54].

The VD consisted of three cylindrical layers of silicon strip detectors that surrounded the beam pipe centred on the interaction point. The layers had radii of 6.3, 9.0 and 10.9 cm. Particles with polar angles in the range $44° < \theta <$

136° traversed all three layers. The first and third layer had strips orthogonal to each other on the opposite sides of the detector wafer, allowing measurements to be obtained both in the ϕ and z directions. In the ϕ direction, the position precision is 7 μm. In the z direction, the accuracy depends on the incidence angle of the particle. At best, when the track is perpendicular to the detector, the precision is 9 μm. The impact parameter resolutions in the $R\phi$ and Rz planes are in average of the order of 70 μm and 80 μm respectively, of which the latter depends more strongly on the momentum of the particle [55].

Lepton identification in this case refers to the identification of muons and electrons. The neutral leptons, neutrinos, are observed only indirectly through missing energy and momentum, and the tau leptons are too short-lived and only their decay products are seen. Only particles with sufficient energy are considered. Typically a momentum greater than 3 GeV/c is required.

The muon identification is based on the muon chambers (MUC). The majority of hadrons are stopped by HCAL, and only muons with momenta above 2 GeV/c penetrate MUC. There remains some residual activity from hadronic tracks in MUC, which requires further discrimination. The particle trajectories reconstructed in the central detector are extrapolated through the solenoid and HCAL, taking into account the magnetic return field in the region. The extrapolated tracks are compared with the hits in MUC, and the track is identified as a muon if the χ^2 value of the fit of the hits with the extrapolated track is good. Regions with poor geometrical acceptance are excluded by requiring that the polar angle, θ_μ, of the muon satisfies $0.03 < |\cos\theta_\mu| < 0.62$ or $0.68 < |\cos\theta_\mu| < 0.95$. This way, the muon identification efficiency is estimated to be 0.82 ± 0.01, with a hadron mis-identification probability of $(0.52 \pm 0.03)\%$ in the barrel and $(0.36 \pm 0.06)\%$ in the forward region.

The electron identification is based on a neural network [56] that uses information from HPC, TPC and the RICH detectors. Particle trajectories in the region of HPC with high acceptance ($0.03 < |\cos\theta_e| < 0.72$) are first extrapolated to HPC and then associated to detected showers. In order to maintain a constant selection efficiency (65%) over the full momentum range, a momentum-dependent cut is applied. The cut was defined using a sample of simulated electrons from b and c decays. The mis-identification probability of hadrons has been evaluated to be $(0.40 \pm 0.02)\%$. This electron identification procedure was designed specifically for studies of semileptonic B decays [10]. An alternative identification is available for cases when the identification efficiency may depend on the electron momentum [53].

Chapter 4

B hadrons at LEP

The bottom quark (b) is the heaviest quark produced at LEP. The lowest-order Feynman diagram for the production process is shown in Figure 4.1. The electron and positron annihilate to produce a Z^0 boson, which subsequently decays into a b anti-b ($\bar{b}$) pair. The branching fraction for this decay is about 15% [57–61].

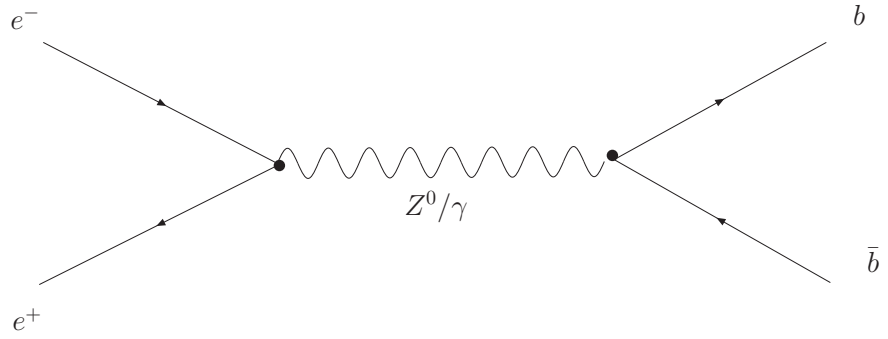

Figure 4.1: The lowest-order Feynman diagram for $b\bar{b}$ production at LEP.

The evolution of an event is depicted in Figure 4.2. The two energetic quarks fly in opposite directions. As the distance between the quarks increases, the strength of the colour field between them also increases. Due to the force exerted by the colour field, the quarks emit bremsstrahlung, soft gluons. The gluons then split into quark anti-quark pairs. This phase is governed by perturbative QCD.

The next phase is known as hadronisation. The quarks form colour-neutral hadrons, either mesons made of one quark and one anti-quark, or baryons,

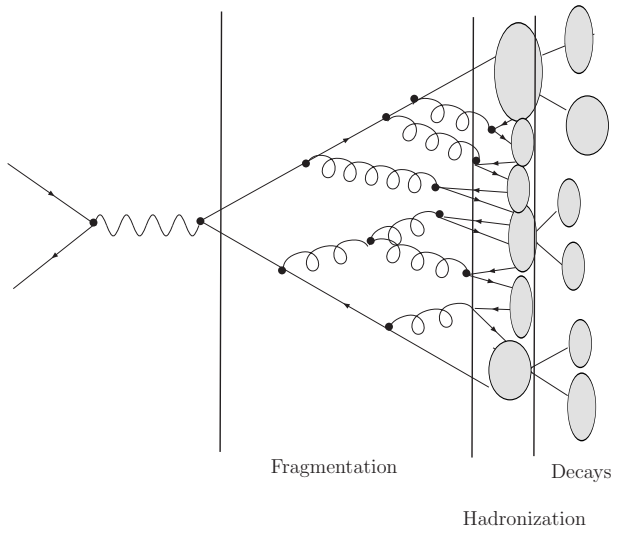

Figure 4.2: A schematic drawing of the different phases of a hadronic event.

made of three quarks or three anti-quarks. In the majority of cases, a meson is produced. At LEP, in about 10% of the cases the b quark ends up bound into a baryon [4].

At the last stage of the evolution, the short-lived hadrons decay into photons, leptons and longer-lived hadrons.

The perturbative phase, the hadronisation process and the decays of hadrons are described in more detail in the following sections.

4.1 Gluon emission off energetic quarks

The energy spectrum of the quarks after gluon radiation has been studied both experimentally and theoretically. The experimental studies concentrate on trying to extract the shape of the quark energy spectrum just before hadronisation [62]. On the theoretical side, phenomenological models describing the quark energy spectrum have been introduced [63–67] and detailed calculations of the gluon emission spectrum have been performed [68]. In the case of energetic heavy quarks, the gluon emission results in a so-called dead cone effect.

The gluon energy distribution with respect to the quark energy can be derived from the improved first order gluon emission probability [68], including the finite quark mass and the running coupling effects. The calculation yields

two characteristics momentum scales related to the maximum and minimum momentum loss of the quark. The gluon energy distribution contains an integration over the variable t, which is related to the transverse momentum of the radiation, $t = x \cdot k_\perp^2$. Here, x is the scaled quark energy $x = 2E_Q/W$, where W denotes the center-of-mass energy of the heavy quark pair and E_Q the energy of the heavy quark, and the transverse gluon momentum $k_\perp \approx \omega_g \theta$, where ω_g is the gluon energy. Lower limit for t can be obtained from the requirement that it must be larger than the minimim momentum loss, $t \geq \kappa^2$, with $\kappa^2 \approx m_Q^2(1-x)^2/x$ [68]. The inequality becomes

$$t = \frac{2E_Q}{W}(\omega_g \theta)^2 \geq \kappa^2 = m_Q^2(1-x)^2/x = m_Q^2 \left(\frac{2\omega_g}{W}\right)^2 \frac{W}{2E_Q}, \tag{4.1}$$

and after simplification,

$$\theta \geq m_Q/E_Q \equiv \Theta_0. \tag{4.2}$$

The angle Θ_0 is the minimum angle of gluon emission.

The radiation pattern of the primary soft gluon with energy ω from a massive relativistic quark with energy $E_Q \gg m_Q$ and small emission angle $\Theta \ll 1$, is thus given by [69]

$$d\sigma_{Q\to Q+g} = \frac{\alpha_S}{\pi} C_F \frac{\Theta^2 d\Theta^2}{(\Theta^2 + \Theta_0^2)^2} \frac{d\omega}{\omega}. \tag{4.3}$$

The minimum angle for gluon emission, Θ_0, creates a cone around the energetic heavy quark where no gluons are expected. This cone is known as the dead cone.

This phenomenon is characteristic for bremsstrahlung off a massive particle. It reflects the conservation of the projection of the total angular momentum on the heavy quark momentum. Soft radiation cannot change the quark helicity and forward emission is forbidden.

At larger emission angles, $\Theta \approx 1$, the emission becomes insensitive to the quark mass m_Q and appears to be identical to the gluon emission off a light quark,

$$d\sigma_{q\to q+g} = \frac{\alpha_s}{\pi} C_F \frac{d\Theta^2}{\Theta^2} \frac{d\omega}{\omega}. \tag{4.4}$$

The dead cone will not be filled by gluons from further branchings of the emitted gluon. The colour coherence inside jets gives rise to a phenomenon known as angular ordering [70]. The permitted decaying angle between two quarks produced in gluon conversion, or the angle between the parent gluon and a secondary gluon emitted by it, is restricted to be smaller than the original

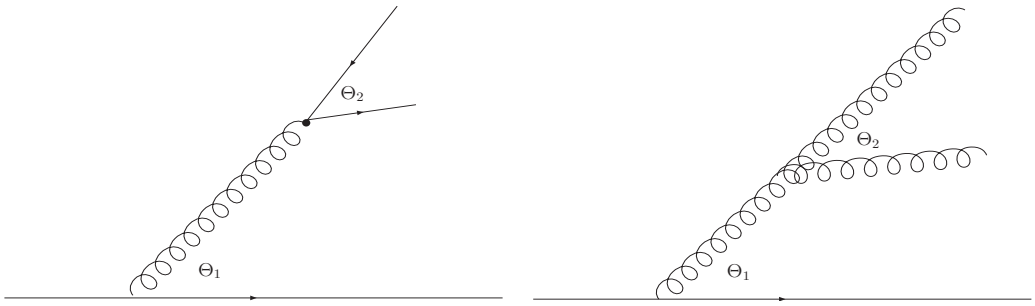

Figure 4.3: Illustration of angular ordering in case of gluon conversion to a quark-antiquark pair (left) or gluon emitting secondary gluons (right). In both cases $\Theta_1 > \Theta_2$.

gluon emission angle Θ (Figure 4.3). After a few successive branchings, the permitted emission angle has shrunk to very small values.

According to the hypothesis of local parton-hadron duality, the hadrons from the emitted gluons will follow the angular distribution of the gluons; consequently, the particles observed in the final state will exhibit a depletion of particles in the direction of the original heavy quark.

In addition to the relatively depopulated cone around the heavy quark, the minimum angle of gluon emission has other important consequences [71].

First of all, the minimum angle restricts the emission of energetic gluons with relatively small transverse momenta, which is normally where the radiation is most intense. Due to this, a heavy quark is expected to retain a larger fraction of its energy than lighter quarks do. This can be seen in the distributions of fractional energy, or fragmentation functions, of heavy and light quarks: the most probable energy of the hadron formed by the b quark is about 75% of the beam energy, while for the lighter c quarks, it is about 45% and for the light quarks (u, d, s), the mean energy of the corresponding hadron is only about 35% of the beam energy. This is illustrated in Figure 4.4, where the distributions of fractional energy are shown.

A second consequence is that the multiplicity of light hadrons from the gluon radiation accompanying the heavy quark is less than in a light quark jet. The multiplicity difference between heavy and light quark jets depends solely on the heavy quark mass and does not, for example, depend on the quark energy. This has been experimentally confirmed by DELPHI, where the multiplicity difference was measured at a number of different energies. It was observed to be constant and independent of the energy, while naive models predict the difference to decrease with increasing quark energy [72, 73].

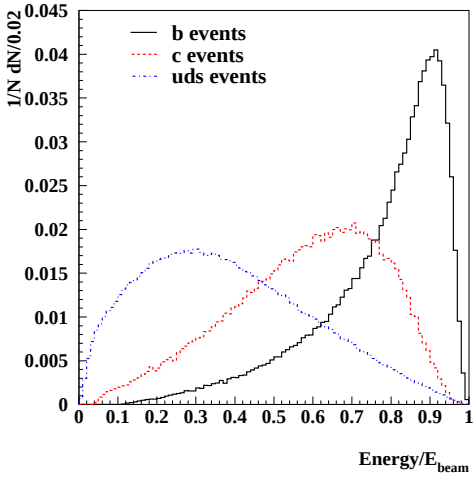

Figure 4.4: The distributions of fractional energy for b, c and u, d, s quarks. The heavier the quark is, the larger fraction of the available energy it retains. The distributions are obtained from simulation adjusted to reproduce the DELPHI data.

As a third consequence, the energy spectrum of the accompanying light hadrons is affected, showing a depletion at comparatively large momentum fractions compared to light quark jets.

The parton shower phase terminates when the partons have lost energy to the extent that their dynamics are no longer described by perturbative QCD, and non-perturbative effects become important.

4.2 Hadronisation

Hadronisation is the process where the partons are converted into the observed hadrons. Non-perturbative effects dominate hadronisation and at present only models for hadronisation exist.

The models are based on the hypothesis of local parton-hadron duality, where one supposes that the flow of momentum and quantum numbers at the hadron level tend to follow the flow at the parton level [74]. Therefore, for example, the depletion of gluons at small angles with respect to the primary heavy quark is expected to be reproduced as a depletion of hadrons with respect to the hadron containing the primary heavy quark.

The two most widely used models are string fragmentation and cluster fragmentation.

1. String fragmentation
   The string fragmentation scheme considers the colour field between the quarks and gluons to be the fragmenting entity rather than the partons themselves. The string can be viewed as a colour flux tube formed by gluon self-interaction as two coloured partons move apart. This idea was first introduced by X. Artru and G. Mennessier [75], and the most popular string fragmentation model is the so-called Lund model [76].

   Emitted energetic gluons are regarded as kinks on the string that carries energy and momentum. When the stored energy in the string is sufficient, a $q\bar{q}$ pair may be created from the vacuum. Thus, the string breaks up repeatedly into colour singlet systems as long as the invariant mass of the pieces of string exceeds the mass of a hadron. Due to the dependence on the parton mass and hadron mass, the production of strange and heavy quark hadrons is suppressed. The PYTHIA event generator [77, 78] uses the string fragmentation model.

2. Cluster fragmentation
   The cluster fragmentation model is based on the idea of preconfinement [79]. The gluons remaining at the end of the parton shower evolution are split into quark-antiquark pairs. Then, colour singlet clusters with masses of the order of a couple of GeV are formed. These clusters are made to decay directly into hadrons, except if they are too heavy or too light. Overly heavy clusters are forced to decay into two clusters, and too light clusters decay into a single hadron. The decay of a cluster into two hadrons is assumed to be isotropic in the rest frame of the cluster. A decay channel is chosen based on the phase-space probability, the density of states, and the spin degeneracy of the hadrons. Cluster fragmentation has a compact description with only a few parameters, due to the phase-space dominance in the formation of hadrons. The HERWIG event generator [80] is the most widely used event generator based on cluster fragmentation.

Both models give a good overall description of data.

The production fractions of different b hadron species can only be studied at LEP or at TEVATRON at FERMILAB. The so-called B-factories that have the largest samples of B decays produce only the lightest states, B^0 (B_d) and B^+ (B_u), because they are operated at a center-of-mass energy that is not sufficient for the production of heavier states.

In Figure 4.5, a schematic picture of the B hadron production process is shown. The estimated production rates are indicated both for the primary mesons and for the weakly decaying mesons. The rates have been taken from PYTHIA simulation tuned to best reproduce the event shape and charged particle inclusive distributions as well as identified particle data recorded by DELPHI [81]. The decay processes of the primary mesons into the weakly decaying mesons are discussed in Section 4.3.

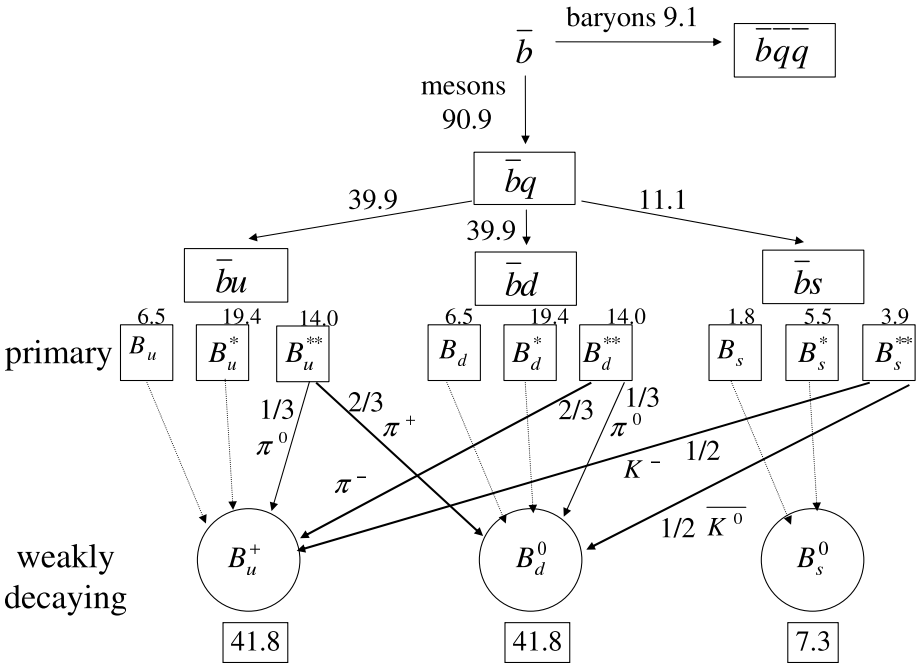

Figure 4.5: Schematic picture of the production of B mesons, adapted from Ref. [82]. The rates are given in percentage terms and are taken from the simulation. The electromagnetic decays (γ emission) are denoted by dotted arrows and strong decays (π, K emission) by solid arrows. The dashed lines indicate cases where no decays take place. B_u^+, B_d^0 and B_s^0 decay weakly.

In about 91% of cases a B meson, formed of a (anti-)b quark and a lighter quark, is produced, while in the remaining 9% of cases, a b-baryon consisting of a b quark and two lighter quarks is produced. The probability of having a $\overline{b}u$ or $\overline{b}d$ meson is equal, while heavier $\overline{b}s$ mesons are produced with a probability that is smaller by nearly a factor of four. Recently production of heavy and rare B_c ($\overline{b}c$) state has been confirmed by the CDF collaboration [83].

B baryons are produced in only about 9% of cases, and 90% of the baryons produced consist of a b quark and u or d quarks, while the remaining baryons contain a b quark, s quark and either a u or a d quark.

The fraction of $\bar{b}$-quarks fragmenting into positively charged weakly decaying B hadrons has been measured by DELPHI to be $f^+ = 0.4209 \pm 0.0082 \pm 0.0098$, and the production rate of $\overline{b}u$ mesons, obtained by removing the contribution due to positively charged B baryons, was measured to be $f_{\overline{b}u} = 0.4099 \pm 0.0082 \pm 0.0111$ [82]. Fragmentation fractions have also been measured by other collaborations [84–88].

A large proportion of the hadrons produced are in an excited state. The first excited meson states are usually denoted by B^* and the heavier states by B^{**}. The production of the exited states has been studied in detail by the DELPHI collaboration [89, 90] and other collaborations [91–96].

4.3 B decays

None of the B hadrons are stable. The exited states are very short-lived and they decay instantly. The lightest states, B_u^+, B_d^0, B_s^0 and the baryon Λ_b, can only decay through the weak interaction and therefore have longer lifetimes.

The B^* states decay through the electromagnetic interaction by photon emission. This decay does not change the quark content of the meson.

The B^{**} states decay through strong interaction. The B_u^{**} and B_d^{**} can decay by emitting either a charged or a neutral pion, for example $B_d^{**} \to \pi^- B_u^+$. Emission of a neutral pion does not change the quark content of the meson, but charged pion emission changes the flavour of the quark accompanying the heavy quark from u to d or vice versa. The B_s^{**} decay by emitting a charged ($B_s^{**} \to K^- B_u^+$) or neutral ($B_s^{**} \to K^0 B_d^0$) kaon.

The B^0 and B^+ mesons decay by flavour-changing weak interactions. Since the b quark is much heavier than its partner quark, the B decay can be described as the decay of the b quark (spectator model). The dominant decay mode of a b quark is $b \to cW^*$, where the virtual W^* decays either to a pair of leptons (semileptonic decay) or a pair of quarks that subsequently hadronise (hadronic decay). The heavy c quark produced in the decay will then take the place of the b quark in the heavy meson, producing a D meson, often in an excited D^* or D^{**} state. The D meson will then further decay to lighter mesons.

An alternative to the $b \to cW^*$ is the Cabibbo-suppressed decay $b \to uW^*$. There are also other decay modes, such as $b \to s\gamma$, which occur even more rarely, since they only take place through higher order diagrams.

Many data analyses use samples consisting of only semileptonic B decays, where the lepton is either an electron or a muon, for several reasons. First of all, the semileptonic decays are easier to treat theoretically than the hadronic ones. In the final state of a semileptonic decay there are strong interactions only between the spectator quark and the c or u quark produced in the b quark decay, while in hadronic decays, the quarks from the W^* decay also need to be taken into account. Secondly, the decays are easy to identify experimentally due to the energetic lepton produced in the decay. In addition, reasonable statistics are available due to the large value of the semileptonic branching ratio, $\Gamma_{\rm sl}/\Gamma_{\rm tot} = 0.21$ [4,10,12–18], where $\Gamma_{\rm sl}$ is the semileptonic decay width and $\Gamma_{\rm tot}$ is the total decay width of the B. The fourth advantage is that the inclusive or exclusive reconstruction of the charm hadron decay vertex is facilitated by the absence of hadrons from the B decay. On the other hand, hadronic decays allow the study of several effects related to strong interactions.

In the study of semileptonic decays, there is a sizable contamination from events where the lepton is produced by some other process than the weak B meson decay, and these events appear as background in the study of the semileptonic decays.

The most important background source are semileptonic decays of D mesons. The semileptonic decay width of the D meson is 0.20 [4], therefore often the hadronic decay of a B meson will be followed by a semileptonic decay of the D meson. This background is known as cascade background. In addition, in about 9.3% [97–99] of the hadronic events, the virtual W^* decays into a charmed meson ($b \to cW^*$, $W^* \to \bar{c}s$). The sign of this charm quark is opposite to the charm quark produced directly in the b decay, which is why this background is known as wrong sign charm.

Due to the lower mass of the D mesons compared with the B mesons, there is less phase space available in the decay; hence the lepton cannot have as much energy in the rest frame of the decaying D meson as in the case of B meson decays. This is often used to reduce the background originating from charm decays in the semileptonic B decay sample. The selection removes a whole kinematical region from the analysis, however, which in some cases can be a significant drawback. If the event sample is very large, one can also choose to use only events with two leptons, with minimum energy requirement for one of the leptons, which gives very good control of the cascade background.

Leptons can also be produced in other decays. Sometimes hadrons are misidentified as leptons.

Chapter 5

Heavy Meson Decay Models

Heavy mesons are comparable to hydrogen atoms: they can be thought to consist of a heavy quark, around which the lighter quark circulates. The first approximation to a theoretical description of the meson decay is naturally to view it as a weak decay of a free heavy quark. The strong interaction effects between the heavy quark and the spectator quark are significant, and therefore this approximation is not accurate enough for most purposes.

Better descriptions of heavy meson decay are needed, since the favoured methods for measuring the CKM matrix elements $|V_{cb}|$ and $|V_{ub}|$ use inclusive distributions in semileptonic heavy flavour decays. In order to extract the matrix elements from data, the strong interaction effects need to be disentangled from the weak decay.

The first approach to describe the meson decay was the ACCMM model [100] that treats the decay as a free-quark decay, to which the effect of the motion of the heavy quark inside the heavy meson is included. The ISGW model takes into account the mass spectrum of the charmed hadrons produced in the B meson decay and is based on the summation of different exclusive channels [101]. The most recent approaches are based on Operator Product Expansion (OPE) [102] applied to effective heavy quark theory and heavy quark expansion.

5.1 The ACCMM model

The ACCMM model, named after Altarelli, Cabibbo, Corbò, Maiani and Martinelli [100], was one of the first models to describe decays of B hadrons and to attempt to predict the shape of the lepton energy spectrum in semileptonic B meson decays. The idea was to describe the meson decay as a semileptonic

b-quark decay with corrections due to QCD and from the bound-state structure of the B meson. This had already been applied to charm mesons [103] resulting in a good description of the data.

An important concept first introduced in Ref. [103], and further developed in Ref. [100], is to treat the effects due to the bound-state structure of the hadron by attributing Fermi motion to the heavy quark within the heavy meson with mass M_B. The spectator antiquark is treated as a particle of definite mass, $m_{\rm sp}$ and momentum, p, while the heavy quark is treated as a virtual particle of invariant mass W,

$$W^2 = M_B^2 + m_{\rm sp}^2 - 2M_B\sqrt{p^2 + m_{\rm sp}^2}. \tag{5.1}$$

The spectator momentum is assumed to have a Gaussian distribution with an adjustable parameter P_F,

$$\phi(|p|) = \frac{4}{\sqrt{\pi}P_F^3}\exp\left(-\frac{|p|^2}{P_F^2}\right). \tag{5.2}$$

The spectrum of the lepton energy, E, is then obtained from folding $\phi(|p|)$ with the decay of a quark of effective mass, W, as

$$\frac{d\Gamma_B}{dE} = \int_0^{p_{\rm max}} \phi(|p|)p^2dp\frac{d\Gamma_q}{dE}(W,p,E). \tag{5.3}$$

The limit of integration, $p_{\rm max}$, is the maximum allowed value of $|p|$, and $d\Gamma_q/dE$ is the energy spectrum of the leptons from the decay of a quark of mass W. The distribution $d\Gamma_q/dE$ can be found in Ref. [100].

Denoting $\epsilon = m/m_Q$, where m_Q is the heavy quark mass and m is the mass of the quark produced in the decay, and defining the shorthand notation

$$x = \frac{2E_\ell}{M_Q} \leq 1 - \epsilon^2 \equiv x_M, \tag{5.4}$$

the lepton energy distribution is given by

$$\frac{d\Gamma}{dx} = \frac{d\Gamma^{(0)}}{dx}\left(1 - \frac{2}{3}\frac{\alpha_s}{\pi}G(x,\epsilon)\right). \tag{5.5}$$

For the decay $b \to c$,

$$\frac{d\Gamma^{(0)}}{dx} = \frac{G^2M_Q^5}{96\pi^3}x^2\frac{(x_M - x)^2}{(1-x)^3}[(1-x)(3-2x) + (1-x_M)(3-x)], \tag{5.6}$$

and

$$G(x,\epsilon) \underset{x\to x_M}{\sim} \frac{1}{x_M} 2\ln(x_M - x)[2x_M + (2-x_M)\ln(1-x_M)]. \tag{5.7}$$

The model was able to predict the branching ratios and absolute rates of semileptonic B decays with reasonable accuracy, considering the experimental data available at the time of the construction of the model. Attempts to measure the value of P_F, however, gave inconsistent and even unphysical results [104]. The *ad hoc* nature of the parameters has also been criticised [105]. When the results of the ACCMM model are compared with the lepton spectrum obtained using operator product expansion in terms of the mass of the heavy quark, the results are remarkably similar to the ACCMM results, after the latter have been scaled with a normalisation factor.

5.2 ISGW model

The ISGW model [101], after its authors Isgur, Scora, Grinstein and Wise, concentrates on the end-point region of the lepton energy spectrum. The ACCMM model did not predict the shape and normalisation of the lepton energy spectrum correctly near the upper edge of the kinematically allowed region. This is due to the almost discrete masses of the low-mass hadronic states whose production populates the end-point region. The ISGW model takes this into account by summation over the spectra generated by the exclusive decay channels.

In the ISGW model, the differential decay rate for the decay $\bar{B}^0 \to X_q^+ e\bar{\nu}_e$, with m_X being the mass of the hadronic system X_q, is

$$\begin{aligned}\frac{d^2\Gamma}{dx\,dy} &= |V_{qb}|^2 \frac{G_F^2 m_B^5}{32\pi^3} \times \\ &\left(\frac{\alpha}{m_B^2} y + 2\beta_{++}\left[2x(1 - \frac{m_X^2}{m_B^2} + y) - 4x^2 - y\right] - \gamma y(1 - \frac{m_X^2}{m_B^2} - 4x + y)\right),\end{aligned} \tag{5.8}$$

where $x = E_\ell/m_B$ and $y = (p_B - p_X)^2/m_B^2$. The expressions for α, β_{++} and γ are given in Ref. [101].

The model gives rather accurate predictions for the end-point region that is populated by the production of only the two lightest charm meson states, D and D^*. In order to extract the full spectrum, the contributions from the broader D^{**} are needed, which complicates the calculation.

5.3 Heavy Quark Expansion

The most developed theoretical description of heavy meson decays combines Operator Product Expansion [102] with Heavy Quark Effective Theory [106, 107].

The strong interactions affect the free-quark decay model in two ways: Firstly, corrections related to gluon radiation and exchange, calculated in terms of α_S, can be treated using perturbative QCD. The one-loop corrections, of order α_S, to some differential distributions were calculated already 20 years ago [100, 108–112], and to the total width in 1989 [113]. The $\mathcal{O}(\alpha_S^2\beta_0)$ corrections (the BLM [114] corrections) to the total width have been known for ten years [115, 116].The BLM corrections to order $\mathcal{O}(\alpha_S^n\beta_0^{n-1})$ have also been calculated [117]. Secondly, non-perturbative corrections related to the bound state dynamics of the meson and hadronisation after the decay require performing an expansion in terms of inverse powers of the heavy quark mass, m_Q. The OPE is used to describe these corrections. The corrections are not as well known as the radiative corrections and they contain parameters whose values need to be determined experimentally.

The QCD Lagrangian has the form

$$\mathcal{L}_{\mathrm{QCD}} = -\frac{1}{4g_s^2}(G^a_{\mu\nu})^2 + \sum_q \bar{q}(i\not{D} - m_q)q, \tag{5.9}$$

where $G^a_{\mu\nu}$ is the gluon field strength tensor and $G_{\mu\nu} = t^a G^a_{\mu\nu}$ is its matrix representation, and the gauge-fixing term has been left out. The sum extends over all the quarks q. All the operators are defined at a specified normalisation point, μ, and all couplings are functions of μ. In an effective theory describing the low-energy properties of heavy hadrons, the normalisation point μ must be below the mass of the heavy quark m_Q. This changes the generic form of the Lagrangian and a series of operators of higher dimension appear, whose coefficients contain inverse powers of m_Q. These effective operators need to be Lorentz scalars. To order $1/m_Q^2$ the Lagrangian becomes [118]

$$\begin{aligned}\mathcal{L} = &-\frac{1}{4g_s^2}(G^a_{\mu\nu})^2 + \bar{Q}(i\not{D} - m_Q)Q + \sum_q \bar{q}(i\not{D} - m_q)q + \frac{c_G}{4m_Q}\bar{Q}i\sigma_{\mu\nu}G_{\mu\nu}Q \\ &+ \sum_q \frac{f_q}{m_Q^2} m_q \bar{q} i\sigma_{\mu\nu}G_{\mu\nu}q + \sum_{\Gamma,q}\frac{d^{(\Gamma)}_{Qq}}{m_Q^2}\bar{Q}\Gamma Q\bar{q}\Gamma q + \sum_{\Gamma,q,q'}\frac{d^{(\Gamma)}_{qq'}}{m_Q^2}\bar{q}\Gamma q\bar{q}'\Gamma q' \\ &+ \frac{h}{m_Q^2}\mathrm{Tr}(G_{\mu\nu}G_{\nu\rho}G_{\rho\mu}) + \mathcal{O}(1/m_Q^3),\end{aligned} \tag{5.10}$$

where Γ are four-fermion operators and Q is the heavy quark field. All masses, couplings and the coefficients of higher dimension operators depend on the renormalisation scale.

The leading contribution to the meson decay width, corresponding to the free-quark decay, is obtained from the term $\bar{Q}m_Q Q$ of the Lagrangian, given by an effective operator of the form

$$\hat{\Gamma}_0 = \frac{G_F^2}{192\pi^3} N_c |V^{\mathrm{CKM}}|^2 m_Q^5 \bar{Q}Q, \tag{5.11}$$

where N_c is the number of colours and V^{CKM} the CKM matrix element related to the decay.

There cannot be terms that are of the order of $1/m_Q$, since they can only arise from dimension four operators. Such an operator is either a total derivative, which has to vanish due to equations of motion, or a scalar that can be absorbed in an overall constant of Eq. (5.11).

The first non-leading operators in the expansion are therefore of dimension five. One of them is the chromomagnetic dipole operator for the heavy quark Q:

$$D_G = \bar{Q} i\sigma_{\mu\nu} \hat{G}_{\mu\nu} Q, \tag{5.12}$$

where the gluonic field strength tensor $\hat{G}_{\mu\nu} = \frac{1}{2} g G^a_{\mu\nu} \lambda^a$, and $\sigma^{\mu\nu} = \frac{1}{2}(\gamma^\mu\gamma^\nu - \gamma^\nu\gamma^\mu)$. The expectation value

$$\frac{1}{2M_{H_Q}} \left\langle H_Q | \bar{Q} \frac{i}{2} \sigma_{\mu\nu} G^{\mu\nu} Q | H_Q \right\rangle \equiv \mu_G^2 \tag{5.13}$$

defines the parameter μ_G^2, when H_Q denotes the heavy hadron. In an alternative parametrisation, where the expansion is performed in terms of the heavy quark pole mass instead of the running mass utilised here, the corresponding parameter is denoted by λ_2, with approximately $\mu_G^2 = 3\lambda_2$. The value of μ_G^2 can be determined from the mass difference of B and B^* mesons.

The other dimension five operator is related to the kinetic energy of the heavy quark inside the heavy hadron. The operator is

$$O_\pi = -\bar{Q}\vec{D}^2 Q = \bar{Q}\vec{\pi}^2 Q, \tag{5.14}$$

where $\vec{\pi} = -i\vec{D}$ is the covariant momentum operator for the heavy quark, with the expectation value

$$\frac{1}{2M_{H_Q}} \left\langle H_Q | \bar{Q}\vec{\pi}^2 Q | H_Q \right\rangle \equiv \mu_\pi^2. \tag{5.15}$$

Physically μ_π^2 corresponds to the average squared spacial momentum of the heavy quark inside the heavy hadron. In the pole mass scheme μ_π^2 is known as $-\lambda_1$.

The relevant dimension six operators are the Darwin term $\rho_{\rm D}^3$ and the spin-orbit term $\rho_{\rm LS}^3$ [119],

$$\rho_{\rm D}^3 \equiv \frac{1}{2M_{H_Q}}\big\langle H_Q|\bar{Q}\big(-\frac{1}{2}\vec{D}\cdot\vec{E}\big)\big)Q|H_Q\big\rangle \tag{5.16}$$

and

$$\rho_{\rm LS}^3 \equiv \frac{1}{2M_{H_Q}}\big\langle H_Q|\bar{Q}(\vec{\sigma}\cdot\vec{E}\times i\vec{D})Q|H_Q\big\rangle, \tag{5.17}$$

where $\vec{E}$ denotes the background chromoelectric field.

To summarise, there are no corrections to the free quark decay model that are of order $1/m_b$. The non-perturbative corrections of order $1/m_b^2$ are flavour independent and affect the heavy meson decays in a uniform way independent of the flavour of the light antiquark. The $1/m_b^3$ corrections do also depend on the flavour, and generate differences in the lifetimes and semileptonic branching ratios between heavy hadrons. The semileptonic width is given by [119]

$$\Gamma_{\rm sl}(b\to c) = \hat{\Gamma}_0(1+A_{\rm ew})A^{\rm pert}(r,\mu)\bigg(z_0(r)+\frac{\Gamma_2}{m_b^2}+\frac{\Gamma_3}{m_b^3}+\mathcal{O}(1/m_b^4)\bigg), \tag{5.18}$$

with

$$\Gamma_2 = \frac{z_0(r)}{2}(\mu_\pi^2-\mu_G^2)-4(1-r)^4\mu_G^2 \tag{5.19}$$

and

$$\Gamma_3 = \bigg(\frac{z_0(r)}{2}+2(1-r)^4\bigg)(\rho_D^3+\rho_{\rm LS}^3)+d(r)\rho_D^3. \tag{5.20}$$

All the parameters m_b, μ_π^2, μ_G^2, ρ_D^3 and $\rho_{\rm LS}^3$ depend on the normalisation scale μ. The mass ration is given by $r = m_c^2/m_b^2$. The electroweak correction $1+A_{\rm ew}\approx 1.014$ and for $\sqrt{r}=0.25$ and $\mu = 1$ GeV the perturbative contributions $A^{\rm pert}\approx 0.908$. The phase space factor $z_o(r)$ is given by

$$z_0(r) = 1-8r+8r^3-r^4-12r^2\ln r \tag{5.21}$$

and

$$d(r) = 8\ln r+\frac{34}{3}-\frac{32}{3}r-8r^2+\frac{32}{3}r^3-\frac{10}{3}r^4. \tag{5.22}$$

The lepton energy spectrum calculated using this approach contains singular terms at the end-point of the spectrum. The chromomagnetic interaction

effectively shifts the spectrum by changing the energy of either the initial or the final state, and the motion of the b quark inside the heavy hadron Doppler shifts the spectrum [120]. The expression contains a δ function and its derivatives. The observable spectrum and the expression obtained from heavy quark expansion can only be compared outside a finite neighbourhood of the end-point region or by integrating over the spectrum. This is why experimental studies of the lepton spectrum measure the statistical moments of the spectrum rather that just the shape of it.

The first three statistical moments of the lepton energy spectrum in $b \to c$ transitions are defined as

$$\begin{aligned} M_1^{\ell} &= < E_{\ell}^{*} > \\ M_2^{\prime\ell} &= < (E_{\ell}^{*} - < E_{\ell}^{*} >)^2 > \\ M_3^{\prime\ell} &= < (E_{\ell}^{*} - < E_{\ell}^{*} >)^3 >, \end{aligned} \tag{5.23}$$

where $< E_{\ell}^{*} >$ denotes the mean value of the lepton energy distribution in the rest frame of theB. The moments of the hadron mass distribution can be defined either with respect to the spin-averaged D meson mass $m_{\rm spin} = 1.97375$ GeV/c^2,

$$M_n^H = < (m_H^2 - m_{\rm spin}^2)^n > \tag{5.24}$$

or with respect to the mean value of hadronic mass squared,

$$M_n^{\prime\ell} = < (m_H^2 - < m_H^2 >)^n > . \tag{5.25}$$

The moments can be expressed in terms of the parameters μ_G^2, μ_π^2, ρ_D^3 and ρ_{LS}^3 and the quark masses m_b and m_c. The values of these parameters can then be determined by measuring several of these moments. They also provide a useful testing ground for OPE [121]. At lowest order in OPE (the free quark model) the final hadronic state has fixed invariant mass $s_H = m_q^2$, and therefore moments of $(s_H - m_q^2)$ directly probe the physics beyond the free quark model. Similarly, the maximum hadron energy is $(m_b^2 + m_q^2)/2m_b$, and the region above this endpoint is populated only by gluon bremsstrahlung and non-perturbative effects.

The LEP experiments, like DELPHI, are well-suited for the measurement of these moments. The amount of data does not match that available at B-factories, but the high energy of the B mesons produced allows the performance of the measurement using the full spectrum of the lepton energy in the rest frame of the decaying B. The high energy does, of course, introduce other complications to the event reconstruction, but they are more straightforward to solve than accounting for the degradation of the reliability of the theoretical descriptions, and even biases, brought about by not being able to use a significant part of the lepton energy spectrum [122, 123].

Chapter 6

Top quark production at CLIC

In electron-positron colliders the colliding particles are basic constituents of matter and therefore the full center-of-mass energy is available for the physics process. In hadron colliders the constituents of the hadrons collide. The quarks and gluons have only a fraction of the total energy, and therefore the center-of-mass energy of the interaction is lower than the center-of-mass energy of the hadrons and it varies from one interaction to the other. In circular accelerators, the energy losses of electron and positron beams due to synchrotron radiation become intolerable at energies larger than those reached at LEP, and future electron-positron colliders are therefore foreseen to be linear.

At the moment, the technology exists to build a 500-1000 GeV linear electron-positron collider, known as the International Linear Collider, or ILC, to complement the existing proton-antiproton collider TEVATRON and the proton-proton collider LHC that is being prepared for operation. It is expected that new particles will be found at LHC. If their masses are above 1 TeV, they cannot be studied in detail at ILC, but instead a higher-energy electron-positron collider will be needed.

The CLIC collider is a linear collider concept for center-of-mass energies of 3 TeV [124] and beyond being developed at CERN. Despite its higher center-of-mass energy, the length of the accelerator would be about the same as that of ILC. In addition to allowing the study of high-mass particles found elsewhere, it would open a new frontier for even higher energies and the possible unforeseen physics phenomena.

The CLIC accelerator design contains several new concepts. One of the most interesting features is that the acceleration will be provided by a secondary particle beam travelling parallel to the primary beam. When the primary beam has absorbed most of the energy of the secondary beam, the secondary beam is

replaced with a new one. This enables much larger acceleration gradients than achieved with more conventional methods, and despite the much larger center-of-mass energy, the length of the CLIC accelerator would be approximately the same as that of the ILC, about 35 km. The other dimensions of CLIC would also be very compact, the radius of the beam pipe would be just a few centimetres and the dimensions of the magnets of the order of 20 cm. The small size gave CLIC its full name, Compact Linear Collider.

It is important to perform physics studies already at an early stage of the design of the accelerator. The studies help define the optimal center-of-mass energy for the collider and possibly add insight into the merits of different scenarios for the accelerator performance[1]. The studies also help in understanding the requirements for the detectors to be used in the experiments. Most importantly, the studies help illustrate the physics possibilities offered by the collider. The study of the top quark production cross-section and forward-backward asymmetry serves these purposes.

Currently, the top quarks are produced and studied only at the TEVATRON collider at FERMILAB, and after the 2007 start-up of LHC at CERN even more of them will be produced. By the time CLIC could start operation, around 2020, the properties of the top quark, such as its mass and decay fractions, will be known to a high accuracy. There may also be additional information about physics beyond the Standard Model. The Higgs boson should have been found by then, and perhaps also supersymmetric particles have been found at LHC.

There are extensions to the Standard Model, such as the E_6 inspired models [125–130] and the left-right symmetric models [131, 132] that contain extra gauge bosons Z'. For a review of these models, see Ref. [133].

The masses of Z' bosons may be in the energy region reachable with CLIC, but they may just as well be considerably heavier. In the latter case, they can still be observed indirectly. There would be mixing between the Z^0 and the Z', which affects the cross-sections and production asymmetries of fermions. The expressions for cross-sections and asymmetries depend on which model is being studied. By precision measurements of the cross-section and asymmetries of the fermion production, Z' bosons with masses above 10 TeV could be observed with a 3 TeV collider through observing values that deviate from the expected Standard Model values.

[1]In the case of CLIC, there are two different luminosity scenarios, one with a higher luminosity ($\mathcal{L} = 10 \cdot 10^{34}$ cm^{-2}s^{-1}) but with a larger spread of the center-of-mass energy, and another with a lower luminosity ($\mathcal{L} = 8 \cdot 10^{34}$ cm^{-2}s^{-1}) but with a center-of-mass energy with a smaller spread [124].

The Standard Model production process of quark-antiquark pairs is the same as in lower energies, $e^+e^- \to Z/\gamma \to q\bar{q}$. The extensions with additional gauge bosons would also add $e^+e^- \to Z' \to q\bar{q}$, changing the cross-section, and the interference would affect the forward-backward asymmetry.

Simulation studies with the PYTHIA event generator were performed to estimate the accuracy with which the top quark pair production cross-section and the forward-backward asymmetry could be measured, taking into account the $\gamma\gamma \to$ hadrons events accompanying the electron-positron collisions and the realistic beam energy distributions, as described in [124]. Only the dominating background, W^+W^- production, was considered. The accuracy of the cross-section measurement was estimated based on the efficiency of $t\bar{t}$ event identification. To estimate the accuracy of the forward-backward measurement, the charge of the top quark was determined based on the charge of the charged lepton produced in the top decay. Combining these results with similar studies for bottom quarks and muons, it has been shown that after four years of CLIC running at the design luminosity the existence of a 30 TeV Z' boson could be established [134].

The lifetime of the top quark is short, 10^{-24} s [4], and it decays as a free quark, not having time to form a hadron. The dominant decay mode of the top quark is $t \to W^+b$. The W can then decay either to leptons, $e^+\bar{\nu}_e$, $\mu^+\bar{\nu}_\mu$ or $\tau^+\bar{\nu}_\tau$, or to quarks, $u\bar{d}$ or $c\bar{s}$. Thus the signature of an event with $t\bar{t}$ pair is two b-tagged jets accompanied by either four non-b jets, or two jets, a lepton and missing energy, or two leptons and missing energy. The invariant mass of a b jet combined with the appropriate non-b jets should be close to the top quark mass.

Chapter 7

Decay reconstruction

Depending on the purpose, the decay vertex of a heavy quark can be reconstructed with varying accuracy and complexity.

The simplest reconstruction is used in the study of top quark production at CLIC (publication VII). In this case, the main purpose is to identify events in which a top quark has been created, and thus only the mass of the decaying object is of interest. The most accurate decay reconstruction is required in the study of the lepton energy spectrum (publications I-IV), where the energy and momentum of the decaying B meson need to be reconstructed with a very high accuracy, since any uncertainty on the decay vertex will directly affect the accuracy of the determination of the lepton energy in the rest frame of the B. The reconstruction algorithm described here corresponds to the final version of publication I, and the one used in, for example, publication IV is somewhat simpler, even though the approach is the same.

In this chapter, the three reconstruction methods are described, starting with the simplest one used in the top quark analysis for CLIC, followed by the B decay vertex reconstruction used to separate B decay products from fragmentation particles in the DELPHI dead cone analysis (publication VI) and finally the detailed reconstruction needed to measure the lepton energy spectrum at DELPHI.

7.1 Top identification

In order to measure the $t\bar{t}$ production cross-section at 3 TeV center-of-mass energy at CLIC (publication VII), the events need to be identified. This can be done by reconstruction of the two top quark decays in the event.

According to the Standard Model, the top quark decays in nearly all cases to a b quark and a W boson. The W can then decay either to leptons (a charged lepton and the corresponding anti-neutrino) or to hadrons (a quark and an anti-quark). Since the top quarks are produced in pairs in e^+e^- collisions, the events can be either fully leptonic (10%), fully hadronic (46%), or semileptonic (44%), where one of the W bosons decays into leptons and the other into hadrons.

The reconstruction starts by counting the number of energetic leptons ($E_\ell > 50$ GeV) identified in the event. If none are found, the event is assumed to be fully hadronic. If there is one lepton, the event is assumed to be semileptonic, and if there are two or more leptons, the event is presumed to be a fully leptonic event. The lepton is required to be energetic, since leptons with lower energies are also produced in semileptonic decays of the b and c quarks.

If the event is classified as fully leptonic, no further analysis is performed. The fully leptonic events consist of two energetic charged leptons and two b jets, while the neutrinos remain undetected. The top decays cannot be satisfactorily reconstructed in this case due to the large amount of missing energy.

If the event is fully hadronic, the particles in the event are clustered into exactly six jets using the JADE algorithm [135]. These six jets correspond to

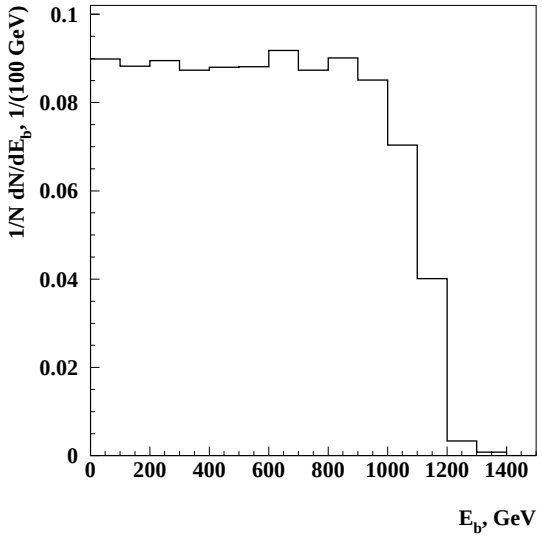

Figure 7.1: The energy distribution of the b quarks produced from top quark decays at $\sqrt{s} = 3$ TeV in $e^+e^- \to t\bar{t}$ events according to PYTHIA Monte Carlo.

the two b jets from the two top quark decays and two non-b jets from the decay of each of the W bosons. If the event is semileptonic, four jets are required, corresponding to the two b jets and two non-b jets from the hadronic decay of one of the W bosons.

The b jets are identified using b-tagging. Based on a previous study [136], it is assumed that b jets are correctly identified with a 85% efficiency and the rates to falsely identify c jets and light quark jets as b jets are 30% and 10%, respectively.

Optimally, the reconstruction would combine two non-b-tagged jets with one b-tagged jet. In practice, the jet reconstruction does not always resolve the jets correctly. The b jets can have very low energies despite the large center-of-mass energy (Figure 7.1) and can therefore be combined with one of the more energetic jets from the W, while the other jet from W decay is split in two or a gluon-initiated jet forming the sixth jet in the event. In addition, the angle between the two jets from the W decay is typically small (Figure 7.2) and these jets are easily merged together.

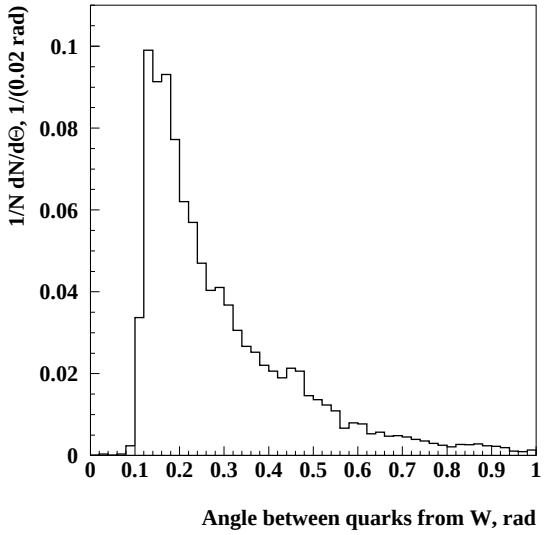

Figure 7.2: The angle between the two quarks from decays of a W boson produced in top quark decay in $e^+e^- \to t\bar{t}$ events at $\sqrt{s} = 3$ TeV.

The possible problems in the jet reconstruction are accounted for by considering any combination of one b-tagged jet and between one and three non-b-tagged jets, and looking for the combination that gives an invariant mass

closest to the nominal top quark mass. Among the non-b-tagged jets, a combination giving an invariant mass close to the W boson mass is searched for.

The combination that minimises the mass difference with respect to the nominal top and W masses m_t and m_W

$$D = |m_t^{\mathrm{rec}} - m_t| + |m_W^{\mathrm{rec}} - m_W| \tag{7.1}$$

is selected as the top candidate of the event. In fully hadronic events, the masses of the two top candidates are considered simultaneously. Each jet is allowed to be included only in one of the reconstructed top quarks.

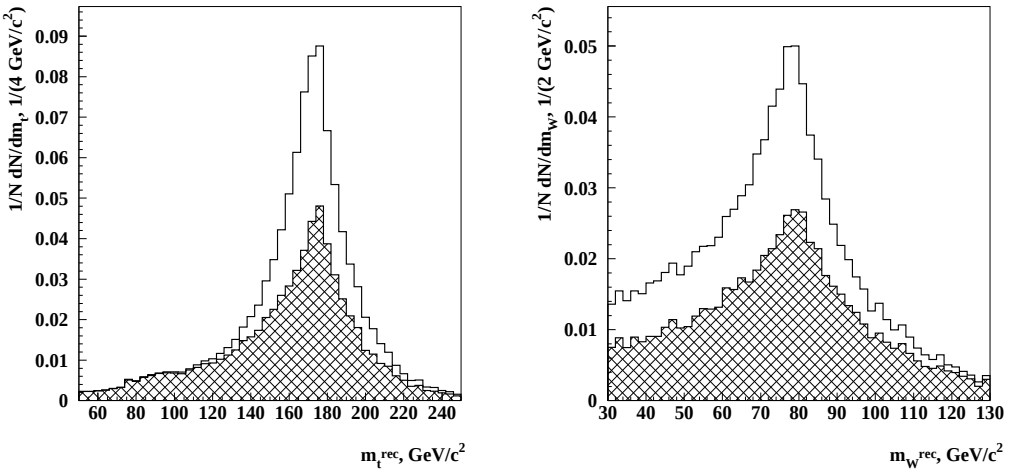

Figure 7.3: The reconstructed mass for the top quark candidates that minimise the mass difference D (left). The reconstructed mass of the W candidates (right). The shaded area represents events that do not contain top quarks, mainly from the process $e^+e^- \to W^+W^-$.

The mass distributions of the top candidates and of the W candidates are shown in Figure 7.3.

7.2 Simple B decay reconstruction

In the dead cone analysis (publication VI) studying the angular distribution of fragmentation particles in events at DELPHI containing heavy quarks, the vertex reconstruction is performed in order to separate the fragmentation particles from those originating from the heavy meson decay.

First the event is divided into two hemispheres with a plane perpendicular to the thrus axis[1]. One of the hemispheres is randomly seleced to be used in the analysis, and only particles in that hemisphere are considered.

Only charged particles that were detected in the silicon vertex detector are used. The momentum is required to be greater than 0.5 GeV/c. For each particle, impact parameter significance (IPS) is defined. The impact parameter is the distance of closest approach between the particle trajectory and the primary vertex, and IPS is obtained by dividing the absolute value of the impact parameter with the uncertainty on the measured value. For particles with impact parameter defined both in the $R-\phi$ and the $R-z$ plane, the one with larger IPS is used.

An iterative procedure starts with the particle with the largest momentum and the particle with the largest IPS. If the particle with the largest IPS is also the most energetic particle, the particle with the second largest IPS is used. First, a common vertex of the two particle trajectories is calculated. The common vertex of the two particles is required to satisfy

1. The invariant mass of the particles in vertex $m_{\rm vtx} < 5.5$ GeV/$c^2 \approx m_B$.
2. The distance of the vertex from the main vertex of the event $L < 2$ cm and $L/\Delta L > 2.9$.
3. The vertex fit $\chi^2 < 3.0$, or, when adding further particles to the vertex, the change in the fit χ^2 satisfies $\Delta\chi^2 < 3.0$.

All the selected particles are iteratively tested for inclusion in the vertex in the order determined by IPS. The particles are included in the vertex if after their addition the vertex satisfies the above criteria. When a new particle is included in the vertex, the vertex parameters are updated. When no further particles can be added to the vertex without violating the criteria listed above the first stage of the iteration is ended.

If the vertex of the two particles does not satisfy the above criteria, the particle with the largest IPS is replaced with the particle with the second largest IPS.

[1]The thrust, T, of the event is defined as

$$T = \max \frac{\sum_i |\vec{p}_i \cdot \vec{n}|}{\sum_i |\vec{p}_i|},$$

in which $\vec{p}_i$ are the particle momenta and $\vec{n}$ is an arbitrary unit vector. The $\vec{n}$ that maximises the expression defines the thrust axis.

If no two-particle vertex containing the most energetic particle is found, a vertex using the particles with the largest and second largest IPS are used to start the reconstruction.

After the first stage, the reconstruction is continued by considering all charged particles in the hemisphere with a momentum above 0.5 GeV/c. For each remaining particle, the χ^2 values of fits to the main vertex of the event and to the reconstructed secondary vertex are evaluated. Of the particles that have a smaller χ^2 with respect to the secondary vertex than to the main vertex, the one with the lowest χ^2 is included in the secondary vertex, if this new vertex satisfies the criteria above. Then, the χ^2 values for all the remaining charged particles are re-evaluated, and again the one with the lowest χ^2 is included in the secondary vertex. This is continued until all the remaining particles either are more compatible with the main vertex of the event or do not satisfy the criteria to be included in the vertex.

The mass distribution of the reconstructed B decay vertices is shown in Figure 7.4. The most probable value of the vertex mass is close to the D meson mass, 1.8 GeV/c^2. The typical reconstructed mass is significantly lower than

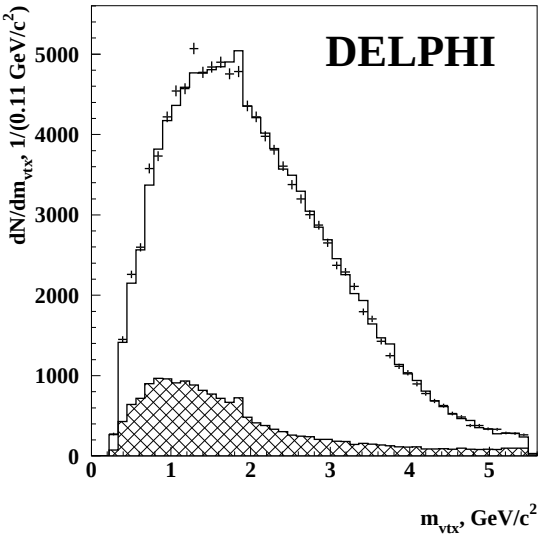

Figure 7.4: The reconstructed mass of B vertices using the simple B reconstruction algorithm. The points corresponds to the data and the histogram to simulated events. The shaded region represents background events that do not contain a B decay.

the B mass, 5.2 GeV/c^2, since only charged particles are used in the reconstruction. Inclusion of energetic neutral particles would increase the reconstructed mass closer to the nominal mass. The neutral particles are not included, since the aim of the analysis is to compare the angular distributions of particles in heavy and light jets, and the trajectories of neutral particles cannot be accurately reconstructed.

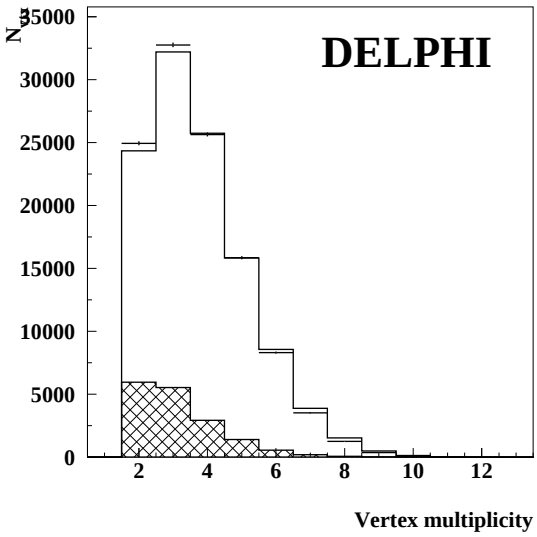

Figure 7.5: The charged multiplicity of B vertices using the simple B reconstruction algorithm. The data is shown as points with error bars and histograms represent the simulation. The shaded region corresponds to background.

The multiplicities of the vertices are shown in Figure 7.5. The average charged multiplicity in B decays is 4.97±0.07 [137]. The most probable multiplicity of the reconstructed vertices is three, with average value of 3.7, suggesting that in average one charged B decay product is not included in the vertex.

The fraction of true B decay products in the reconstructed vertices is shown in Figure 7.6. Since the fraction is calculated for each event as the ratio the number of the B decay products out of total number of particles in the vertex it takes such values as 2/3, 4/5 or 2/2. Over 60% of the reconstructed vertices contain only true B decay products. There is also a small fraction of events with no true B decay products in the vertex.

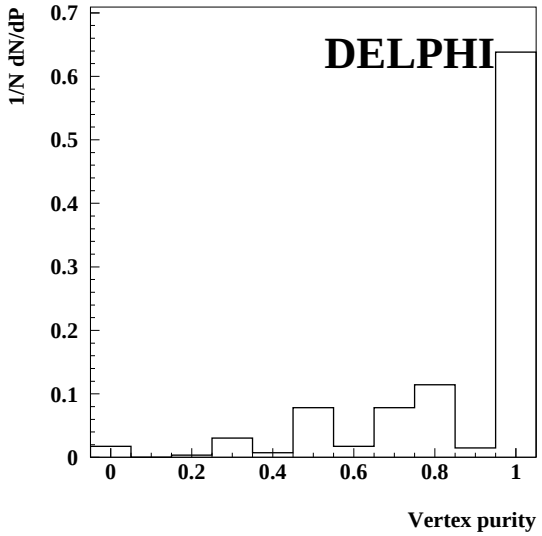

Figure 7.6: The fraction of true B decay products in the reconstructed secondary vertex using the simple B reconstruction algorithm according to simulated events. The fraction is defined only for signal events.

7.3 Elaborate B decay reconstruction

Accurate reconstruction of the B system is crucial in the measurement of the lepton energy spectrum at DELPHI (publication I). The lepton is Lorentz-boosted to the rest frame of the B meson; hence, any inaccuracies in the reconstruction of the energy or the momentum of the B directly affect the measured lepton energy.

The B decays studied are semileptonic decays $B \to X_c \ell \overline{\nu}_\ell$, where the charm hadron, X_c, subsequently decays into lighter hadrons. The reconstruction of the B decay requires the identification of the charged lepton, the reconstruction of the neutrino from the missing energy, the missing momentum and the missing mass in both hemispheres of the event, and the reconstruction of the charm decay vertex. From these, it is then possible to estimate the energy and momentum of the B meson.

The reconstruction of the charm decay vertex is based on the simple B reconstruction algorithm described in the previous subsection. It has been developed further to achieve the accuracy needed.

First, the charged lepton is identified as described in Chapter 3.

Then, all charged particles belonging to the same jet as the lepton are considered. The jets are reconstructed using the LUCLUS algorithm [138]. For each particle in the jet, the point where the particle trajectory crosses the jet axis is calculated. The distance between the main event vertex and this crossing point is called the crossing distance. The sign of the crossing distance is negative, if the crossing point is in the hemisphere opposite to the one in which the particle and the jet are.

Ideally the crossing distance is compatible with zero for particles originating from the main event vertex, when the uncertainty on the distance is considered. The crossing of the lepton with the jet axis is at a significantly larger distance in a semileptonic B decay. The particles produced in the subsequent decay of the D meson have the largest crossing distances (see Figure 7.7).

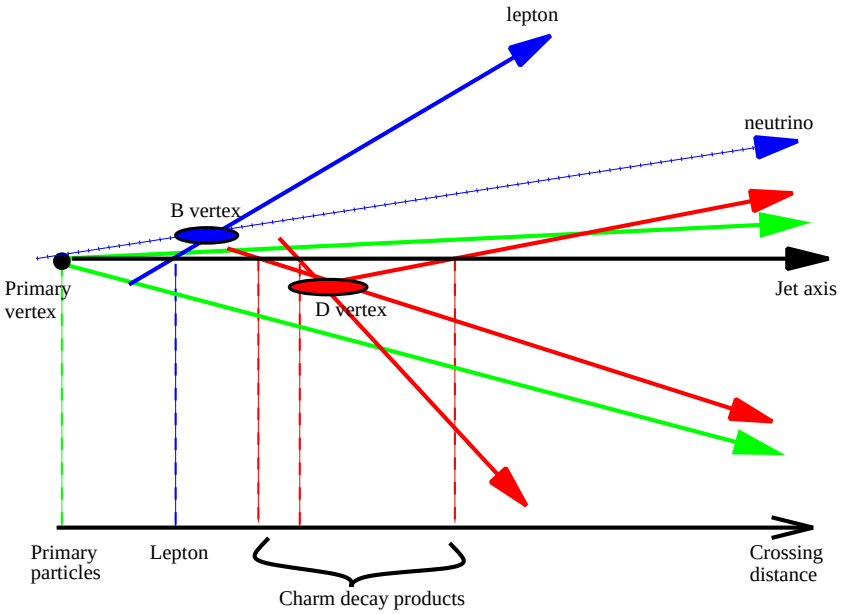

Figure 7.7: Schematic illustration of a semileptonic B decay showing the jet direction and the crossing distances of the charged particles projected on the jet axis. The solid lines represent the particle trajectories and the dashed lines lead to the projection of each crossing point to the distance from the main vertex. The crossing distances are related to the origin of the particles.

An attempt was made to use these crossing distances as a basis of the vertex reconstruction. The D decay vertex was formed by those charged particles whose crossing distances with the jet axis were compatible with each other. Several different ways of identifying and combining these particles were tested,

but the required vertex reconstruction performance level was not achieved. An important advantage of this approach is that it is very sensitive to those D decays where only one energetic charged particle is produced, accompanied by one or more neutral particles.

The evaluated crossing distances are used in the vertex reconstruction to help identify the particles with which to start the iterative reconstruction process. The particles are ordered according to their impact parameter significance, as in the simple reconstruction. If there is a charged particle with a crossing at least 1σ distance away from the main event vertex and further away than the lepton crossing, it is used to start the iteration process. The crossing distance must not exceed 15 cm, which would indicate that the particle is probably not produced in a D meson decay. If there is no particle with a large crossing distance, the iteration starts with the most energetic charged particle in the hemisphere.

The target mass of the vertex is set to 1.8 GeV/c^2, the nominal mass of the D^0 and D^+ mesons. New particles are added to the vertex only if their addition brings the invariant mass of the vertex closer to this value.

Apart from the target mass, the reconstruction in the first stages proceeds as in the case of the simple reconstruction. If, after the full iteration process, the vertex mass exceeds the target mass or the χ^2/n.d.f of the vertex is larger than 2.0, each particle is removed from the vertex one by one. If the removal of one of the particles results in a mass closer to the target mass or significantly improves the χ^2 value of the vertex, the particle is permanently removed.

At the last stage of the reconstruction of the charm system, neutral particles are considered. The trajectories of the neutral particles cannot be reconstructed as accurately as those of the charged particles, and thus a complete vertex fit that would give the χ^2 value of the vertex as well as its position, cannot be performed. The invariant mass of the vertex can be evaluated, and it is used to estimate the compatibility of the neutral particle with the reconstructed vertex. If the addition of a neutral particle brings the invariant mass of the vertex closer to the target value, the neutral particle is included. Among neutral particles, combinations of either two neutral pions that are compatible with originating from a neutral kaon or two photons compatible with a neutral pion are also considered, even if the momenta of the single pions or photons are below the required 0.5 GeV/c.

If no vertex is found using the particles in the same jet as the lepton, the process is repeated using all charged particles in the hemisphere of the lepton.

In the event of no vertex of at least two particles being found, a single charged particle is accepted to represent the decay vertex. In this case, the particle

with the largest crossing distance is used, or the most energetic particle, or the particle with the largest impact parameter significance, in decreasing order of preference.

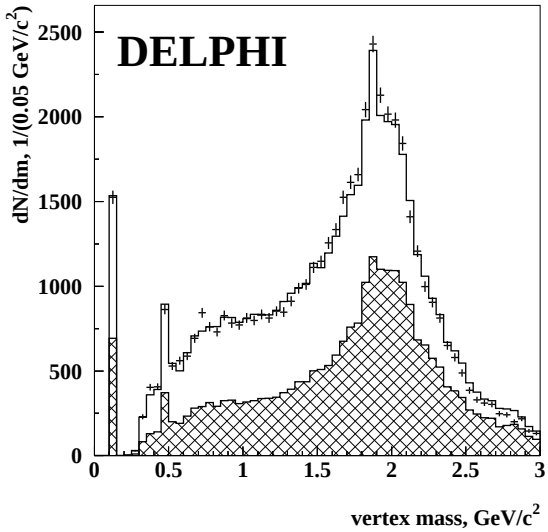

Figure 7.8: The reconstructed mass of the D vertices when the elaborate reconstruction is used. The points with error bars are DELPHI data and the simulation is shown as a histogram. The shaded histogram represents the background, which also contains events with genuine D mesons.

The mass distribution of the reconstructed vertices peaks at the target mass 1.8 GeV/c^2 (see Figure 7.8). The background is also peaked at the D mass, due to the fact that it contains also events with genuine D mesons, such as events with Z^0 decays to charm and anti-charm or hadronic B decays to charmed mesons. The peaks at 0.14 GeV/c^2 and 0.49 GeV/c^2 correspond to vertices of a single π or K meson, respectively.

The neutrino is reconstructed using the visible energy, momentum and mass in both hemispheres. The neutrino energy is obtained from the missing energy $E_{\rm beam} - E_{\rm vis}$ in the hemisphere, corrected by the missing mass in the hemisphere $M_{\rm mis} = \sqrt{E_{\rm vis}^2 - p_{\rm vis}^2}$. For missing mass less than 4 GeV/c^2, the correction has essentially the same effect as adding the missing mass to the missing energy. If the missing mass is larger than 4 GeV/c^2, the estimated missing energy is increased by about 5 GeV/c^2. The energy of the neutrino can be reconstructed with a resolution of 2.9 GeV (Figure 7.9).

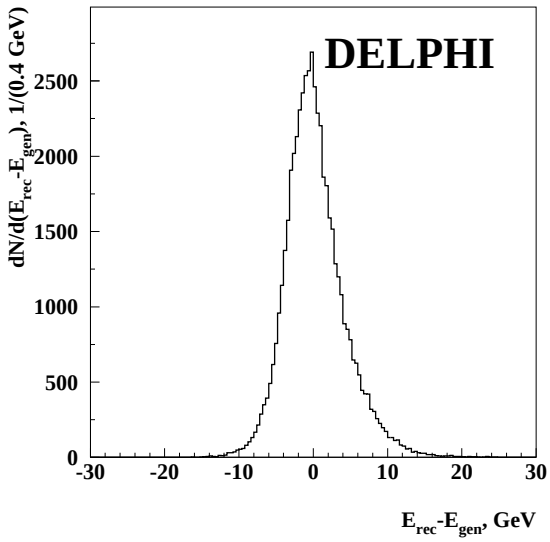

Figure 7.9: The resolution of missing energy reconstruction according to simulated events.

The total energy and the mass of the B meson is then obtained by summing the lepton, the missing energy and the charm decay vertex. Events to be used are required to have the reconstructed B mass between 4 GeV/c^2 and 9 GeV/c^2. The lower limit significantly reduces events without a semileptonic B decay and the upper limit rejects badly reconstructed signal events. The energy resolution of the B meson for the selected events is about 10%.

The momentum of the B is obtained by combining the momenta given by two separate estimators.

One estimator is the momentum sum of the lepton, the neutrino, and the D vertex. The estimator is available for all selected events, but its accuracy varies with the reconstructed mass of the B. When the reconstructed mass differs significantly from the nominal B mass of 5.28 GeV/c^2, the direction of the reconstructed momentum is deteriorated. Typically, in these cases, the direction of the missing momentum is incorrectly reconstructed due to some particles having escaped detection.

The second estimator is independent of the neutrino reconstruction. A vertex fit is performed using the charged particles in the D vertex and the lepton, and the flight direction is obtained from the vector connecting the reconstructed D-ℓ vertex with the main vertex of the event. The uncertainty is obtained

from the covariance matrix of the main vertex and the reconstructed vertex, and the accuracy of the direction estimation depends on $s_d = d/\sigma_d$, where d is the distance between the two vertices and σ_d its estimated uncertainty. If $s_d < 10$, the accuracy is not good enough to be useful.

The accuracies of these two estimators are estimated based on the mass of the reconstructed B for the first and s_d for the second, and the final momentum direction is their weighted sum. The weights are defined event-by event based on the relative estimated accuracies of the two estimators in that event. The combined estimator resolves the B direction with a 14 mrad precision in ϕ and with a 15 mrad precision in θ for the majority of the events.

When the lepton energy in the rest frame of the reconstructed B is calculated, the reconstructed energy has a 170 MeV resolution. The reconstructed lepton energy spectrum in semileptonic B decays is shown in Figure 7.10.

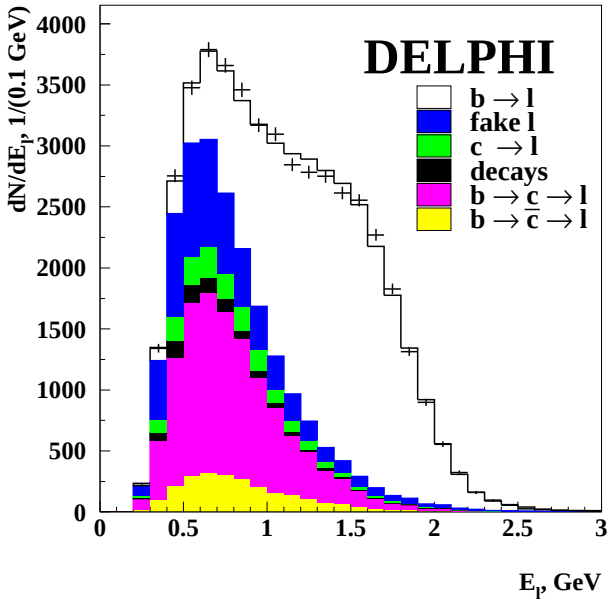

Figure 7.10: The reconstructed lepton energy spectrum in the rest frame of the B meson in semileptonic B decays. The points with errors are data and the histograms represent simulated events. The background components shown are, from top: hadrons identified as leptons; $Z^0 \to c\bar{c}$ events; leptons from decays of particles other than B or D mesons; cascade $b \to cW^*$, $c \to s\ell\nu$ and wrong sign $b \to c\bar{c}s$, $\bar{c} \to \bar{s}\ell\nu$.

Chapter 8

Background reduction

After the reconstruction of the decay, a large amount of background still remains in the event sample. Often the background is reduced by using a separating variable. The selected events are required to lie within a certain, optimised interval of that variable. As an example, the b-jet sample for the study of the dead cone effect in publication VI is selected by requiring that the probability of all the particles in the hemisphere originating from the event main vertex is less than 0.01. The sample obtained consists of 81% of b jets and 19% of jets of other flavours. Requiring a reconstructed secondary vertex improves the purity of the sample even further.

Such a simple selection is not always possible. A distinct variable may not exist that would give clear enough separation, or the variable achieving it would also introduce a bias in the quantity being measured. Instead, several variables with some separating power and unrelated to the quantity being measured may be found. Placing strict requirements on all of these variables would yield too low a selection efficiency for signal events considering the available data. The information contained in these variables, however, can be combined into one single variable, which is then used to select the events to be used for the analysis. This approach was used to select simulated CLIC $e^+e^- \to t\bar{t}$ events out of a sample that contained 20 times more $e^+e^- \to W^+W^-$ events (publication VII), to separate $Z \to c\bar{c}$ events from other events containing a reconstructed D meson at DELPHI (publication IV), and to select events that contained a semileptonic B decay for the lepton spectra analysis at DELPHI (publications I, III and IV). In all of the cases, the basic idea was the same and it was adapted for each specific case.

From simulated events, a probability density distribution is obtained for each of the variables used for separation. The probability P^{s} of the event being a signal event based on a variable i can be determined from a binned probability

density distribution. Using N variables, the total probability of the event being a signal event before normalisation is

$$P^{s'} = \prod_{i=1}^{N} P_i^{\mathrm{s}}, \tag{8.1}$$

and, correspondingly, the probability of the event being a background event is

$$P^{b'} = \prod_{i=1}^{N} P_i^{\mathrm{b}}. \tag{8.2}$$

The normalised variable is then

$$P^{s} = \frac{P^{s'}}{P^{s'} + P^{b'}}, \tag{8.3}$$

which takes values between 0 and 1.

As an example, let us look at a simplified case with just one variable with probablity distributions for signal and background as in Figure 8.1. In this case, the background has a flat distribution, while the distribution for signal shows linear growth. Suppose that a value of 0.25 has been measured. Then,

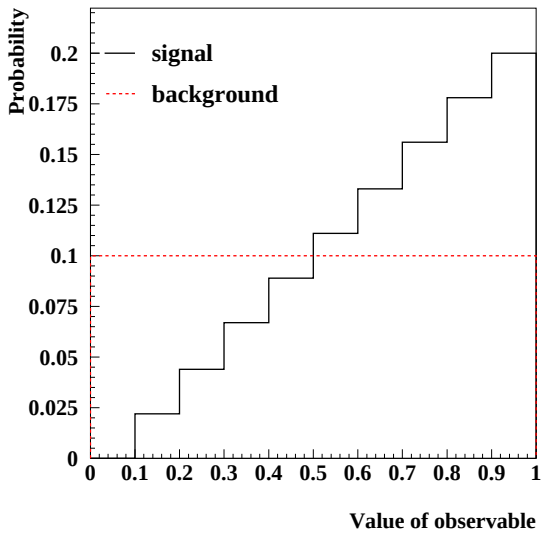

Figure 8.1: Sample binned probability density distributions in ten bins for signal (solid line) and background (dashed) .

reading from the probability density distributions, $P_1^{\mathrm{s}} = 0.044$ and $P_1^{\mathrm{b}} = 0.100$, and $P^s = \frac{0.044}{0.144} = 0.306$, or the event is signal at a probability of 31% and background with 69% probability.

If the individual probabilities are small and the number of separating variables, N, is large, the multiplication of the probabilities may lead to a numerical underflow in the calculation. For example, sharp changes in the probability density distribution of a continuous variable require using a large number of narrow bins. The average probability is $1/N_{\mathrm{bin}}$, and when the number of bins is large, it may be beneficial to normalise P_i^{s} and P_i^{b} to $P_i^{\mathrm{s}} + P_i^{\mathrm{b}} = 1$ before performing the multiplication. An additional benefit is that all the probabilities to be multiplied are approximately of the same order of magnitude, regardless of into how many bins the probability density distributions were initially divided. The final variable P^s has the same value with or without the additional normalisation and the calculation becomes numerically more stable when such a normalisation is introduced.

In this chapter, the separating variables selected for each of the three analysis are reviewed. First the selection of semileptonic top events at CLIC is discussed. Then the selection of charm jets for the DELPHI dead cone analysis is described, and the chapter concludes with the selection of semileptonic B decays for the lepton spectrum measurement. The selection variables presented in this chapter for the semileptonic B decay selection correspond to the set used for the final version of the analysis, described in publication I. Since the earliest version of the analysis, publication IV, some of the variables have been changed.

8.1 Semileptonic t decay selection at CLIC

W^+W^- pair production is the most significant source of background in the measurement of $t\bar{t}$ production cross-section at $\sqrt{s} = 3$ TeV (publication VII). The cross-section of W^+W^- production, 500 fb [139], is about a factor of 25 larger than the Standard Model cross-section for $t\bar{t}$ production, 20 fb [139]. The W^+W^- events do not contain the two b jets present in the $t\bar{t}$ events, but there may be extra jets in the event. These extra jets, combined with the jets produced in the W decay, may give an invariant mass close to the top mass. Light quark jets can also be mis-identified as b jets [136].

There are also other background processes that produce $bWbW$ final states, but their combined cross-section is 2.6 fb [139] and they are therefore insignificant compared to the W^+W^- background.

The following requirements significantly reduce the number of W^+W^- events in the sample, while keeping the $t\bar{t}$ events:

1. Between one and three of the jets in the event are identified as b jets.
2. The reconstructed top mass is between 100 and 1300 GeV/c^2.
3. The reconstructed W mass is between 20 and 160 GeV/c^2.

These requirements reduce the background to a tolerable level for the cross-section measurement, yielding a sample of $t\bar{t}$ events in which only 20% are W^+W^- events.

If the event contains an energetic, isolated lepton, only one reconstructed top decay filling the above criteria is required, while in events without a lepton both top candidates are required to satisfy the criteria. In the measurement of the forward-backward asymmetry only events with leptons are used.

In Figure 8.2 the mass distribution of hadronically decaying top quark candidates is shown in events that have been pre-selected for the measurement of

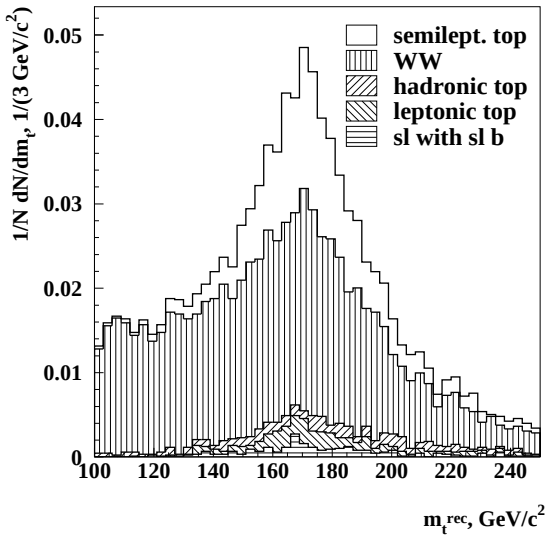

Figure 8.2: The mass distribution of the hadronic top candidates in the selected semileptonic $t\bar{t}$ event sample. The backgrounds shown are W^+W^- events, fully hadronic $t\bar{t}$ events, fully leptonic $t\bar{t}$ events, and semileptonic $t\bar{t}$ events, where the selected lepton was produced in a semileptonic b decay.

the forward-backward asymmetry. The contribution from background sources is significant. Since the measurement only uses semileptonic top events, the background in this case also includes the fully hadronic and fully leptonic top events.

The strategy of the measurement is to use the charge of the lepton from the leptonic decay to identify the charge of the top (t or $\bar{t}$). The reconstructed hadronically decaying top provides the angle of the top with respect to the electron beam direction.

When only one fully reconstructed top quark is expected in the event, the mass selection criteria are not as efficient in reducing the W^+W^- background as they are when two reconstructed top quarks are required. There are also energetic leptons in W^+W^- events from leptonic decays of the W boson.

The different backgrounds can also bias the measured asymmetry. Fully hadronic top decays, where the lepton is most probably produced in the decay of the b quark, $t \to bW$, $b \to c\ell^+\nu$, contain a lepton with the opposite charge from the expected in $t \to bW \to b\ell^-\nu$ decay and therefore tend to diminish the asymmetry. The leptons from b decays have, in average, less energy than those from t decays. The requirement of lepton energy larger than 50 GeV helps reduce the b background, but does not remove it completely.

In fully leptonic top decays, the lepton gives a correct charge, but the direction of either of the top quarks is not reconstructed. In principle, these events could be used to count the number of top quarks (as opposed to anti-top quarks) in the forward and backward directions.

The third kind of background $t\bar{t}$ events are semileptonic top decays accompanied by a semileptonic b decay, where the lepton from the b decay has been selected instead of the proper lepton. The false lepton charge results in an opposite bias.

The important difference between signal and background events is that the signal events are supposed to contain four jets and an isolated, energetic lepton. Two of the four jets are expected to be b jets, and the other two should be light quark jets. The jet reconstruction in the background events may have failed, and produced four jets and a lepton, but this failure in the reconstruction will lead to different distribution for jet energies and multiplicities.

The jet energy distributions are shown in Figure 8.3.

In signal events, all the jets are reasonably energetic. The W^+W^- events differ from the others in that they contain one very energetic jet and the average energy of the other jets is lower than in other event types. In fully hadronic $t\bar{t}$ events, the jets tend to have roughly equal energies. In fully leptonic events, the jets are soft, since the two b jets and two charged leptons are forced to

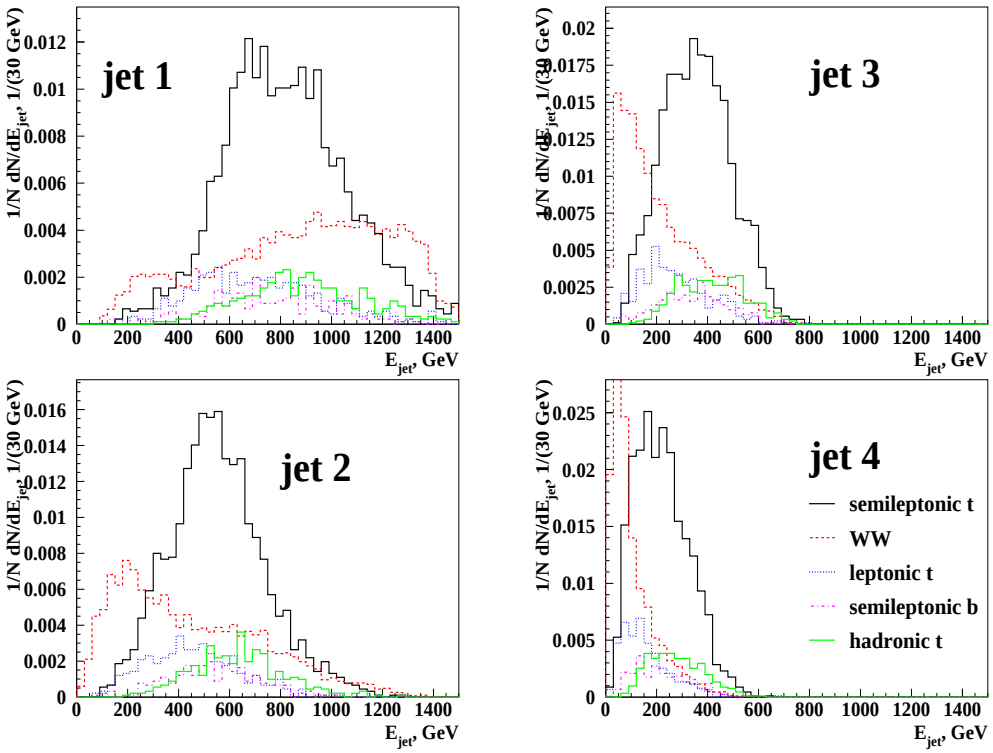

Figure 8.3: The energy distributions of jets in semileptonic $t\bar{t}$ events, W^+W^- events, fully hadronic, fully leptonic, and semileptonic $t\bar{t}$ events with $b \to \ell$ decay. The W^+W^- contribution has been scaled down by a factor of 5.

make up altogether four jets. The semileptonic top events with the lepton from a b decay behave similarly to the signal semileptonic events.

The numbers of particles in each jet are shown in Figure 8.4. The signal events tend to have jet multiplicities of the order of 20 in all the jets. In the W^+W^- events and fully leptonic $t\bar{t}$ events, the jets have low multiplicities, while fully hadronic and semileptonic background events behave similarly to the signal events.

The probabilities for the event to be fully hadronic, semileptonic, or fully leptonic are evaluated. The distributions of the probability for an event to be a semileptonic top event are shown in Figure 8.5 for both signal and all the background sources.

The most part of the W^+W^- background can be discarded by requiring sep-

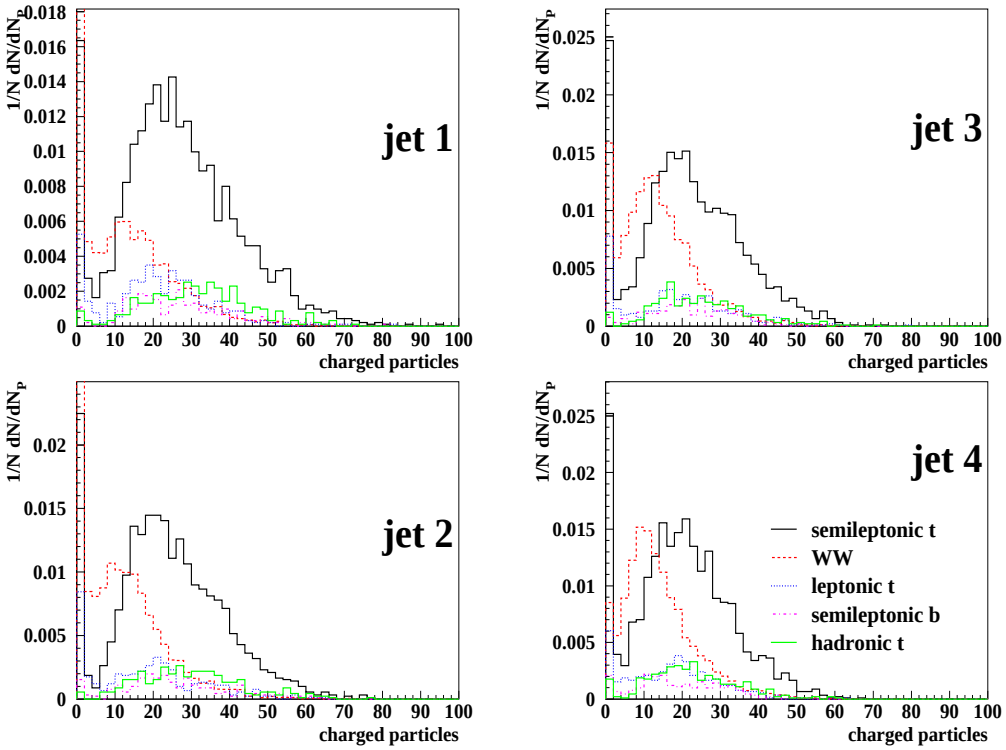

Figure 8.4: The multiplicity distributions of jets ranked according to their energy, for semileptonic $t\bar{t}$ events, as well as W^+W^- events, fully hadronic $t\bar{t}$ events, fully leptonic $t\bar{t}$ events, and semileptonic $t\bar{t}$ events where the lepton was produced in b decay. The W^+W^- contribution has been scaled down by a factor of 5.

arating variable values higher than 0.15. A significant reduction of the background from $t\bar{t}$ events will affect the selection efficiency of the signal events. The final selection was performed with a combination of the hadronic, leptonic and semileptonic probabilities. The sample obtained consisted of 68% semileptonic signal events, with W^+W^- events as the largest background component with 10%.

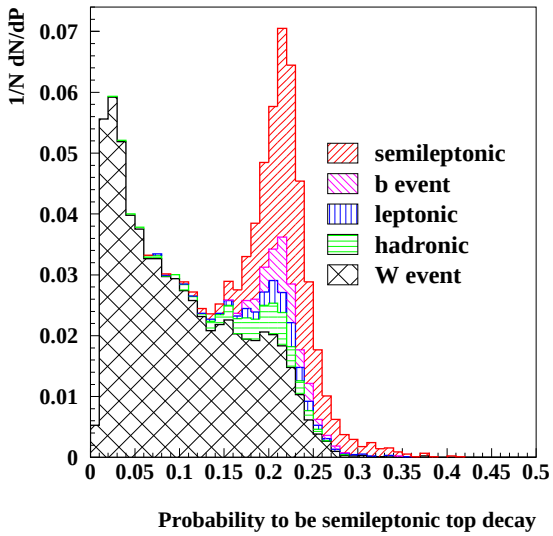

Figure 8.5: The distribution of the probability for an event to be semileptonic $t\bar{t}$ events for events that contain an energetic, isolated lepton and a top candidate and a W candidate with their masses within the mass limits.

8.2 Charm jet selection

The selection of charm jets for the study of the angular distribution of fragmentation particles in jets of different flavours at LEP also requires the construction of a separating variable (publication VI). The b jets can be selected using the standard DELPHI b-tagging combined with a requirement of a reconstructed secondary vertex, and light quark (u, d, s) jets can be selected by anti-b-tagging and requiring that no decay vertices were reconstructed in the event.

The starting point for the charm jet selection is a set of exclusively reconstructed charm decay vertices in a number of different decay channels. The reconstruction method is described in Ref. [140]. The first selection is performed by requiring the mass of the reconstructed vertex to be within a predefined region of the nominal D meson mass, which reduces the combinatorial background to a large extent. The background also contains genuine D mesons, for example in b jets, where the b quark has decayed into a c quark, and this background cannot be reduced using the mass selection.

Information on the topology and the kinematics of the event can be used to

distinguish between D mesons originating from c jets and b jets. A small contribution from light quark (u, d, s) jets also remains, where no genuine D mesons are expected. The topologies of the b, c and light quark events are illustrated in Figure 8.6.

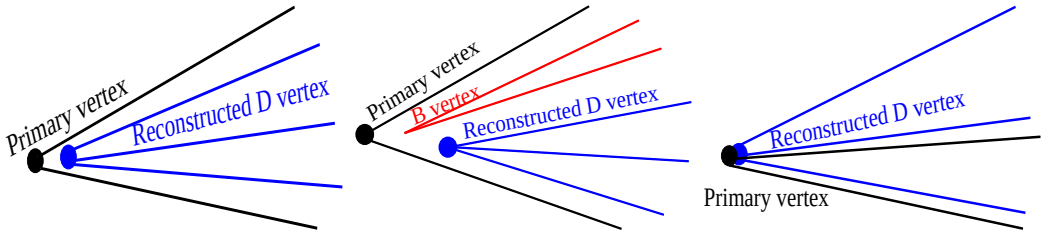

Figure 8.6: Typical topologies of events with a reconstructed D decay vertex candidate in charm (left), beauty (center) and light quark (right) jets.

In b jets, the D mesons produced typically have lower energies than in c jets, due to the fact that the D mesons are secondary decay products of the B mesons and the other decay products take part of the energy. The energy distribution of the reconstructed D mesons are shown in Figure 8.7 for charm, beauty, and light quark jets.

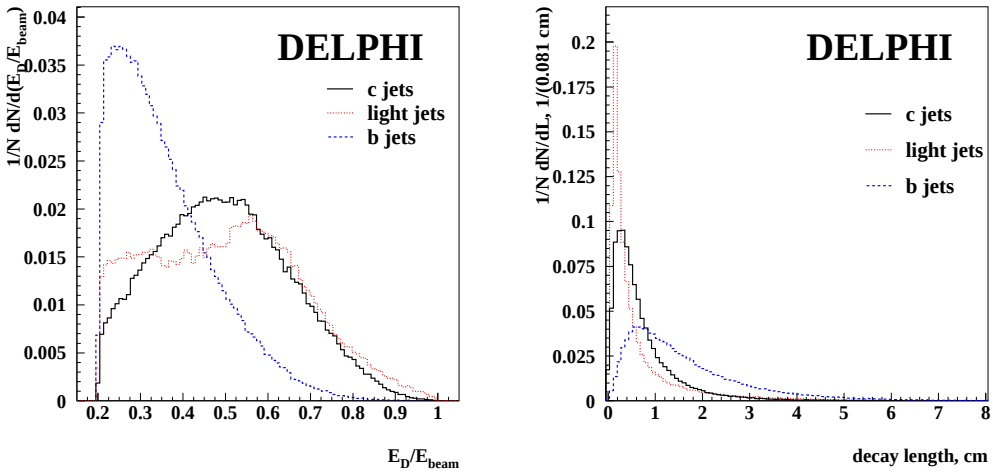

Figure 8.7: The distribution of energy normalised to the beam energy (left) and the decay distance distribution (right) for b, c and light quark (u, d, s) jets.

The distances, L, between the primary vertex of the event and the reconstructed D decay vertex, or decay distances, differ for the three flavours. In light quark jets, the D meson is reconstructed from particles that truly originate from the primary vertex of the event, resulting in a short decay distance. In b jets, where the D is produced in the decay of the B, the meson is already displaced from the primary vertex when it is produced. Therefore, the decay distance L is the sum of the typical flight distance of a B meson and that of a D meson. The decay distance distributions for the three event flavours are shown in Figure 8.7.

The topology of the event can be considered by calculating the probability of all the particles in the hemisphere of the reconstructed D meson originating from the main event vertex. For light quark jets, this probability should be rather large, while in the jets with b or c quarks the decay products of the heavy quark decrease this probability.

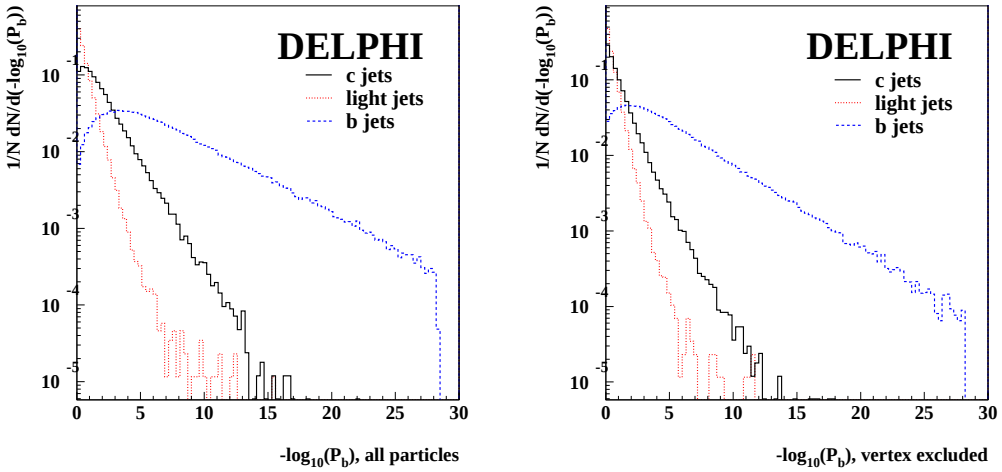

Figure 8.8: The probability of all the particles in the hemisphere (left) and all particles except those associated with the D decay (right) originating from the main vertex of the event for b, c and u, d, s jet.

Further separation is obtained by excluding the particles associated with the D decay and recalculating the probability of all the remaining particles in the hemisphere originating from the main vertex of the event. The probability should be large for u, d, s and c jets, while it should remain small for the b jets due to the B decay vertex contained in the hemisphere.

The probability distributions including and excluding the D decay vertex are

shown in Figure 8.8.

The distributions are considered separately for each decay mode. It is assumed that the fraction of background contained in the simulated event sample is accurate, which is a reasonable assumption based on how well the simulations are known to describe the DELPHI data. Therefore, the probability of the event being a c event, for example, is not estimated based on the fraction of c events contained in the same bin of the distribution, but on the fraction of c events in that bin out of all events in the bin. The probability of the event being a b, c or light quark event are considered separately, and in the end the three probabilities are normalised to sum to unity.

The distribution of the separating variable related to the probability of the event being a c event is shown in Figure 8.9.

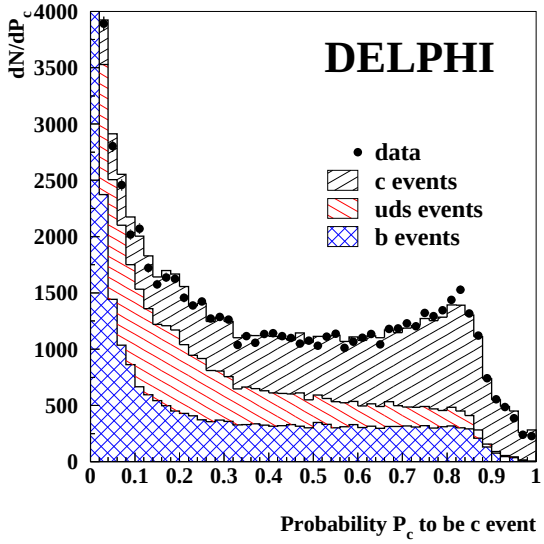

Figure 8.9: The separating variable related to the probability of the event being a c event for $Z \to c\bar{c}$, $Z \to b\bar{b}$ and $Z \to u\bar{u}$, $Z \to d\bar{d}$ or $Z \to s\bar{s}$ events.

The selection value is defined individually for each decay mode to give final samples of approximately equal purities. The decay modes with higher statistics are required to have higher purities than the rest. The selection values are tabulated in publication VI.

8.3 Selection of semileptonic B decays

The reconstructed lepton energy spectrum for semileptonic B decays before background subtraction is shown in Figure 7.10. The spectrum contains large contributions from various background sources. The most significant, and easiest to control, are the events where the lepton comes from the decay of a D meson that was produced in the B decay. The lepton energy in these events is lower than in signal events, which affects the shape of the measured spectrum. Typical methods used to select semileptonic B decays utilise the lower energy and require the leptons to have at least a certain amount of energy in the rest frame of the decaying B. This removes the lower end of the spectrum, the sensitivity to which is the main strength of the analysis (publication I).

In the majority of D decays, the decaying c quark was produced in $b \to cW^-$ decays, ("cascade decays", labelled "$b \to c \to \ell$" in Figure 7.10) and in the consequent decay of the c, the sign of the lepton is opposite to the sign of the lepton that would have been produced, had the b quark decayed semileptonically. In some cases, the virtual W from the b quark decay decays into $s\overline{c}$ and the observed lepton is a decay product of the $\overline{c}$ ("wrong sign charm", labelled "$b \to \bar{c} \to \ell$" in Figure 7.10). In this case, the lepton charge is the same as in the b decay. Topologically, the event differs from semileptonic b decays. The different topologies are illustrated in Figure 8.10.

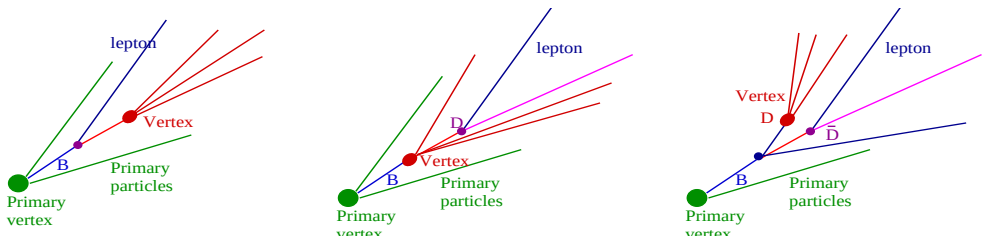

Figure 8.10: Typical topologies of semileptonic b decays, cascade decays $b \to c \to \ell$, and wrong sign decays $b \to \overline{c} \to \ell$.

In semileptonic B decays, the lepton production vertex, the B decay vertex, is located between the main vertex of the event and the reconstructed hadronic system. In semileptonic D decays, the lepton is mostly produced further away from the main vertex than the reconstructed secondary system.

The other backgrounds are either less significant, like $Z \to c\bar{c}$ events that are only 3% of the sample, or do not offer a practical handle to discriminate from the signal events. Examples of the latter case are the fake lepton events, where the particle identified as a lepton is in fact a hadron, and the events

that contain leptons produced in other decays. The cascade and wrong sign backgrounds are the only background components that seriously distort the measured lepton spectrum, if not treated properly.

Two sets of variables were identified to be used to select signal events: topological variables and charge variables. A separating variable was constructed separately for each of these two variable sets and only in the end the two variables were combined. The charge variables are not quite as efficient in separating the background from the signal as the topological ones; nevertheless they add important information on the event.

The topological variables are the lepton impact parameters with respect to the reconstructed secondary vertex, the number of particles in the secondary vertex, the number of particles in the hemisphere not associated with the secondary vertex, the χ^2 value of the vertex, and the topology of particles other than the lepton in the hemisphere. The charge variables are the correlation of the lepton charge with the charge of the secondary vertex, the charge of the alternative secondary vertices in both the hemisphere of the lepton and the opposite hemisphere, the jet charge in the opposite hemisphere, and charge of the leading kaon candidate. Some of the variables have been changed since the

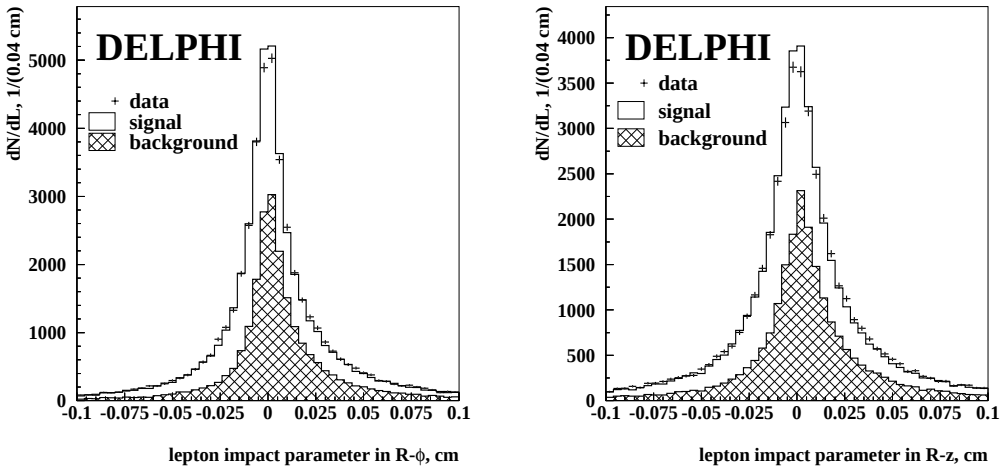

Figure 8.11: The lepton impact parameter with respect to the reconstructed secondary vertex in $R-\phi$ and $R-z$ planes. The background includes the cascade background $b \to c \to \ell^-$, the wrong sign background $b \to \bar{c} \to \ell^+$, $Z \to c\bar{c}$ events, leptons from other decays and hadrons that have been identified as leptons.

first report on the measurement of the moments of the lepton energy spectrum, in publication IV.

The lepton impact parameter with respect to the reconstructed secondary vertex is the distance of closest approach between the lepton trajectory and the vertex. The impact parameter has a negative sign, if the point in the lepton trajectory closest to the secondary vertex is on the same side of the secondary vertex as the main vertex, and a positive sign, if the point is on the opposite side. The signal leptons are expected to have a negative sign and background leptons to have a positive sign. In reality, the distributions are smeared by the reconstruction resolution (Figure 8.11).

The average charged multiplicity of D decays is lower than that of B decays. The most common D decay modes produce two or three charged particles, while the average charged multiplicity of B decays has been measured to be 4.97±0.07 [137]. Therefore, events where the reconstructed vertex contains more than four charged particles (Figure 8.12) are typically either background events, where a B decay has been reconstructed, or signal events where a fragmentation particle has been included in the vertex.

In addition to the vertex multiplicity, the number of particles in the hemisphere

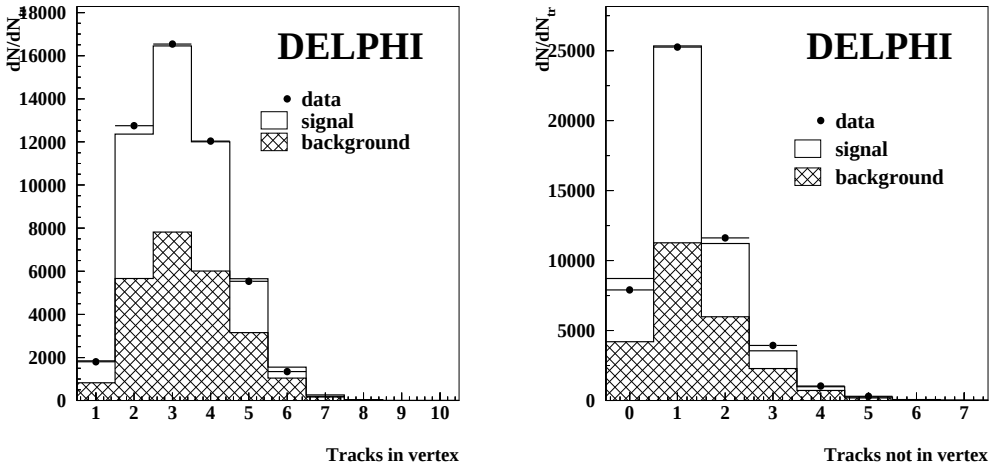

Figure 8.12: The number of particles in the secondary vertex (left). The number of particles in the hemisphere that are not associated with the secondary vertex (right). The background includes the cascade background $b \to c \to \ell^-$, the wrong sign background $b \to \bar{c} \to \ell^+$, $Z \to c\bar{c}$ events, leptons from other decays and hadrons that have been identified as leptons.

that are not associated with the secondary vertex, N_P, also proved to be useful. In signal events, only particles originating from the main event vertex are not associated with the secondary decay, if the event was properly reconstructed. In cascade decays, in addition to the particles originating from the primary vertex, more unassociated particles are expected from the decay of the B. The distribution of N_P for signal and background events is shown in Figure 8.12.

The χ^2 value of the vertex tests the quality of the vertex fit. A well-reconstructed D meson decay vertex will have a relatively low χ^2 value, while background events tend to have higher χ^2 values (Figure 8.13).

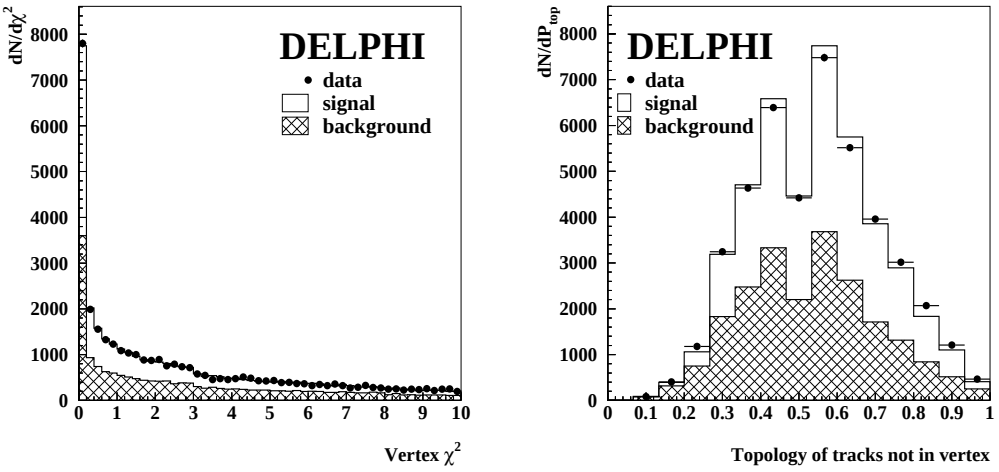

Figure 8.13: The χ^2 distribution of the reconstructed secondary vertices (left). The likelihood of the event containing a semileptonic B decay based on the the distances at which the charged particles of the event, excluding the lepton, cross the jet axis (right). The background includes the cascade background $b \to c \to \ell^-$, the wrong sign background $b \to \bar{c} \to \ell^+$, $Z \to c\bar{c}$ events, leptons from other decays and hadrons that have been identified as leptons.

The last topological variable describes the topology of all the particles other than the lepton in the hemisphere. Based on the crossing distances of the particles with the jet axis (see Section 7.3), a likelihood that the event contains a semileptonic B decay is estimated. The distribution of this variable for signal and background events is shown in Figure 8.13.

The charge correlation variables are constructed by multiplying the charge of a vertex, a jet or a single particle in the event by the lepton charge. The majority of the variables by themselves do not provide much separation between the

signal and the background, but all of them combined a separation is achieved.

The most obvious charge product to consider is the correlation of the lepton charge and the charge of the reconstructed hadronic vertex (Figure 8.14). Correctly reconstructed charm decay vertices should have charge ± 1 or 1. The reconstructed vertices with larger charges are either missing a charged particle or two that would bring the total charge closer to zero, or they contain charged particles that were not produced in the D decay. The fraction of background events is larger in these bins than in the bins with the expected charge. The dominance of the zero-charge bin is due to it containing both $B^+ \to \overline{D}^0 \ell^+ \nu$ and $B^- \to D^0 \ell^- \bar{\nu}$.

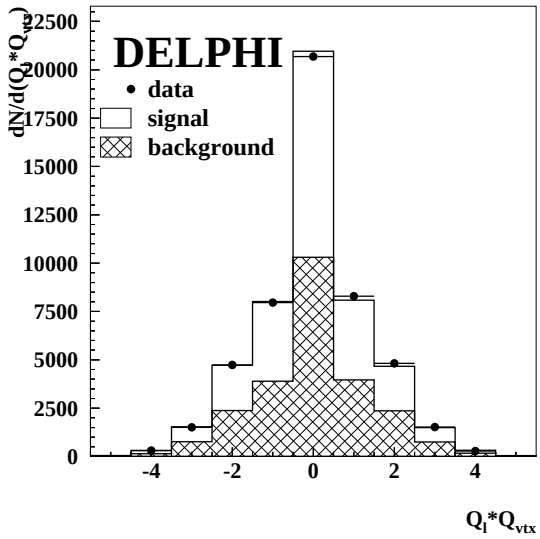

Figure 8.14: The product of the lepton charge and the charge of the reconstructed D decay vertex. The background includes the cascade background $b \to c \to \ell^-$, the wrong sign background $b \to \bar{c} \to \ell^+$, $Z \to c\bar{c}$ events, leptons from other decays and hadrons that have been identified as leptons.

The DELPHI BSAURUS [141] neural network package reconstructs an alternative decay vertex in the hemisphere. One should note that this vertex is the B meson decay vertex, and not the charm decay vertex as in the previous variable. The neural network assigns to each charged particle a probability, p_B, to originate from the B decay vertex rather than from the primary vertex and

based on that a weighted vertex charge is formed

$$Q_v = \sum_i^{N_{\text{particles}}} p_B^i \cdot Q_i. \tag{8.4}$$

Since the charge definition contains all the particles, the lepton charge is also included in the charge determination of the vertex in the hemisphere of the lepton. The vertex charges in both the hemisphere of the lepton and in the opposite hemisphere are considered (Figure 8.15). Because of the weighting, the vertex charge is not restricted to integer values. The vertex charge distribution before multiplication with the lepton charge has three distinct peaks: the highest for zero-charge vertex and the lower ones around charge ± 1.

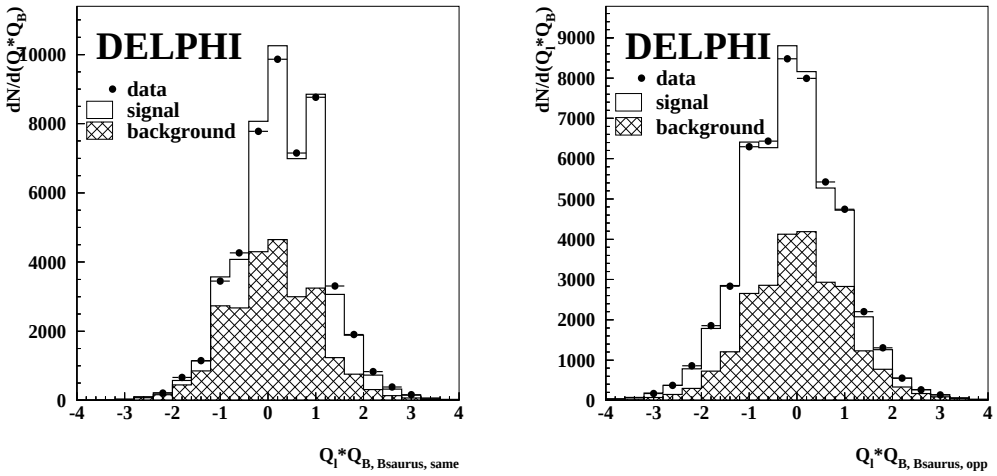

Figure 8.15: The product of the lepton charge and the charge of B decay vertex reconstructed by the BSAURUS package in the hemisphere of the lepton (left) and in the opposite hemisphere (right). The background includes the cascade background $b \to c \to \ell^-$, the wrong sign background $b \to \bar{c} \to \ell^+$, $Z \to c\bar{c}$ events, leptons from other decays and hadrons that have been identified as leptons.

In the hemisphere of the lepton, the multiplication by the lepton charge retains the peak at zero and enhances the peak at $+1$ for signal, as expected for $B^+ \to \overline{D}^0 \ell^+ \nu$ ($Q_{\text{vtx}} = +1, Q_\ell = +1$) and $B^- \to D^0 \ell^- \bar{\nu}$ ($Q_{\text{vtx}} = -1, Q_\ell = -1$). In the case of cascade background, the lepton charge is the opposite and the product of the two charges tends to take negative values. The wrong sign background behaves similarly to the signal.

In the opposite hemisphere, the correlation is not as direct. If the charge of the lepton in a signal event is negative, the opposite hemisphere must contain an anti-b quark, if the $B^0 - \overline{B}^0$ mixing is not taken into account. The meson in the opposite hemisphere can then be either B^0 or B^+. Hence, the product of the lepton and the meson charges is either 0 or -1. In practice, the charge peaks are not as distinct in the opposite hemisphere as they are in the same hemisphere. Nevertheless, the signal events tend to take negative values for the product of the two charges, while the background seems more symmetrical around zero.

The jet charge Q_J is defined by

$$Q_J = \frac{\sum |p_L|_i^\kappa Q_i}{\sum |p_L|_i^\kappa}. \tag{8.5}$$

The sum extends over all charged particles and p_L is the momentum component longitudinal to the thrust axis of the event. The value $\kappa = 0.6$ is used. The most weight is given to the most energetic particles. The product of the jet charge and the lepton charge is shown in Figure 8.16 for the jet in the opposite hemisphere. Since the weighting is based on particle momentum, using the jet charge of the jet in the hemisphere of the lepton would introduce a bias on the lepton energy spectrum, as energetic leptons would have a large weight. The jet charge is related to the charge of the B meson in the hemisphere and is expected to behave similarly to the B vertex charge in the opposite hemisphere. In fact, the product of the lepton charge and the jet charge is typically negative for signal events, while for background events it is more likely to be positive than negative.

The last charge correlation variable is the correlation of the lepton charge and the charge of the leading kaon candidate, if there is one. The leading kaon is typically the kaon that has the largest rapidity with respect to the B hadron direction. The leading kaon has most likely been produced in the decay of a D meson. The connection between the kaon charge and the lepton charge is not very straightforward.

In the decay of a D^+ meson a K^- is produced in about 24% of cases, K^0 or $\overline{K}^0$ in about 60% of cases, and K^+ in about 6% [4]. Since the D^+ is accompanied at production by ℓ^-, the majority of the signal events would have the product zero. The identification of the neutral kaons is more difficult than that of charged ones and their trajectories are usually not reconstructed.

Out of five charged kaons in $\overline{B}^0 \to D^+\ell^-\bar{\nu}$, one is expected to have a charge product of -1, while the rest have a product +1.

In the case of $B^- \to D^0\ell^-\bar{\nu}$, the large majority of kaons from the D^0 decay

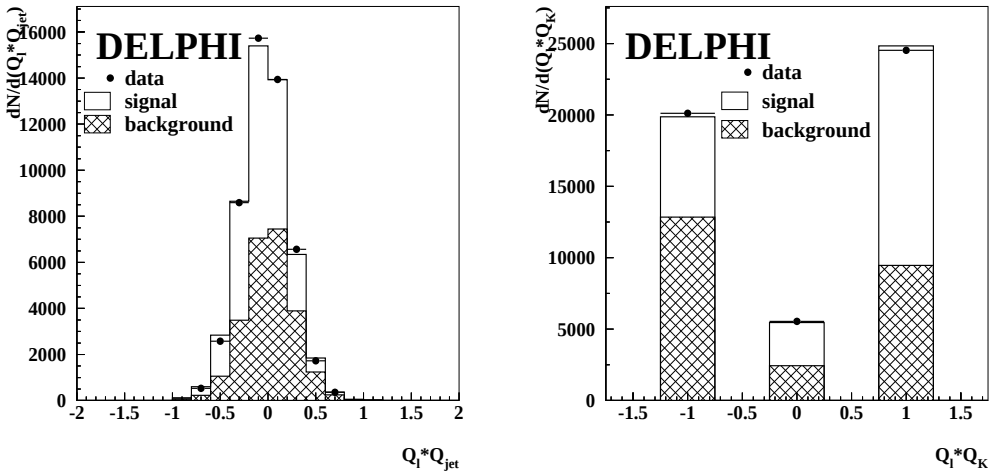

Figure 8.16: The product of the lepton charge and the jet charge of the jet in the other hemisphere (left) and the product of the lepton charge and the charge of the leading kaon in the hemisphere of the lepton (right). The $Q_\ell \cdot Q_K = 0$ case correspond to neutral leading kaon candidates. The background includes the cascade background $b \to c \to \ell^-$, the wrong sign background $b \to \bar{c} \to \ell^+$, $Z \to c\bar{c}$ events, leptons from other decays and hadrons that have been identified as leptons.

have a charge -1, and about 5% have a charge +1, resulting in the charge product of +1 for the most of the cases.

In background events, if the charged lepton and the kaon are produced in the same D^0 meson decay, they generally have the opposite charges and thus a charge product of -1. In $D^\pm$ decays the kaon is often neutral.

It is also possible that the selected leading kaon is in fact a fragmentation particle, in which case the correlation between the kaon charge and lepton charge is quite random.

The distribution of the charge product of the lepton and the kaon (Figure 8.16) generally behaves as expected: in the case of background, the product is somewhat more likely to be negative and in the case of signal a positive product is more likely. Also some neutral kaon candidates have been observed, but they offer little aid in the separation of the signal and the background.

The two-dimensional distributions of the signal and background in terms of the two separating variables are shown in Figure 8.17. The signal events tend to have high values in terms of both variables and the background events low

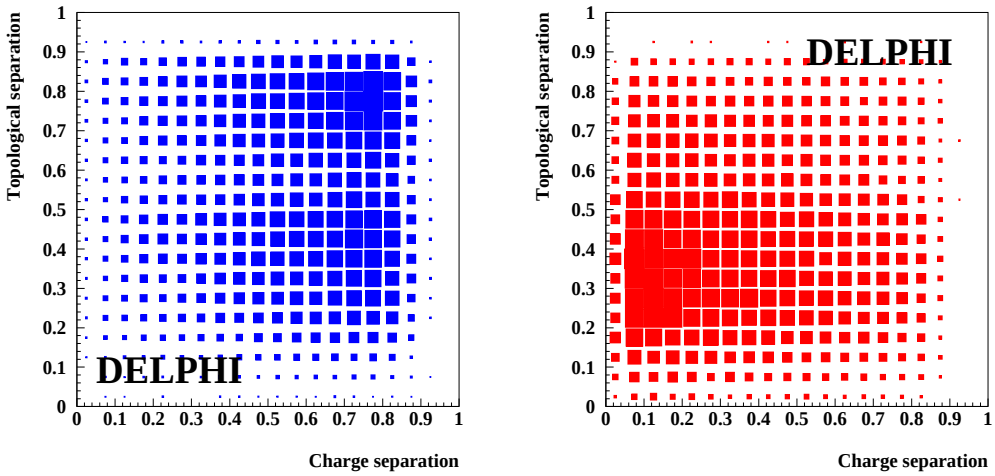

Figure 8.17: The two-dimensional distribution of signal (left) and background (right) events of the topological and charge separating variables. The background includes the cascade background $b \to c \to \ell^-$ and the wrong sign background $b \to \bar{c} \to \ell^+$.

values, but the separation is not perfect and signal events can be found in the region mainly populated by background and vice versa. The final separating variable was obtained as the fraction of signal events out of all events in each bin of the two-dimensional distribution. This relies on the assumption that the relative amounts of signal and background are properly reproduced in the simulation. The assumption was checked by comparing the lepton energy distributions in data and simulation for different intervals of the separating variable. The data and simulation were found to be compatible in all the cases.

The advantage of defining the separating variable as the fraction of signal events has the advantage that the value of the separating variable corresponds directly to the purity.

The signal events were selected by requiring the selection variable value higher than 0.58, which resulted in a sample of 14364 events with 81% purity. The lepton energy spectrum in the rest frame of the B meson for the selected events is shown in Figure 8.18. The event selection efficiency as a function of the lepton energy is reasonably independent of the energy, as desired.

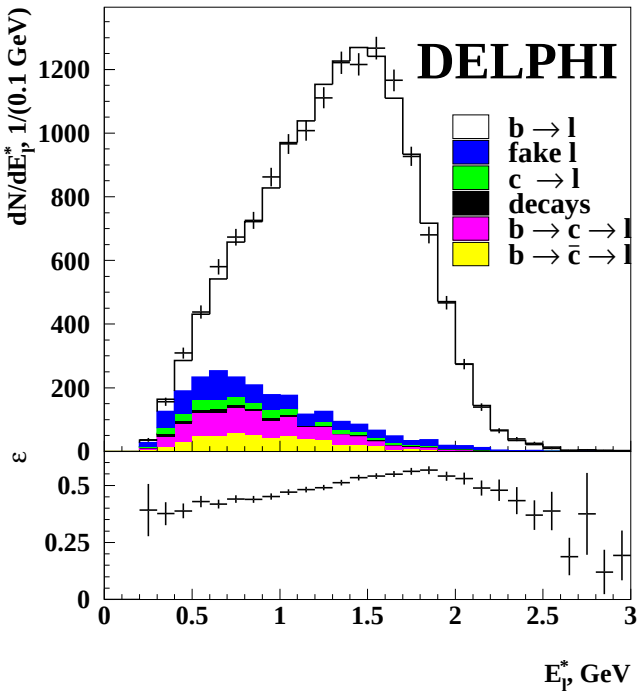

Figure 8.18: The lepton energy spectrum after background reduction (top) and the selection efficiency as a function of the lepton energy (bottom) in the rest frame of the B hadron.

Chapter 9

Conclusions

Measurements of the statistical moments of the lepton energy spectrum and hadronic mass spectrum in semileptonic B decays have attained a significant amount of attention recently. Several experimental collaborations, in addition to DELPHI, have measured the moments and some of them have also used the measurements to extract the OPE parameters. The theoretical expressions that connect the moments with the OPE parameters and the CKM-matrix element V_{cb} have been improved by calculations of higher order corrections. Extractions of the OPE parameters using measured values from several collaborations have also been published [142, 143].

The pioneering work toward the measurement of the moments was done by the CLEO collaboration. In 1996, they published the first extraction of $\bar{\Lambda}$ and λ_1 based on the lepton energy spectrum in semileptonic B decays [144,145]. In 2003, extractions of several of the parameters with over-constrained fits with more systematical approach to the estimation of uncertainties due to higher order corrections were published, publication II and Ref. [2]. Both of these used the preliminary results of publication IV and Ref. [146], Ref. [2] also used other results available at the time. The more systematical approach started a flurry of new measurements.

CLEO reported new preliminary numbers [147] and currently they have an another analysis in preparation [148] that uses both the lepton [149] and hadron [150] spectra, as well as the photon spectrum [151] in the $B \to X_s\gamma$ process. The BABAR collaboration has extracted the OPE parameter values and the value of V_{cb} [152] using measurements of the hadron mass spectrum [153] and lepton energy spectrum [154]. They have also measured the related photon energy spectrum [155]. The CDF collaboration has measured the first two moments of the hadron mass spectrum and used it to extract the values of $\bar{\Lambda}$ and λ_1 [156]. The BELLE collaboration has reported preliminary results regarding

the hadron moments [157] and the lepton moments [158] as well as a measurement of the photon energy spectrum [159]. The most important difference between the DELPHI measurement and the other measurements is that only at DELPHI the full lepton energy spectrum can be used for the analysis. In the other experiments, a minimum requirement on the lepton energy (E_{cut}) needs to be placed in order to obtain a sample of accurately reconstructed leptons.

In this chapter, the different measurements are compared, starting with the lepton energy moment results. Subsequently, the results for the OPE parameters are compared, and finally the values obtained for V_{cb} are compared. The DELPHI results used in the comparison are the final values from publication I. Another interesting result from the DELPHI analysis of the moments is the measurement of $m_b(m_b)$, which can be compared with the DELPHI measurement of $m_b(m_Z)$ [160]. These measurements make DELPHI the first experiment to measure the mass of the b quark, m_b, at two distinct energy scales. In the last sections, the conclusions of the study of the angular distribution of fragmentation particles in jets with heavy quarks and of the top reconstruction at CLIC are presented.

9.1 Moments of lepton energy spectrum

Measurements of the statistical moments of the lepton energy spectrum are available from four collaborations. The DELPHI measurement, described in this thesis, provides the first three moments with no requirement for the lepton energy in the B rest frame (publication I). The BABAR collaboration has measured the first three moments with two different requirements for the energy of the leptons, $E_{\mathrm{cut}} = 0.6$ GeV and $E_{\mathrm{cut}} = 1.5$ GeV, resulting in a total of six values [154]. The CLEO collaboration has reported the first two moments for ten different values of E_{cut}, from 0.6 GeV to 1.5 GeV [149]. The preliminary BELLE results give the first three moments for six values of E_{cut} in the range between 0.4 and 1.5 GeV [158].

The measured values cannot be compared as such due to the different requirements for the minimum energy of the leptons used in the analyses. Using expressions from Ref. [117], obtained as a FORTRAN code from the authors, the values of the moments can be computed for arbitrary E_{cut} for certain values of the OPE parameters. The parameter values have been taken from the DELPHI determination, where the central values give the solid line in the Figures 9.1-9.3 and an approximate 1σ contour is obtained by varying all the parameters by $\pm 1\sigma$. This approach does not properly take into account the correlations between the parameters, and the true 1σ contours will in reality be slightly

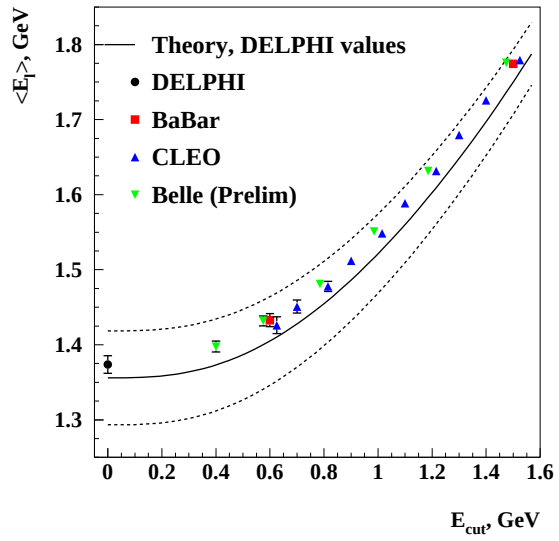

Figure 9.1: Comparison of measurements of the first statistical moment of the lepton energy spectrum in semileptonic B decays, the mean energy of the leptons. The solid line gives the expected behaviour based on the OPE parameter values set by the combined DELPHI measurement, and the dashed lines, the approximate 1σ contours obtained by varying the parameters simultaneously by $\pm 1\sigma$

narrower than those shown in the Figures 9.1-9.3.

The measurements of the first moment are depicted in Figure 9.1. All the measurements appear consistent with the parameter values obtained from the DELPHI measurement. The DELPHI measurement is not situated right on top of the central value curve defined by the DELPHI measurements since the OPE parameter determination also includes the DELPHI measurement of the moments of the hadronic mass spectrum. The 1σ band gets narrower at high values of $E_{\rm cut}$. This means that the first moment is less sensitive to the OPE parameters when a high value of $E_{\rm cut}$ is used. On the other hand, the combined statistical and systematic errors of the measurements with high $E_{\rm cut}$ are smaller than in the DELPHI measurement.

The measurements of the second moment of the lepton energy spectrum are summarised in Figure 9.2. Again most of the points are compatible with the 1σ limits.

Measurements of the third moment of the lepton energy spectrum (Figure 9.3)

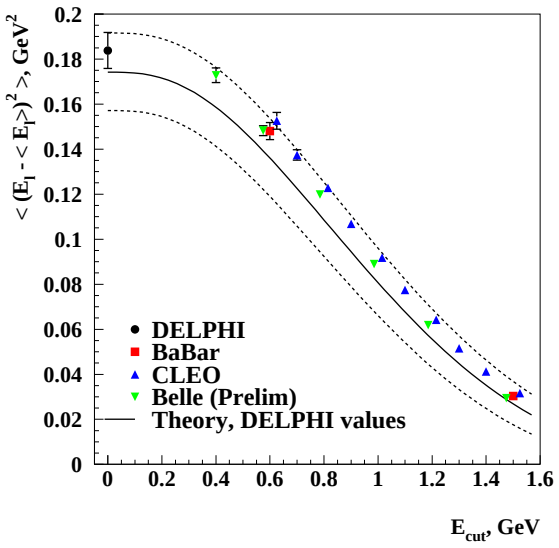

Figure 9.2: Comparison of the measurements of the second leptonic moment, the variance of the energy spectrum of the leptons. The solid line gives the expected behaviour based on the OPE parameter values set by the DELPHI measurement, and the dashed lines, the approximate 1σ contours obtained by varying the parameters by $\pm 1\sigma$

have been reported by the DELPHI, BABAR and BELLE collaborations. The decrease in the third moment after $E_{\rm cut} = 1$ GeV reduces the reliability of the 1σ band above that point; nevertheless the BABAR measurement at 1.5 GeV seems to be located right on the curve defined by the DELPHI parameters. The BELLE measurements are also consistent with the 1σ band.

To summarise, based on the Figures 9.1, 9.2 and 9.3 all the other measurements of the lepton energy moments are compatible with the DELPHI measurements given in publication I.

9.2 OPE parameters

The OPE parameter values are determined by finding a set of parameter values that best correspond to the measured values of the statistical moments of the lepton spectrum and hadron mass spectrum in semileptonic B decays, as described in publication II. Additional constraints are needed to ensure that

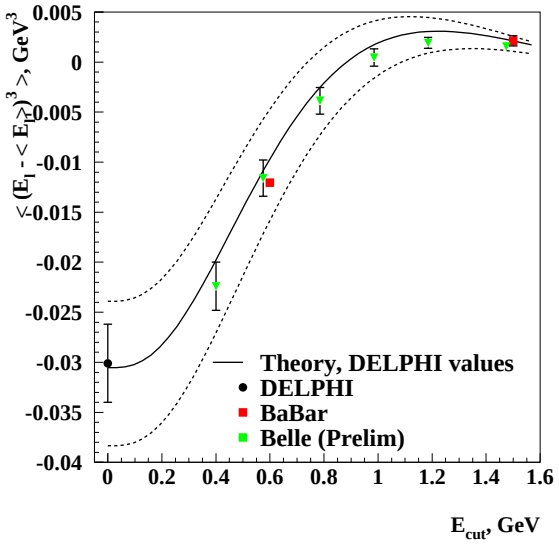

Figure 9.3: Comparison of measurements of the third leptonic moment, the skewness of the lepton energy distribution. The solid line gives the expected behaviour based on OPE parameter values set by the DELPHI measurement, and the dashed lines, the approximate 1σ contours obtained by varying the parameters by $\pm 1\sigma$

the fit converges to a physically meaningful region in the parameter space.

The results of the OPE parameters can in principle be compared only when they are evaluated to the same order in the $1/m_b$ and α_S expansions. The majority of the determinations include corrections up to the order of $1/m_b^3$ and $\alpha_S^2\beta_0$. The theoretical uncertainty quoted with the measurement usually contains an estimate of the effect of the higher order terms.

There are several possible schemes for defining the OPE parameters. A summary of the schemes, although a subjective one, is presented in Ref. [142]. The parameters of the two schemes used in the DELPHI analysis (publication I), the kinetic mass scheme and the pole mass scheme, are presented in Section 5.3 of this thesis.

In this section, the DELPHI results are compared with results from the other collaborations that have presented the results in the same schemes as DELPHI. Results in the kinetic mass scheme are available from BABAR, as well as preliminary results from CLEO. An extraction using all the experimental measurements [143] also exists, denoted in the following by B&F after its authors. In

the pole mass scheme, preliminary results from CLEO are available, as well as $\bar{\Lambda}$ and λ_1 based on the hadronic moments at CDF. A fit using all the available moment measurements [142] (BLLMT) yields a value of λ_1.

9.2.1 Kinetic mass scheme

The parameters determined by DELPHI in the kinetic mass scheme are the quark masses m_b and m_c, the b quark kinetic energy squared μ_π^2 and the Darwin term ρ_D^3. The following constraints are applied: $\mu_G^2 = 0.35 \pm 0.07$ GeV^2 and $\rho_{\rm LS}^3 = -0.15 \pm 0.10$ GeV^3, based on the $B^* - B$ mass difference and sum rules, respectively. In addition, it is required that $m_b(1\text{ GeV}) = 4.61 \pm 0.17$ GeV/c^2 and $m_c(1\text{ GeV}) = 1.14 \pm 0.10$ GeV/c^2, converted from the current values of $m_b(m_b)$ and $m_c(m_c)$ [4]. The requirement on m_b has the same effect as including a measurement of the mean energy of photons in $B \to X_s\gamma$ decays.

The values can be compared with the BABAR results [152], the preliminary results from CLEO [148] and a global fit to all available measurements (B&F) [143]. The CLEO results contain only the evaluation of the experimental uncertainties. The total error for the CLEO measurement for the purpose of comparison

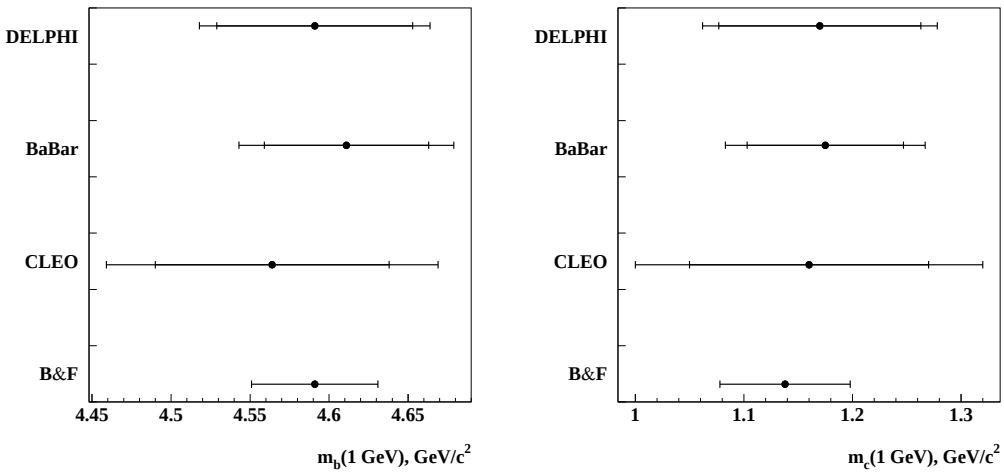

Figure 9.4: Comparison of the DELPHI, BABAR and preliminary CLEO measurements of the quark masses m_b (left) and m_c (right), as well as results from a fit to all available moment measurements (B&F). The error bars shown correspond to experimental and total uncertainties.

is estimated by assuming that the theory uncertainty is of the same magnitude as the experimental uncertainty, as is the case for both the DELPHI and the BABAR determinations. The global fit result is reported with just the total uncertainty.

The four determinations of m_b and m_c are compared in Figure 9.4. All the values are compatible with the DELPHI value already at the level of the experimental accuracy. The theoretical uncertainties between the measurements are partly correlated.The combination of all the measurements (B&F) has the smallest overall uncertainty.

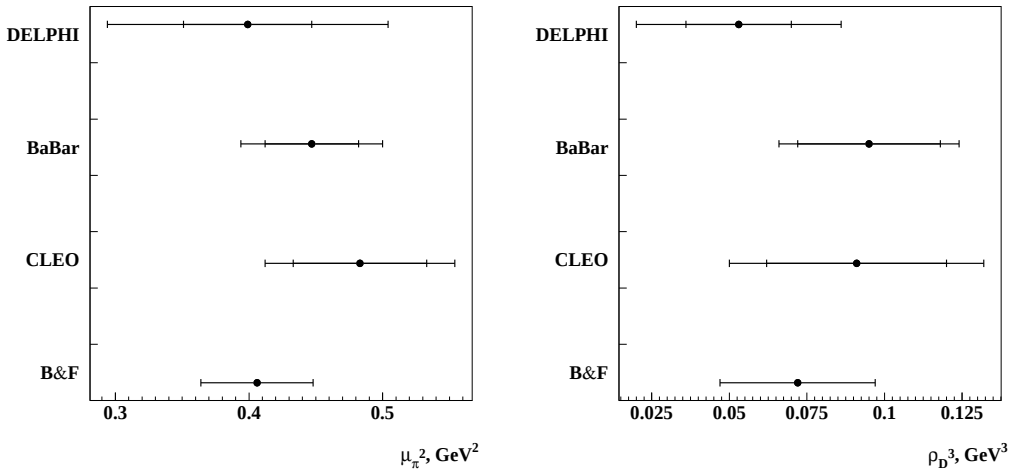

Figure 9.5: Comparison of the DELPHI, BABAR and preliminary CLEO measurements of the mean energy squared of the b quark μ_π^2 and the Darwin operator $\tilde{\rho}_D^3$ (right) together with the result of a global fit (B&F). The error bars shown correspond to experimental and total uncertainties.

The values of μ_π^2 and $\tilde{\rho}_D^3$ are compared in Figure 9.5. Even though all the four values of μ_π^2 are compatible, the DELPHI value is slightly lower than the BABAR and CLEO determinations. The global value (B&F) is very close to the DELPHI determination. All the determinations satisfy the lower bound $\mu_\pi^2 \geq \mu_g^2$ obtained from the requirement that the operator $(\vec{\sigma} \cdot \vec{\pi})^2 = \vec{\pi}^2 - \sigma \cdot \vec{B}$ is not negative [1, 161].

The other experiments obtain higher values of $\tilde{\rho}_D^3$ than DELPHI. The results are within the estimated accuracy of each other. The global fit value falls between the DELPHI value and the other two. One should note that BABAR

and B&F report the value of ρ_D^3, while DELPHI and CLEO give the value of $\tilde{\rho}_D^3$. The two parameters are related through $\tilde{\rho}_D^3 \backsimeq \rho_D^3 - 0.1\,\mathrm{GeV}^3$ [162]. All the results have been converted to $\tilde{\rho}_D^3$ for Figure 9.5.

9.2.2 Pole mass scheme

In the pole mass scheme, DELPHI has extracted parameters $\bar{\Lambda}$, λ_1, λ_2, ρ_1 and ρ_2. In this case, the constraints needed were the restriction of $M_{B^*} - M_B$ and $M_{D^*} - M_D$ to the measured values and fixing the parameters $\mathcal{T}_i$ appearing at $1/m_b^3$ $\mathcal{T}_i = 0.0$ GeV^3. The obtained parameter values can be compared with $\bar{\Lambda}$ and λ_1 from hadronic moments at CDF [156] and the preliminary values from CLEO in 2003 [147], and λ_1 from the extraction using all available moment measurements in two different schemes [142]. In addition, the results of the B&F determination performed in the kinetic mass scheme have been converted to the pole mass scheme. The CLEO numbers are given separately for two determinations, one using the first two moments of the lepton energy

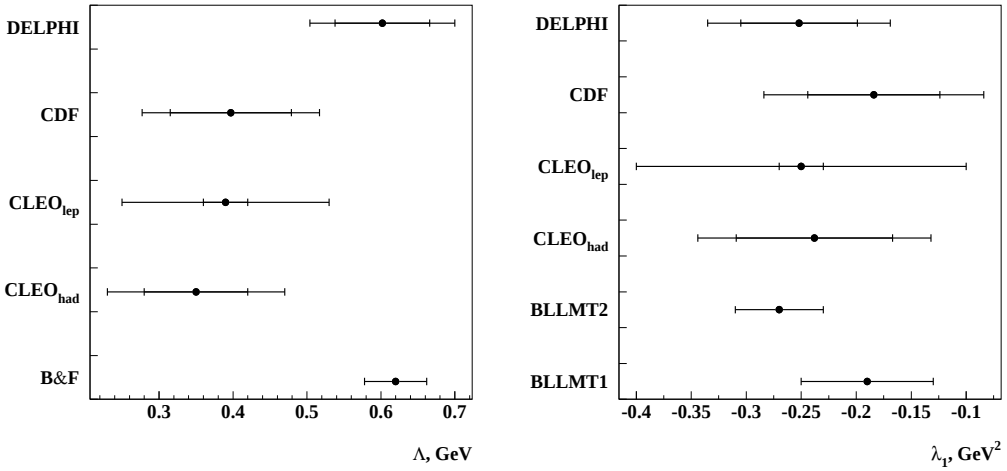

Figure 9.6: Comparison of the DELPHI, CDF and preliminary CLEO measurements separately for lepton moments and the first hadron mass and photon energy moment, of the parameter $\bar{\Lambda}$ and the B&F result obtained in the kinetic mass scheme converted to the pole mass scheme (left). Comparison of the values of parameter λ_1 also including two determinations using all available measured moments (BLLMT1 and BLLMT2) in two schemes (right).

spectrum and the other using the mean mass of the hadron system and the mean energy of a photon in $B \to X_s\gamma$ decays.

The measured values are depicted in Figure 9.6. While the three other measurements of $\bar{\Lambda}$ yield values very close to each other, the DELPHI value is higher, as is the B&F value. One should note, however, that the CLEO extraction does not contain the $1/m_b^3$ corrections. The CDF extraction includes the correction. They use fixed values for the parameters appearing at that order and include the variation in the systematical uncertainty. The DELPHI determination also extracts the higher order parameters ρ_1 and ρ_2 form the measured moments.

The determinations of λ_1 by the experimental collaborations are compatible with each other.The two extractions using all the available moments (BLLMT1 and BLLMT2) are consistent with the values obtained by experiments.

9.3 The CKM-matrix element $|V_{cb}|$

The values of the CKM-matrix element $|V_{cb}|$ offer the best comparison of the moment measurements for those cases where it is available. All the dependence of the particular scheme, the corrections included in terms of $1/m_b$ and α_S, and the minimum lepton energy requirements should not affect the measured value of $|V_{cb}|$, as long as they are treated consistently within each measurement. In addition, there are complementary methods for the measurement of $|V_{cb}|$ with which to compare.

The $|V_{cb}|$ values obtained in different moment analyses are summarised in Figure 9.7. The current world average of inclusive determinations [4] is shown as a shaded band with a vertical line representing the central value. The CLEO results are all preliminary and the most recent one, labelled "CLEO04", still lacks evaluation of theoretical uncertainty. Only the experimental uncertainty is shown in that case. The BELLE result [17] is an old inclusive measurement. The difference between the theory uncertainty in the BELLE measurement and the other measurements reflects the improvement in the accuracy brought about by the moment measurements leading to more accurate knowledge on the values of the OPE parameters. For the sake of comparison, the world average of the complementary exclusive $|V_{cb}|$ determination is also shown.

All the measured values of $|V_{cb}|$ included in the Figure are compatible. The most recent measurements (DELPHI, BABAR, CLEO04) tend to yield higher values than the average inclusive $|V_{cb}|$. The recent values are close to the central value of the exclusive world average. A similar development can be observed

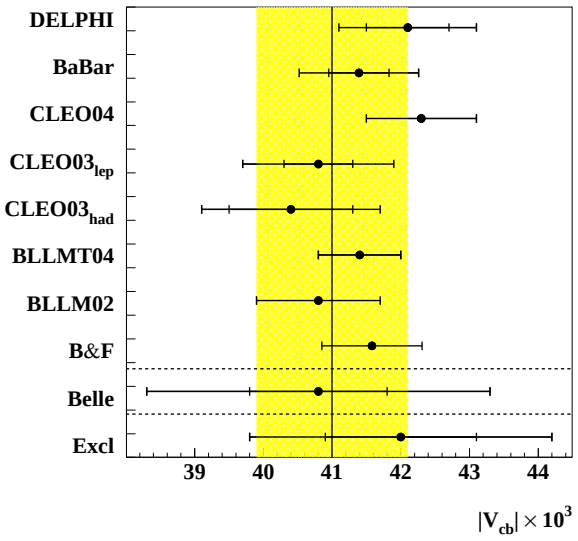

Figure 9.7: Comparison of the inclusive determinations of $|V_{cb}|$. The vertical line corresponds to the world average [4], and its 1σ limits are shown as the shaded band. The world average of the exclusive measurement [4] is also shown. The points included have been obtained through analysis of the moments, with the exception of the BELLE result, which is an older inclusive determination. The new preliminary CLEO04 value is obtained in the kinetic mass scheme, while the older, also preliminary, CLEO03 values use the pole mass scheme.

in the result using moments from all the collaborations. The recent values from 2004 (BLLMT04) and 2005 (B&F) are higher than the value obtained in 2002 (BLLM02) [2]. The uncertainty has also decreased, due both to improvements in the theoretical treatment as well as more experimental moment measurements available.

The improvement in the accuracy of $|V_{cb}|$ attributable to the OPE parameter determination using the statistical moments of the lepton energy spectrum and the hadronic mass spectrum is significant. In the BELLE measurement that does not utilise the new information, the theoretical uncertainty is about 6%, while in the new DELPHI determination (publication I) the theoretical uncertainty is about 2%.

9.4 The running b-quark mass

The extraction of the parameters in the kinetic mass scheme (publication I) was also performed without constraints on the quark masses m_b and m_c. This gave $m_b(1\text{ GeV}) = 4.67 \pm 0.22\text{ GeV}/c^2$, which is fully consistent with the value obtained with the constraints, but with a larger uncertainty. The value corresponds to the $\overline{\text{MS}}$ mass of $m_b(m_b) = 4.31 \pm 0.20\text{ GeV}/c^2$.

The DELPHI collaboration has also performed another measurement of m_b, at the Z^0 pole mass m_Z [160]. The rate of b events with three jets is related to the value of $m_b(m_Z)$ and by comparing the three-jet rate in $Z \to b\bar{b}$ and $Z \to q\bar{q}$, $q = u,\ d,\ s$ events, $m_b(m_Z)$ was determined.

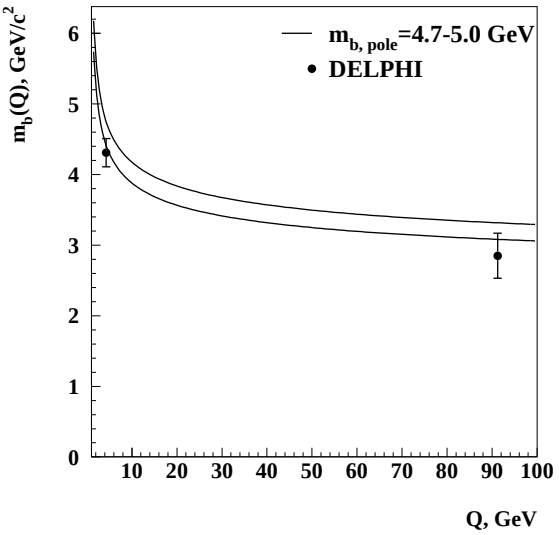

Figure 9.8: The measurement of m_b at two energy scales with DELPHI, from moment analysis at m_b and at m_Z using the three-jet rate. The solid lines give the expected behaviour for b quark pole mass between 4.7 and 5.0 GeV/c^2.

These two measurements make DELPHI the first experiment to measure m_b at two different energy scales. The results (Figure 9.8) are consistent with the running of the b quark mass expected using renormalisation group equations in the $\overline{\text{MS}}$ renormalisation scheme, shown as the band defined by the two solid lines in the Figure. The value of $m_b(m_b)$ from the measurement of the moments in B decays (publication I) is also compatible with the current world average of $m_b(m_b) = 4.24 \pm 0.11\text{ GeV}/c^2$ [4].

9.5 The dead cone effect

The objective of the measurement of the angular distributions of fragmentation particles in jets with heavy and light flavours (publication VI) was to study the dead cone effect, i.e. the absence of fragmentation particles at small emission angles. The results are summarised in Figure 9.9.

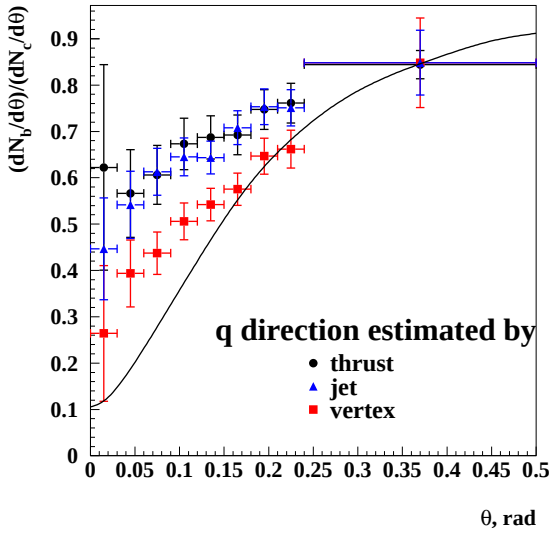

Figure 9.9: The ratio of the angular distribution of fragmentation particles in b and c jets, with the angle with respect to the event thrust axis (circle), the jet direction (triangle) and the flight direction of the vertex (square) direction. The solid line represents the theoretical expectation convoluted with the expected experimental accuracy.

The direction of the b quark has been estimated in three different ways: the direction of the thrust axis, the direction of the jet and the flight direction of the vertex were used as the estimator. The differences between the different estimators give an estimate of the systematic uncertainty of the measurement. The error bars shown only correspond to the statistical uncertainty.

The theoretically preferred estimator [163], the vertex direction, shows the most significant depletion. One should note that the normalisation is based on the last bin, where the statistical uncertainty is large, especially in the case of the vertex direction as the estimator. From the experimental point of view the vertex direction is the estimator that has the largest expected bias. The

distributions using the thrust or jet direction show depletion of fragmentation particles at small angles in b jets, but not to the expected extent.

9.6 Top quark pair production at CLIC

The simulation studies performed to understand the accuracy at which the cross-section and forward-backward asymmetry of $t\bar{t}$ could be performed at CLIC (publication VII) had two purposes. On the one hand, the resulting numbers were needed to asses the possibility of observing Z' bosons beyond the center-of-mass energy of the collider. On the other hand, it was a test to see whether the foreseen detector accuracies and running conditions would allow the reconstruction and identification of events with top quarks. An additional benefit was a reconstruction method for top quarks that could be applied in other analyses, such as the one looking for supersymmetric top quarks, or stops [164].

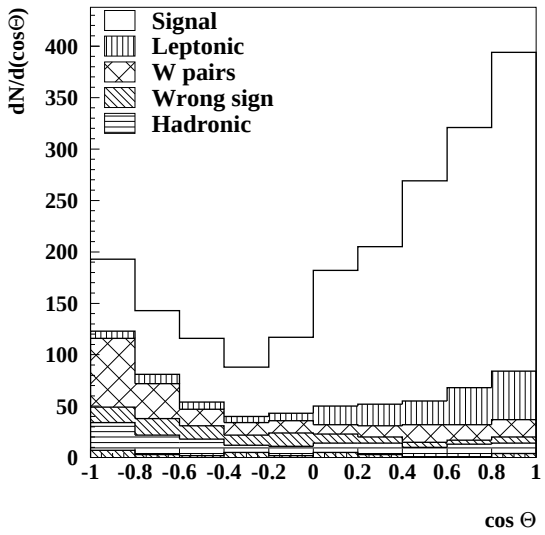

Figure 9.10: The reconstructed $\cos\Theta$ distribution of the top quark direction with respect to the beam electron direction.

The asymmetry distribution is shown in Figure 9.10. The study shows that it is feasible to measure the production cross-section of top quarks at CLIC at an accuracy of $\Delta\sigma_{t\bar{t}}/\sigma_{t\bar{t}} = 0.014$ and the forward-backward asymmetry at

accuracy $\Delta A_{\mathrm{FB}}^{t\bar{t}}/A_{\mathrm{FB}}^{t\bar{t}} = 0.042$ for 1 ab^{-1} of data. The data corresponds to one year of accelerator running. Combining the top quark results with results for b quarks and muons indicates that, for example, the existence of a 30 TeV/c^2 Z' boson could be established after four years of CLIC running [124].

Chapter 10

Summary

In this thesis, analyses on three distinct topics are presented. The three analyses have two significant steps in common: the reconstruction of the heavy quark decay and the separation of the signal from the background. Each of the analyses had different requirements for the performance of these, while the basic principles were the same.

The most important analysis is the study of the lepton spectrum in semileptonic B decays at DELPHI (publications I-IV). Using the statistical moments of the energy spectrum, together with the moments of the hadronic mass spectrum, OPE parameters can be extracted. These parameters are an important part of the current theoretical description of the decays of heavy mesons and are crucial in the extraction of the CKM-matrix element V_{cb}, a parameter of the Standard Model. The DELPHI measurement is important as it is the only one performed using the full electron energy spectrum.

The OPE parameter values obtained are in the region expected based on theoretical considerations, and they are also compatible with the other determinations. The uncertainty on the value of V_{cb} has been reduced.

In the second analysis (publication VI), the angular distribution of fragmentation particles in b, c and light quark jets was studied using the DELPHI data. The ratio of the distributions show a depletion of particles at small angles, as expected for the dead cone effect predicted by perturbative QCD.

The simulation studies regarding the reconstruction of top quark decays at center-of-mass energy of 3 TeV (publication VII) showed that the reconstruction and signal event selection is feasible even under these demanding conditions. The results were used to estimate the possibility of indirectly observing heavy gauge bosons beyond the center-of-mass energy of the collider.

Bibliography

[1] M. B. Voloshin, Phys. Rev. **D51** (1995) 4934, hep-ph/9411296.

[2] C. W. Bauer, Z. Ligeti, M. Luke, and A. V. Manohar, Phys. Rev. **D67** (2003) 054012, hep-ph/0210027.

[3] F. Halzen and A. Martin, *Quarks and Leptons: An Introductory Course in Modern Particle Physics* (John Wiley & Sons, 1984).

[4] S. Eidelman *et al.*, (Particle Data Group), Phys. Lett. **B592** (2004) 1, and 2005 partial update for edition 2006 (URL: http://pdg.lbl.gov).

[5] P. Abreu *et al.*, (The DELPHI Collaboration), Nucl. Phys. **B418** (1994) 403.

[6] The CDF Collaboration, the DØ Collaboration and the Tevatron Electroweak Working Group, "Combination of CDF and D0 results on the top-quark mass", hep-ex/0507091.

[7] N. Cabibbo, Phys. Rev. Lett. **10** (1963) 531.

[8] M. Kobayashi and T. Maskawa, Prog. Theor. Phys. **49** (1973) 652.

[9] C. Jarlskog, Phys. Rev. Lett. **55** (1985) 1039.

[10] P. Abreu *et al.*, (The DELPHI Collaboration), Eur. Phys. J. **C20** (2001) 455, hep-ex/0105080.

[11] H. Albrecht *et al.*, (The ARGUS Collaboration), Phys. Lett. **B318** (1993) 397.

[12] G. Abbiendi *et al.*, (The OPAL Collaboration), Eur. Phys. J. **C13** (2000) 225, hep-ex/9906041.

[13] M. Acciarri *et al.*, (The L3 Collaboration), Eur. Phys. J. **C13** (2000) 47, hep-ex/9909045.

[14] A. Heister *et al.*, (The ALEPH Collaboration), Eur. Phys. J. **C22** (2002) 613, hep-ex/0108007.

[15] B. Barish *et al.*, (The CLEO Collaboration), Phys. Rev. Lett. **76** (1996) 1570.

[16] S. Henderson *et al.*, (The CLEO Collaboration), Phys. Rev. **D45** (1992) 2212.

[17] K. Abe *et al.*, (The BELLE Collaboration), Phys. Lett. **B547** (2002) 181, hep-ex/0208033.

[18] B. Aubert *et al.*, (The BABAR Collaboration), Phys. Rev. **D67** (2003) 031101.

[19] J. Abdallah *et al.*, (The DELPHI Collaboration), Eur. Phys. J. **C33** (2004) 213, hep-ex/0401023.

[20] D. Buskulic *et al.*, (The ALEPH Collaboration), Phys. Lett. **B395** (1997) 373.

[21] G. Abbiendi *et al.*, (The OPAL Collaboration), Phys. Lett. **B482** (2000) 15, hep-ex/0003013.

[22] R. A. Briere *et al.*, (The CLEO Collaboration), Phys. Rev. Lett. **89** (2002) 081803, hep-ex/0203032.

[23] B. Aubert *et al.*, (The BABAR Collaboration), (2003), hep-ex/0308027.

[24] K. Abe *et al.*, (The BELLE Collaboration), Phys. Lett. **B526** (2002) 247, hep-ex/0111060.

[25] B. Aubert *et al.*, BABAR, Phys. Rev. Lett. **95** (2005) 111801, hep-ex/0506036.

[26] A. Limosani *et al.*, (The BELLE Collaboration), Phys. Lett. **B621** (2005) 28, hep-ex/0504046.

[27] P. Abreu *et al.*, (The DELPHI Collaboration), Phys. Lett. **B478** (2000) 14, hep-ex/0105054.

[28] B. Aubert *et al.*, (The BABAR Collaboration), Phys. Rev. Lett. **92** (2004) 071802, hep-ex/0307062.

[29] I. Bizjak *et al.*, (The BELLE Collaboration), Phys. Rev. Lett. **95** (2005) 241801, hep-ex/0505088.

[30] T. Inami and C. S. Lim, Prog. Theor. Phys. **65** (1981) 297, Erratum Prog. Theor. Phys. **65** (1981) 1772.

[31] P. Abreu *et al.*, (The DELPHI Collaboration), Z. Phys. **C76** (1997) 579.

[32] D. Buskulic *et al.*, (The ALEPH Collaboration), Z. Phys. **C75** (1997) 397.

[33] G. Abbiendi *et al.*, (The OPAL Collaboration), Phys. Lett. **B493** (2000) 266, hep-ex/0010013.

[34] M. Acciarri *et al.*, (The L3 Collaboration), Eur. Phys. J. **C5** (1998) 195.

[35] F. Abe *et al.*, (The CDF Collaboration), Phys. Rev. **D60** (1999) 072003, hep-ex/9903011.

[36] Y. Zheng *et al.*, (The BELLE Collaboration), Phys. Rev. **D67** (2003) 092004, hep-ex/0211065.

[37] B. Aubert *et al.*, (The BABAR Collaboration), Phys. Rev. **D67** (2003) 072002, hep-ex/0212017.

[38] J. Abdallah *et al.*, (The DELPHI Collaboration), Eur. Phys. J. **C35** (2004) 35, hep-ex/0404013.

[39] A. Heister *et al.*, (The ALEPH Collaboration), Eur. Phys. J. **C29** (2003) 143.

[40] G. Abbiendi *et al.*, (The OPAL Collaboration), Eur. Phys. J. **C19** (2001) 241, hep-ex/0011052.

[41] F. Abe *et al.*, (The CDF Collaboration), Phys. Rev. Lett. **82** (1999) 3576.

[42] K. Abe *et al.*, (The SLD Collaboration), Phys. Rev. **D66** (2002) 032009, hep-ex/0207048.

[43] J. Hewett, editor, *The discovery potential of a Super B Factory*, , Proceeding of SLAC Workshops, SLAC-R-709, SLAC-R-0709, SLAC-709, SLAC-0709, 2003, hep-ph/0503261.

[44] B. Aubert *et al.*, (The BABAR Collaboration), Phys. Rev. Lett. **94** (2005) 161803, hep-ex/0408127.

[45] K. Abe *et al.*, (The BELLE Collaboration), Phys. Rev. **D71** (2005) 072003, Erratum Phys. Rev. **D71** (2005) 079903, hep-ex/0408111.

[46] B. Aubert *et al.*, (The BABAR Collaboration), Phys. Rev. Lett. **95** (2005) 041805, hep-ex/0503049.

[47] K. Abe *et al.*, (The BELLE Collaboration), "Measurement of the branching fraction, polarization, and CP asymmetry in $B^0 \to \rho^+\rho^-$ decays", BELLE-CONF-0545, UCHEP-05-02, hep-ex/0507039, Contributed paper to LP 2005, Uppsala, Sweden, and to HEPP-EPS 2005, Lisbon, Portugal.

[48] F. Wilczek, Proc. Nat. Acad. Sci. **102** (2005) 8403, hep-ph/0502113.

[49] D. J. Gross, Nucl. Phys. Proc. Suppl. **74** (1999) 426, hep-th/9809060.

[50] H. D. Politzer, Phys. Rev. Lett. **30** (1973) 1346.

[51] D. J. Gross and F. Wilczek, Phys. Rev. **D9** (1974) 980.

[52] P. A. Aarnio *et al.*, (The DELPHI Collaboration), Nucl. Instrum. Meth. **A303** (1991) 233.

[53] P. Abreu *et al.*, (The DELPHI Collaboration), Nucl. Instrum. Meth. **A378** (1996) 57, Erratum Nucl. Instrum. Meth. **A396** (1997) 281.

[54] K. Österberg, *Search for New Physics in the Lepton Sector of the Standard Model at LEP1*, PhD thesis, University of Helsinki, 1998.

[55] V. Chabaud *et al.*, (The DELPHI Collaboration), Nucl. Instrum. Meth. **A368** (1996) 314.

[56] M. Feindt, C. Kreuter, and O. Porobrin, (The DELPHI Collaboration), "ELEPHANT Reference Manual", DELPHI Report DELPHI 96-82 PROG 217, 1996 (unpublished).

[57] P. Abreu *et al.*, (The DELPHI Collaboration), Eur. Phys. J. **C10** (1999) 415.

[58] R. Barate *et al.*, (The ALEPH Collaboration), Phys. Lett. **B401** (1997) 150.

[59] R. Barate *et al.*, (The ALEPH Collaboration), Phys. Lett. **B401** (1997) 163.

[60] G. Abbiendi *et al.*, (The OPAL Collaboration), Eur. Phys. J. **C8** (1999) 217, hep-ex/9810002.

[61] K. Abe *et al.*, (The SLD Collaboration), Phys. Rev. **D71** (2005) 112004, hep-ex/0503005.

[62] G. Barker *et al.*, (The DELPHI Collaboration), "A Study of the b-Quark Fragmentation Function with the DELPHI Detector at LEP I", DELPHI Report DELPHI 2002-069 CONF 603, 2002 (unpublished), Contributed paper for ICHEP 2002, Amsterdam.

[63] V. G. Kartvelishvili, A. K. Likhoded, and V. A. Petrov, Phys. Lett. **B78** (1978) 615.

[64] P. D. B. Collins and T. P. Spiller, J. Phys. **G11** (1985) 1289.

[65] C. Peterson, D. Schlatter, I. Schmitt, and P. M. Zerwas, Phys. Rev. **D27** (1983) 105.

[66] B. Andersson, G. Gustafson, and B. Soderberg, Z. Phys. **C20** (1983) 317.

[67] M. G. Bowler, Zeit. Phys. **C11** (1981) 169.

[68] Y. L. Dokshitzer, V. A. Khoze, and S. I. Troian, Phys. Rev. **D53** (1996) 89, hep-ph/9506425.

[69] V. A. Khoze, W. Ochs, and J. Wosiek, "Analytical QCD and multiparticle production", in *Boris Ioffe Festschrift "At the Frontier of Particle Physics. Handbook of QCD"*, edited by M. Shifman, pp. 1101–1194, World Scientific, Singapore, 2001, hep-ph/0009298.

[70] V. A. Khoze, "The Physics of QCD Jets", in *Proceedings of the 1989 International Symposium on Lepton and Photon Interactions at High Energies, Stanford University*, edited by M. Riordan, pp. 387–401, Singapore, 1990, World Scientific.

[71] Y. L. Dokshitzer, V. A. Khoze, and S. I. Troian, J. Phys. **G17** (1991) 1602.

[72] P. Abreu *et al.*, (The DELPHI Collaboration), Phys. Lett. **B479** (2000) 118, Erratum Phys. Lett. **B492** (2000) 492, hep-ex/0103022.

[73] G. Abbiendi *et al.*, (The OPAL Collaboration), Phys. Lett. **B550** (2002) 33, hep-ex/0211007.

[74] B. R. Webber, "Quantum Chromodynamics", in *Proceedings of the 1992 European School of High Energy Physics*, edited by N. Ellis and M. B. Gavela, , CERN yellow report, CERN 94-04, Geneva, 1994, CERN.

[75] X. Artru and G. Mennessier, Nucl. Phys. **B70** (1974) 93.

[76] B. Andersson, G. Gustafson, G. Ingelman, and T. Sjostrand, Phys. Rept. **97** (1983) 31.

[77] T. Sjöstrand, Comput. Phys. Commun. **82** (1994) 74.

[78] T. Sjöstrand *et al.*, Comput. Phys. Commun. **135** (2001) 238, hep-ph/0010017.

[79] D. Amati and G. Veneziano, Phys. Lett. **B83** (1979) 87.

[80] G. Corcella *et al.*, JHEP **01** (2001) 010, hep-ph/0011363.

[81] P. Abreu *et al.*, (The DELPHI Collaboration), Z. Phys. **C73** (1996) 11.

[82] J. Abdallah *et al.*, (The DELPHI Collaboration), Phys. Lett. **B576** (2003) 29, hep-ex/0311005.

[83] D. Acosta *et al.*, (The CDF Collaboration), "Evidence for the exclusive decay $B_c^{\pm} \to J/\psi\pi^{\pm}$ and measurement of the mass of the B_c meson", FERMILAB-PUB-05-216-E, hep-ex/0505076, Submitted to Phys. Rev. Lett.

[84] P. D. Acton *et al.*, (The OPAL Collaboration), Phys. Lett. **B295** (1992) 357.

[85] D. Buskulic *et al.*, (The ALEPH Collaboration), Phys. Lett. **B361** (1995) 221.

[86] R. Barate *et al.*, (The ALEPH Collaboration), Eur. Phys. J. **C2** (1998) 197.

[87] T. Affolder *et al.*, (The CDF Collaboration), Phys. Rev. Lett. **84** (2000) 1663, hep-ex/9909011.

[88] F. Abe *et al.*, (The CDF Collaboration), Phys. Rev. **D60** (1999) 092005.

[89] Z. Albrect *et al.*, (The DELPHI Collaboration), "A Study of Excited b-Hadron States with the DELPHI Detector at LEP", DELPHI Report DELPHI 2005-011 CONF 731, 2005 (unpublished), Contributed Paper for LP 2005 (Uppsala) and HEP-EPS 2005, Lisbon.

[90] P. Abreu *et al.*, (The DELPHI Collaboration), Phys. Lett. **B345** (1995) 598.

[91] R. Akers *et al.*, (The OPAL Collaboration), Z. Phys. **C66** (1995) 19.

[92] G. Abbiendi *et al.*, (The OPAL Collaboration), Eur. Phys. J. **C23** (2002) 437, hep-ex/0010031.

[93] D. Buskulic *et al.*, (The ALEPH Collaboration), Z. Phys. **C69** (1996) 393.

[94] R. Barate *et al.*, (The ALEPH Collaboration), Phys. Lett. **B425** (1998) 215.

[95] M. Acciarri *et al.*, (The L3 Collaboration), Phys. Lett. **B465** (1999) 323, hep-ex/9909018.

[96] T. Affolder *et al.*, (The CDF Collaboration), Phys. Rev. **D64** (2001) 072002.

[97] J. Abdallah *et al.*, (The DELPHI Collaboration), Phys. Lett. **B561** (2003) 26, hep-ex/0303031.

[98] R. Barate *et al.*, (The ALEPH Collaboration), Eur. Phys. J. **C4** (1998) 387.

[99] T. E. Coan *et al.*, (The CLEO Collaboration), Phys. Rev. Lett. **80** (1998) 1150, hep-ex/9710028.

[100] G. Altarelli, N. Cabibbo, G. Corbo, L. Maiani, and G. Martinelli, Nucl. Phys. **B208** (1982) 365.

[101] N. Isgur, D. Scora, B. Grinstein, and M. B. Wise, Phys. Rev. **D39** (1989) 799.

[102] K. G. Wilson, Phys. Rev. **179** (1969) 1499.

[103] N. Cabibbo, G. Corbo, and L. Maiani, Nucl. Phys. **B155** (1979) 93.

[104] E. H. Thorndike, "Weak Decays of Heavy Fermions", in *Proceedings of the 1985 International Symposium on Lepton and Photon Interactions at High Energies, Kyoto*, pp. 406–445, 1985.

[105] B. Grinstein, M. B. Wise, and N. Isgur, Phys. Rev. Lett. **56** (1986) 298.

[106] E. Eichten and B. Hill, Phys. Lett. **B234** (1990) 511.

[107] H. Georgi, Phys. Lett. **B240** (1990) 447.

[108] A. Ali and E. Pietarinen, Nucl. Phys. **B154** (1979) 519.

[109] M. Jezabek and J. H. Kuhn, Nucl. Phys. **B314** (1989) 1.

[110] M. Jezabek and J. H. Kuhn, Nucl. Phys. **B320** (1989) 20.

[111] A. Czarnecki, M. Jezabek, and J. H. Kuhn, Acta Phys. Polon. **B20** (1989) 961.

[112] A. Czarnecki and M. Jezabek, Nucl. Phys. **B427** (1994) 3, hep-ph/9402326.

[113] Y. Nir, Phys. Lett. **B221** (1989) 184.

[114] S. J. Brodsky, G. P. Lepage, and P. B. Mackenzie, Phys. Rev. **D28** (1983) 228.

[115] M. E. Luke, M. J. Savage, and M. B. Wise, Phys. Lett. **B345** (1995) 301, hep-ph/9410387.

[116] P. Ball, M. Beneke, and V. M. Braun, Phys. Rev. **D52** (1995) 3929, hep-ph/9503492.

[117] V. Aquila, P. Gambino, G. Ridolfi, and N. Uraltsev, Nucl. Phys. **B719** (2005) 77, hep-ph/0503083.

[118] I. I. Bigi, M. A. Shifman, N. G. Uraltsev, and A. I. Vainshtein, Phys. Rev. **D52** (1995) 196, hep-ph/9405410.

[119] D. Benson, I. I. Bigi, T. Mannel, and N. Uraltsev, Nucl. Phys. **B665** (2003) 367, hep-ph/0302262.

[120] I. I. Bigi, M. A. Shifman, N. G. Uraltsev, and A. I. Vainshtein, Phys. Rev. Lett. **71** (1993) 496, hep-ph/9304225.

[121] A. F. Falk, M. E. Luke, and M. J. Savage, Phys. Rev. **D53** (1996) 2491, hep-ph/9507284.

[122] I. I. Bigi, "The Unreasonable Success of CKM Theory", FERMILAB-PUB-05-216-E, hep-ph/0501084, Invited talk at Flavor Physics and CP Violation (FPCP 2004), Daegu, Korea.

[123] D. Benson, I. I. Bigi, and N. Uraltsev, Nucl. Phys. **B710** (2005) 371, hep-ph/0410080.

[124] M. Battaglia, A. De Roeck, J. Ellis, and D. Schulte, editors, *Physics at the CLIC Multi-TeV Linear Collider*, , CERN yellow report, CERN-2004-005, Geneva, 2004, CERN, hep-ph/0412251, Report of the CLIC Physics Working Group.

[125] D. J. Gross, J. A. Harvey, E. J. Martinec, and R. Rohm, Phys. Rev. Lett. **54** (1985) 502.

[126] D. J. Gross, J. A. Harvey, E. J. Martinec, and R. Rohm, Nucl. Phys. **B256** (1985) 253.

[127] D. J. Gross, J. A. Harvey, E. J. Martinec, and R. Rohm, Nucl. Phys. **B267** (1986) 75.

[128] P. Candelas, G. T. Horowitz, A. Strominger, and E. Witten, Nucl. Phys. **B258** (1985) 46.

[129] E. Witten, Nucl. Phys. **B258** (1985) 75.

[130] E. Witten, Phys. Lett. **B149** (1984) 351.

[131] Q. Shafi and C. Wetterich, Phys. Lett. **B73** (1978) 65.

[132] V. Elias, J. C. Pati, and A. Salam, Phys. Lett. **B73** (1978) 451.

[133] J. L. Hewett and T. G. Rizzo, Phys. Rept. **183** (1989) 193.

[134] M. Battaglia, S. De Curtis, and D. Dominici, JHEP **12** (2002) 004, hep-ph/0210351.

[135] W. Bartel *et al.*, (The JADE Collaboration), Z. Phys. **C33** (1986) 23.

[136] M. Battaglia, "Jet Flavour Identification at the CLIC Multi-TeV e^+e^- Collider", in *Physics and experiments with future linear e+ e- colliders*, edited by A. Para and H. E. Fisk, AIP Conference Proceedings, pp. 813–816, New York, 2000, hep-ex/0011099.

[137] P. Abreu *et al.*, (The DELPHI Collaboration), Phys. Lett. **B425** (1998) 399.

[138] T. Sjöstrand, L. Lönnblad, S. Mrenna, and P. Skands, (2003), hep-ph/0308153.

[139] M. Battaglia, Private communication. The values are based on the output of the COMPHEP program, documented in [165].

[140] P. Abreu *et al.*, (The DELPHI Collaboration), Eur. Phys. J. **C10** (1999) 219, hep-ex/9903074.

[141] T. Allmendiger *et al.*, (The DELPHI Collaboration), "BSAURUS- A Package For Inclusive B-Reconstruction in DELPHI", DELPHI Report DELPHI 2000-069 PHYS 868, 2000 (unpublished).

[142] C. W. Bauer, Z. Ligeti, M. Luke, A. V. Manohar, and M. Trott, Phys. Rev. **D70** (2004) 094017, hep-ph/0408002.

[143] O. Buchmüller and H. Flächer, "Fits to Moment Measurements from $B \to X_c \ell \nu$ and $B \to X_s \gamma$ Decays using Heavy Quark Expansions in the Kinetic Scheme", hep-ph/0507253.

[144] M. Gremm, A. Kapustin, Z. Ligeti, and M. B. Wise, Phys. Rev. Lett. **77** (1996) 20, hep-ph/9603314.

[145] B. Barish *et al.*, (The CLEO Collaboration), Phys. Rev. Lett. **76** (1996) 1570.

[146] B. Bloch, A. Oyanguren, P. Roudeau, J. Salt, and A. Stocchi, (The DELPHI Collaboration), "Properties of broad D^{**} production in b semileptonic decays", DELPHI Report DELPHI 2002-070 CONF-604, 2002 (unpublished), Contributed paper for ICHEP 2002 conference, Amsterdam. Included in finalised form in publication I.

[147] D. G. Cassel, (The CLEO Collaboration), ECONF **C0304052** (2003) WG104, hep-ph/0309241, Proceedings of Workshop on the CKM Unitarity Triangle, Durham 2003.

[148] A. B. Smith, (The CLEO Collaboration), Nucl. Phys. Proc. Suppl. **142** (2005) 318.

[149] A. H. Mahmood *et al.*, (The CLEO Collaboration), Phys. Rev. **D70** (2004) 032003, hep-ex/0403053.

[150] S. E. Csorna *et al.*, (The CLEO Collaboration), Phys. Rev. **D70** (2004) 032002, hep-ex/0403052.

[151] S. Chen *et al.*, (The CLEO Collaboration), Phys. Rev. Lett. **87** (2001) 251807, hep-ex/0108032.

[152] B. Aubert *et al.*, (The BABAR Collaboration), Phys. Rev. Lett. **93** (2004) 011803, hep-ex/0404017.

[153] B. Aubert *et al.*, (The BABAR Collaboration), Phys. Rev. **D69** (2004) 111103, hep-ex/0403031.

[154] B. Aubert *et al.*, (The BABAR Collaboration), Phys. Rev. **D69** (2004) 111104, hep-ex/0403030.

[155] B. Aubert *et al.*, (The BABAR Collaboration), "Results from the BABAR Fully Inclusive Measurement of $B \to X_s\gamma$", Babar Report BABAR-CONF-05/05/006, SLAC-PUB-11329, 2005 (unpublished), hep-ex/0507001, Contributed paper to EPS05 Conference, Lisbon, Portugal.

[156] D. Acosta *et al.*, (The CDF Collaboration), Phys. Rev. **D71** (2005) 051103, hep-ex/0502003.

[157] K. Abe *et al.*, (The BELLE Collaboration), "Hadronic Mass Moment in $B \to X_c\ell\nu$ Decays", Belle Report BELLE-CONF-055, EPS05-532, 2005 (unpublished), hep-ex/0509013, Contributed paper to EPS05 Conference, Lisbon, Portugal.

[158] K. Abe *et al.*, (The BELLE Collaboration), "Moments of the Electron Energy Spectrum in $B \to X_c\ell\nu$ decays at Belle", Belle Report BELLE-CONF-0558, EPS05-533, 2005 (unpublished), hep-ex/0508056, Contributed paper to EPS05 Conference, Lisbon, Portugal.

[159] P. Koppenburg *et al.*, (The BELLE Collaboration), Phys. Rev. Lett. **93** (2004) 061803, hep-ex/0403004.

[160] J. Abdallah *et al.*, (The DELPHI Collaboration), "Determination of the b quark mass at the M_Z scale with the DELPHI detector at LEP", CERN Report CERN-EP-PH/2005-020, 2005 (unpublished), Submitted to Eur. Phys. J. C.

[161] M. B. Voloshin, "Topics in Heavy Quark physics", Minnesota University at Minneapolis Report TPI-MINN-94-18-T, 1994 (unpublished), Lectures at the 1994 ITEP Winter School, Surveys High Energ. Phys. **8** (1995) 27.

[162] P. Gambino and N. Uraltsev, Eur. Phys. J. **C34** (2004) 181, hep-ph/0401063.

[163] V. A. Khoze, Private communication.

[164] M. Battaglia and M. Gruwé, "Determining the Mass of Supersymmetric Scalars at the CLIC Multi-TeV e^+e^- Collider", in *Proceedings of Internatinal Workshop on Linear Colliders, Jeju, Korea*, edited by J. S. Kang and S. K. Oh, pp. 199–205, Korean Physical Society, 2002, hep-ph/0212140.

[165] A. Pukhov *et al.*, "CompHEP - a package for evaluation of Feynman diagrams and integration over multi-particle phase space", INP-MSU-98-41-542, hep-ph/9908288.